Doctoral Dissertation

Improvement of Ship Geometry for High Performance in Waves by a Practical Integrated Optimization Method

Muhdar Tasrief

June 2014

Graduate School of Engineering,
Osaka University

Improvement of Ship Geometry for High Performance in Waves by a Practical Integrated Optimization Method

by

Muhdar Tasrief

A dissertation submitted in partial fulfillment for the degree of Doctor of Engineering

in the

Graduate School of Engineering
Department of Naval Architecture and Ocean Engineering
Division of Global Architecture
Osaka University

July 2014

"If anyone travels on a road in search of knowledge, God will cause him to travel on one of the roads of Paradise. The angels will lower their wings in their great pleasure with one who seeks knowledge. The inhabitants of the heavens and the Earth and (even) the fish in the deep waters will ask forgiveness for the learned man. The superiority of the learned over the devout is like that of the moon, on the night when it is full, over the rest of the stars. The learned are the heirs of the Prophets, and the Prophets leave (no monetary inheritance), they leave only knowledge, and he who takes it takes an abundant portion."

Sunan of Abu-Dawood

OSAKA UNIVERSITY

Abstract

Graduate School of Engineering
Department of Naval Architecture and Ocean Engineering

Doctor of Engineering

by Muhdar Tasrief

In order to enhance the performance of a ship in waves, improvement of its hull geometry seems to be important and should be treated appropriately. For this purpose, a practical integrated optimization method is developed and utilized to acquire the improved ship geometry. Namely, the Genetic Algorithm (GA) with binary encoding or so-called Binary-Coded Genetic Algorithm (BCGA) and the Enhanced Unified Theory (EUT) are integrated together to optimize the basis ship geometry through its Sectional Area Curve (SAC).

In this study, the shape function based on the shifting method is adopted to the SAC during optimization. Specifically the position of transverse sections is shifted in longitudinal direction to modify the prismatic coefficient, the longitudinal center of buoyancy and the parallel middle body of the basis ship geometry. For simplicity, the principal dimension i.e. the ship length, breadth and draft must be constant. Needless to say that the main objective function of this optimization is to minimize the added resistance computed by EUT as a core method of computation.

From the results obtained in this study, the added resistance of modified Wigley model decreases in large amount at the desired wavelength region in which the optimization is performed. Furthermore, an optimization with the actual ship, namely SR-108 is also done in order to illustrate the effectiveness of the present method for the practical purpose. Thus it can be concluded that the combination between the BCGA and the EUT may be regarded as a reliable practical tool to improve the performance of a ship in waves, particularly in reducing the added resistance.

Acknowledgements

First and foremost, I would like to deeply thank my academic supervisor, Professor Masashi Kashiwagi, for his continous excellent guidance and encouragement along every step of the way to accomplish my doctoral program at Osaka University. His smart advice and expert criticism throughout my study with his extraordinary patience have been immense importance to me and proved to be invaluable.

I am also truly indebted and thankful to Professor Munehiko Minoura as Associate professor in our laboratory who was giving critical and constructive comments during laboratory meeting, moreover to Dr. Guanghua He for his fruitful discussions.

Furthermore, I should say that I have been blessed with friendly and cheerful Japanese students. It was a great pleasure to spend time with all of them in our English Laboratory Program. I also would like to thank them in providing me halal menu in the party. For all staffs of NAOE Department Osaka University, I should thank them for their kindness and help.

Most importantly, I must thank to my wife (Rani) and my children (Naveed, Naqeeb, Azzam) for their love, support and patience in spending time in Osaka with limited halal food. Also to my parents who always pray for my successfulness in obtaining a high quality level of education and in pursuing the doctor degree.

To the Ministry of Education, Culture, Sports, Science and Technology (MEXT) Japan, I am really grateful for the scholarship given to me. I could count myself to be very fortunate indeed to have been the recipient of it. Special thanks to PT. (Persero) Biro Klasifikasi Indonesia for giving a chance and supporting me to study in Osaka University, Japan.

Finally, I would like to thank everyone who was helping and supporting me and my family during our living in Osaka, Japan.

Osaka, July 2014

Muhdar Tasrief

Contents

List of Figures

List of Tables

Abbreviations

3D	three **D**imensional
BCGA	**B**inary-**C**oded **G**enetic **A**lgorithm
EA	**E**volutionary **A**lgorithm
EEDI	**E**nergy **E**fficiency **D**esign **I**ndex **M**ethod
EUT	**E**nhanced **U**nified **T**heory
GA	**G**enetic **A**lgorithm
IMO	**I**nternational **M**aritime **O**rganization
PMB	**P**arallel **M**iddle **B**ody
PI	**P**erformance **I**ndex
SAC	**S**ectional **A**rea **C**urve

Symbols

A	constant or amplitude of incident wave (m)	
a	random weighting factor	
A_{ij}	hydrodynamic added mass	kg
A_0	non-dimensionalized sectional area curve of basis hull	
A_n	non-dimensionalized sectional area curve of optimized hull	
B	ship breadth	m
B_{ij}	hydrodynamic damping coefficient	kgs^{-1}
B_a	constant of after body	
B_f	constant of fore body	
C	chromosome	
C_a	constant of after body	
C_B	block coefficient of ship	
C_f	constant of fore body	
C_{ij}	hydrodynamic restoring force	kgs^{-2}
C_M	midship coefficient of ship	
C_P	prismatic coefficient of ship	
C_{Pa}	prismatic coefficient of aft-body	
C_{Pf}	prismatic coefficient of fore-body	
C_W	steady wave-making coefficient	
C_{WP}	water plane coefficient of ship	
d	ship draught	m
E_i	diffraction hydrodynamic force	kgs^{-2}
F_i	radiation hydrodynamic force	kgs^{-2}
F_n	Froude number	
f	shape function	

G	center of gravity or Green function	
GM	metacenter height	m
g	gravitational acceleration	ms^{-2}
H	Kochin function	
I	integer value of a gene (decoded binary string)	
$\Im$	imaginary part	
i_E	half angle of entrance of the waterline	degrees
k	fractional lever of second moment of half body about midships	
k_0	wave number at infinite depth water	m^{-1}
k_{yy}	pitch gyrational radius	m
L	ship lenght	m
m	length of gene (number of bits)	
$\boldsymbol{n}$	normal vector	m
O	origin of coordinate system	
OG	distance of center buoyancy to center of gravity	m
P	field point	
p	fractional length of parallel middle body of half body	
P_m	mutation probability	
P_c	crossover probability	
Q	source point	
R	real value of a gene	
r	random number between 0 and 1	
$\Re$	real part	
S	ship wetted surface area	m^2
U	ship forward speed	
x	transverse section	
$\overline{x}$	fractional lever of the second moment of half body about midships	
$\overline{z}$	fractional of LCB from midships of half body	
α	gene	
χ	incident wave angle	
δ_{ij}	Kronecker's delta	
λ	wavelength	m

∇	gradient operator (m^{-1}) or ship dispalcement (m^3)	
ω	angular frequency	$rads^{-1}$
Φ, ϕ, φ, ψ	velocity potential	m^2s^{-1}
ρ	water density	kgm^{-3}

Chapter 1

Introduction

1.1 Background

A ship is a dynamic floating body operated in an environment called ocean. In the ocean, rough weather may occur due to winds and waves. When a ship is moving on such weather, its resistance may increase, especially due to waves. Such inevitable condition may lead to involuntary reduction of ship speed and to perilous circumstance accordingly. Moreover a new regulation of the International Maritime Organization (IMO) regarding the energy efficiency for ships, especially the Energy Efficiency Design Index (EEDI) has come into force. It is definitely a mandatory for the new ships with 400 gross tonnages and above, in which the attained EEDI for those ships should be less than the required EEDI.

One way to lessen the attained EEDI of a ship is by decreasing its propulsion power, which may lead to reduction of its speed. To preserve the speed of a ship while lowering its propulsion power, an improvement of ship hull geometry should possibly be done to enhance its performance. Reducing an increase of resistance in waves, namely the added resistance of a ship will be a worthy choice to realize that.

A simple method to generate a new geometry of ships is by adopting the lines distortion approach in which the new lines are generated from the lines of a basis ship geometry as a parent by modifying some form parameters e.g. prismatic coefficient, block coefficient, longitudinal center of buoyancy, parallel middle body, etc. A former work exploiting this approach is the shifting method. In this method, the Sectional Area Curve (SAC) is distorted by shifting the longitudinal positions of each section in between the ships ends in such a way to modify the form parameters.

However it is recognized that generating the new ship geometry through the line distortion approach does not mean that the new ship geometry will have a better hydrodynamic performance than the original ones. To cope with this matter, an optimization method becomes necessary to acquire the best optimized ship geometry resulting from the line distortion approach. In general, there are two major categories of optimization methods; namely deterministic and stochastic optimization algorithms. However, the deterministic method is never user-friendly and thus the stochastic optimization algorithm, namely Evolutionary Algorithms (EAs) would be exploited to get the best optimized ship geometry in this study.

Among the EAs, the Genetic Algorithm (GA) is the most extended method representing the evolutionary tool based on natural selection. The GA searches for the best solution by involving its genetic operators such as selection, crossover and mutation operators, including elitism. This solution is obtained by means of encoding and decoding mechanisms. A common method for encoding, namely the binary encoding will be used further due to its simplicity and gives many possible solutions even with small disparity. It should be noted that the GA is a stochastic method, and thus slightly different results might be occurred for different runs.

In this dissertation an optimization method based on natural selection, namely the GA with binary encoding or so-called the Binary-Coded Genetic Algorithm (BCGA) is newly constructed by adopting the shifting technique to the SAC of a ship. In the optimization process, the shape function combined with Lagrangian interpolation is introduced for generating an innovative shape of this curve with optimized form parameters; hence increasing performance of a ship. Specifically, at least two parameters in the shape function are optimized to generate the new SAC. One parameter is used to define the magnitude of shape function whether to change the cross sectional area of each station or not, except those at ship ends and middle stations as well as at a fixed station which is defined by another parameter being optimized. The number of these parameters could be increased to generate more various shapes of SAC.

For the purpose of establishing a new BCGA and to examine its performance, a modified Wigley model with blunt-bow coefficients is employed as a basis ship geometry. The objective function used in this optimization is measured from the added resistance owing to ship motions. It will be computed by means of Enhanced Unified Theory (EUT) due to its superiority to the strip theory in that the effect of wave reflection mainly generated near the bow is taken into account through the body boundary condition in the diffraction problem as well as 3D and forward-speed effects ignored in the strip theory are incorporated in the EUT through the matching process.

In order to illustrate effectiveness and efficiency of the present method developed, an actual ship e.g. SR-108 is also employed as a basis ship geometry in addition to a modified Wigley model. In this case the objective function will be based on sensitivity study to the added resistance about its peak. According to the sensitivity study, it is found that both amplitude and phase of the pitch motion give the largest contribution to the peak value of the added resistance. The optimization of SR-108 therefore is extended with multi objective functions, namely the pitch motion component will be the primary fitness function followed by the total added resistance as the secondary fitness function. In addition, the steady wave-making resistance is also computed in order to confirm reduction of the total resistance of such ship.

1.2 Overview

This dissertation is concerned with the ship optimization of hydrodynamic problems. In this case, the optimization will be based on an existing ship as a basis ship geometry to comply with the regulation of IMO regarding the EEDI. The purpose of this regulation is to reduce the emission of the green house gasses from international shipping. It can be attained by improving ship performance which allows us to decrease the main engine power. Particularly, reducing the ship motions and thus minimizing the added resistance is addressed to this study.

The main objective of this study is to develop a computational algorithm, namely a practical integrated optimization method, to obtain an optimal ship geometry with high seakeeping performance. To achieve this objective, an optimization method based on natural selection with binary encoding, namely the BCGA is constructed with a modified Wigley model employed as a basis ship geometry. In this algorithm, the shape function followed by Lagrangian interpolation and the EUT for computing the added resistance are incorporated as subroutines in the main algorithm.

For the purpose of establishing this optimization method, an optimization is performed for two different cases based on the selected operational area of a ship. Namely, the shorter wavelengths ($\lambda/L = 0.30 \sim 0.80$) and longer wavelengths ($\lambda/L = 0.80 \sim 1.30$) regions are chosen. In this case the objective function is to minimize the total added resistance. In addition of optimizing a modified Wigley model, an actual ship SR-108 is also optimized at certain wavelengths region in which the added resistance becomes maximum. The steady wave resistance is also computed to confirm reduction of the total wave resistance.

Chapter 1 of this dissertation describes the introduction, including the background, overview and objectives of the study. In **Chapter 2**, the optimization method is given with the shape function of the SAC. Besides that, the computation method of the added resistance is also elucidated in this chapter. Description of the computed model is provided in **Chapter 3**. **Chapter 4** describes the sensitivity of the peak value of the added resistance to the ship motions. This chapter also discusses the relative importance of each term in the added resistance.

Before optimizing the SAC, it might be useful to understand its characteristics by the shifting method which is given in **Chapter 5**. In order to acquire the best perfromance of the GA, a preliminary and validation of its computation method should be done which is described in **Chapter 6**. The results and discussions of the optimization for both of modified Wigley model and actual ship SR-108 are also given in the same chapter. Finally, the conclusions and recommendations are given in **Chapter 7**.

Chapter 2

Theory of Computation

In the ship optimization problem, there must be an optimization method to obtain the best optimized ship geometry with an optimal performance according to the objective function. In this study, the Genetic Algorithm (GA) with binary encoding or so-called Binary Coded Genetic Algorithm (BCGA) and the Enhanced Unified Theory (EUT) based on the linear potential theory are combined together to optimize the basis ship geometry by computing the added resistance as the objective function. In order to understand these, the theoretical background and calculation methods of this optimization are going to be elucidated in this chapter.

2.1 Optimization Method

2.1.1 General Description of Binary-Coded Genetic Algorithm (BCGA)

In general there are two major classes of the optimization algorithms, namely deterministic and stochastic optimization algorithms. Deterministic algorithm is always having the same solution with the same number of the objective functions under the condition that the search space, starting-point, and termination condition are constant. Although the same solution is always obtained, the deterministic optimization algorithm is not user-friendly due to its complexity. Thus the stochastic optimization algorithm, namely the Evolutionary Algorithm (EA) should be exploited to get the best solution of a problem.

The EA is an attempt to solve problems by mimicking the process in natural evolution. The most extended and popular technique representing the application of this evolutionary theory is the Genetic Algorithm (GA). The GA is actually adaptive heuristic search algorithm based on natural selection and genetic to find the best solution of the problems. It is inspired by the theory of evolution, nameley survival of the fittest.

A set of initial possible solutions or so-called a population inside a certain domain called search space, is randomly generated in GA. A population contains a certain number of potential solutions, sometimes called individuals or chromosomes. A chromosome consists of some genes and it can be expressed as follows

$$C_i = (x_1, x_2, x_3, ..., x_j) \tag{2.1}$$

where x_j represents a gene with j-number of the i-th potential solution. A gene itself represents a special character of chromosome.

In GA, possible solutions from one population are taken and used to form a new population with the motivation that it will be better than the old population. Every individual in a population is assigned according to the fitness function, a measure of its goodness with respect to the problem under consideration. In another word, the value of the fitness function is regarded as the quantitative information to guide in searching the best individual of a population.

To put the GA working on any problems, it is necessary to define a method for encoding a chromosome. There are several kinds of method to encode a chromosome, for instance binary encoding, value encoding, permutation encoding, and tree encoding. In binary encoding, every chromosome is given in form of a string of bits. For value encoding, a chromosome is given as a sequence of some values. In permutation encoding, every chromosome is a string of numbers that represent a position in a sequence and thus it is usually used in ordering problems. In case of tree encoding, every chromosome is a tree of some objects, i.e. functions or commands in programming language.

Among those methods of encoding, the binary encoding is the most common one to encode a chromosome containing some characters on its genes. This is due to its simplicity to be used in any kind of problems. Nevertheless the binary encoding gives many possible solutions even with small disparity. In binary encoding a chromosome given in Eq.(2.1) can be expressed as, for example

$$C = (1101, 1111, 1010, 0110, 0010) \tag{2.2}$$

or simply given as

$$C = (1101\ 1111\ 1010\ 0110\ 0010) \tag{2.3}$$

From this chromosome, it could be understood that it consists of five genes and each gene is constituted with four bits.

After encoding, decoding takes place. Genes of a chromosome in form of binary strings are firstly converted to the integers or decoded binary strings of j-th gene with length

m by using the following formula

$$I_j = \sum_{k=0}^{m_j-1} 2^k S_k \tag{2.4}$$

where S is a bit of strings whether 0 or 1 and represented as $S_{m-1}, ...S_3, S_2, S_1, S_0$. These decoded binary strings are then converted to the real numbers by using the following transformation

$$R_j = R_j^L + \frac{(R_j^U - R_j^L)}{(2^{m_j} - 1)} \times I_j \tag{2.5}$$

with superscripts U and L denote upper and lower limits of the j-th gene. It should be noted here that in this study a term of gene is refer to a parameter being optimized. An example of using these transformations may be given with the first gene of chromosome in Eq.(2.3), i.e. *1101*. In this case we have 4-bits string ($m = 4$), thus its decoded binary string or integer value is equal to

$$I = 2^3 \times 1 + 2^2 \times 1 + 2^1 \times 0 + 2^0 \times 1 = 13$$

Knowing the value of upper and lower limits of this gene, for instance 0.0 and 1.0 respectively, the real value of it may be obtained easily using Eq.(2.5) as follows

$$R = 0 + \frac{(1.0 - 0.0)}{(2^4 - 1)} \times 13 = 0.86667$$

In GA the most important part is the genetic operators involving several operators, such as selection, crossover, and mutation operators including elitism. Its performance is extremely influenced by these operators.

Selection Operator

Selection in the genetic algorithm is the process of choosing parents for mating. Thus it can be said that the selection operator is a genetic operator that chooses a chromosome from the current population for inclusion in the next population. It is believed to be responsible for the convergence of the algorithm. Good individuals based on their fitness value will be selected to be parents for mating. There are several methods available for selection purpose such as

- *Roulette wheel*; A selection operator in which the chance of a chromosome getting selected is proportional to its rank or fitness. In this method, The wheel is spun N times, where N is the number of chromosomes in the population. On each spin, the chromosome under the wheels marker is selected to be in the pool of parents for the next population

- *Tournament*; A selection operator that provides selective pressure by holding a tournament competition among N chromosomes. The best chromosome from the tournament is the one with the highest fitness. It is then chosen as the selected individual for the next population.
- *Rank*; A selection operator which ranks the population and every chormosome receives fitness from the ranking. The worst chromosome has fitness 1 and the best has fitness N.
- *Boltzmann*; A selection operator that simulates the process of slow cooling of molten metal to achieve the minimum function value in a minimization problem of simulated annealing.
- *Top percent*; A selection operator that randomly selects a chromosome from the top N percent of the population as specified by the user.

Although there are some kinds of selection operator, the most commonly used for selection are only the first three operators. For faster convergence, the tournament selection is usually adopted because it selects the winner of a tournament. However it does not mean that the tournament selection is always better than the roulette wheel selection; it depends on the problem encountered.

Crossover Operator

In GA, crossover or reproduction is a genetic operator that mates two parent (old) chromosomes to produce offspring (new) chromosomes depending on the crossover probability (P_c). The idea behind crossover is that the new chromosome may be better than both of the parents if it takes the best characteristics from each of the parents. The main search tool of BCGA relies on this operator. Crossover occurs during evolution according to a user-definable crossover probability. Various crossover techniques can be given as follows

- *Single point*; A crossover operator that randomly selects one crossover point within a chromosome then interchanges the two parent chromosomes at this point to produce two new offspring chromosomes.
- *Two point*; A crossover operator that randomly selects two crossover points within a chromosome then interchanges the two parent chromosomes between these points to produce two new offspring chromosomes.
- *Multi-point (N-point)*; A crossover operator which randomly selects N-number crossover points within a chromosome then interchanges the two parent chromosomes between these points to produce two new offspring chromosomes.

- *Uniform*; A crossover operator that decides which parent will contribute to each of the gene values in the offspring chromosomes based on mixing ratio defined by user. This allows the parent chromosomes to be mixed at the gene level rather than the segment level (as with one and two point crossovers).

- *Heuristic*; A crossover operator that uses the fitness values of the two parent chromosomes to determine the direction of the search. The offspring are created according to the following equations

$$\left.\begin{aligned} Offspring1 &= BestParent + r \times (BestParent - WorstParent) \\ Offspring2 &= BestParent \end{aligned}\right\} \tag{2.6}$$

  where r denotes a random number between 0 and 1.

- *Arithmetic*; A crossover operator that linearly combines two parent chromosome vectors to produce two new offspring chromosomes according to the following equations:

$$\left.\begin{aligned} Offspring1 &= a \times Parent1 + (1 - a) \times Parent2 \\ Offspring2 &= (1 - a) \times Parent1 + a \times Parent2 \end{aligned}\right\} \tag{2.7}$$

  where a is a random weighting factor.

Because of simplicity, the most commonly used crossover operators are single point, N-point, and uniform crossovers.

Mutation Operator

After crossover is performed, mutation takes place. Mutation is a genetic operator that alters one or more gene values in a chromosome from its initial state based on the mutation probability (P_m). This probability should usually be set fairly low (0.01 is a good first choice). If it is set to high, the search will turn into a primitive random search. According to its definition, the main purpose of mutation is to prevent premature convergence or stagnating at any local optima by ensuring population diversity. As the same with selection and crossover operators, the mutation operator also has various kinds given as follows

- *Flip bit*; A mutation operator that simply inverts the value of the chosen gene (0 goes to 1 and 1 goes to 0).

- *Boundary*; A mutation operator that replaces the value of the chosen gene with either the upper or lower bound for that gene (chosen randomly).

- *Uniform*; A mutation operator that replaces the value of the chosen gene with a uniform random value selected between the user-specified upper and lower bounds for that gene. This mutation operator can only be used for integer and float genes.
- *Non-uniform*; A mutation operator that increases the probability that the amount of the mutation will be close to 0 as the generation number increases. This mutation operator keeps the population from stagnating in the early stages of the evolution then allows the genetic algorithm to tune the solution in the later stages of evolution.
- *Gaussian*; A mutation operator that adds a unit Gaussian distributed random value to the chosen gene. The new gene value is clipped if it falls outside of the user-specified lower or upper bounds for that gene.

The first operator is specially used for binary genes and the remaining operators can only be used for integer and float genes. Because in this study the binary encoding is adopted, thus the only available operator for mutation is flip bit operator.

Elitism

In order to keep the highest fitness chromosome in the new population, elitism must be involved. This is because, by elitism the best chromosome in the previous population is always included in the new population and it will be selected directly to be parent if the best chromosome in the current population has lower fitness than the one in the previous population. Performance of the BCGA is improved significantly by this operator.

Generally, the optimization-flow process involving all of such operators can be seen in Fig. 2.1. The optimization is begun with the basis ship geometry followed by creating an initial population at the first generation. Here some individuals or chromosomes which consist of some genes are randomly generated in form of binary strings as given in Eq.(2.2) or Eq.(2.3). These chromosomes are firstly decoded to the integers by using Eq.(2.4) and then transformed to the real-valued parameters by transformation given in Eq.(2.5). The process is then followed by generating various shapes of Sectional Area Curve (SAC) by the shape function. It should be noted here again that each gene represents a parameter being optimized in the shape function.

Once the new sectional area curves have been obtained through the shape function together with Lagrangian interpolation to get the new station positions, the Enhanced Unified Theory (EUT) is then used to find their fitness. Based on their fitness, then the selection is performed, followed by crossover and mutation respectively as well as elitism if necessary to obtain the new individuals which will be used to replace all individuals

of a population in the former generation. This process will be repeated until the result converges at a certain number of generations.

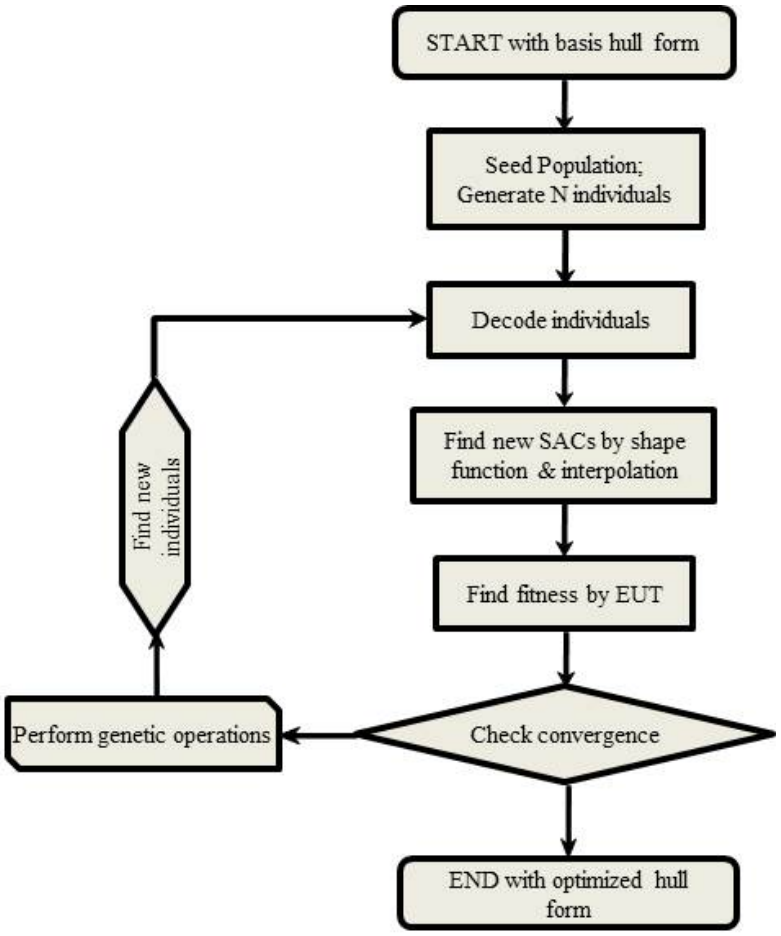

FIGURE 2.1: Flow process of BCGA

It should be kept in mind that a slightly different result for the same problem from one run to another might be obtained as the BCGA is a stochastic method. Further details of GA and its operators might be found in, for example Coley [4], Sivandam and Deepa [5], and Chakraborty [6].

2.1.2 Lines Distortion Approach

Because the shape function is based on the shifting method, it is necessary to explain about this method in obtaining the new ship hull geometry. A simple approach to obtain the ship hull geometry derived from a basis hull is by distorting the Sectional Area Curve (SAC) of the basis hull. In this case the alternative designs are derived with the same principal dimensions but different form coefficients i.e. the block coefficient (C_B), prismatic coefficient (C_P), and longitudinal center of buoyancy (L_{CB}). These can be made by moving aft or forward the shape of sections along the ship's longitudinal

axis (x-axis) in an appropriate way and hence distorts SAC. Therefore by the Lackenby [3] transformation, the block coefficient through prismatic coefficient can be varied independently for the aft- and fore-bodies using the following formulae

$$\delta C_{Pa} = \frac{2[\delta C_{Pt}(B_f - \overline{z}) - \delta\overline{z}(C_{Pt} + \delta C_{Pt})] - C_f\delta p_f + C_a\delta p_a}{(B_f + B_a)} \tag{2.8}$$

$$\delta C_{Pf} = \frac{2[\delta C_{Pt}(B_f + \overline{z}) + \delta\overline{z}(C_{Pt} + \delta C_{Pt})] + C_f\delta p_f - C_a\delta p_a}{(B_f + B_a)} \tag{2.9}$$

Here subscripts a and f denote quantities of the aft- and fore-bodies, respectively. These are subject to the practical limits

$$\delta C_P = \frac{\delta p(1 - C_P) \pm \frac{1}{2}A\left(1 - \frac{\delta p}{1-p}\right)}{1 - p} \tag{2.10}$$

where C_P is the total prismatic coefficient of the basis hull and δC_P the required change in the total prismatic coefficient. $\overline{z}$ means the distance of L_{CB} in the basis hull form from midship expressed as a fraction of the half-length and $\delta\overline{z}$ the required shift of L_{CB} in the derived form. p and δp denote the fractional length of parallel middle body and the required change in the parallel middle body of the half-body, respectively. The position of L_{CB} can be shifted independently by changing the value of $\delta\overline{z}$ and the parallel middle body can be introduced by altering the value of δp which has the following practical limits

$$\delta p = \frac{1 - p}{1 \pm \frac{2(1-C_P)(1-p)}{A}} \tag{2.11}$$

Therefore the general relation between the fractional distance of any transverse section (x) from midship and the necessary shift (δx) in the x-axis can be obtained as follows

$$\delta x = (1 - x)\left\{\frac{\delta p}{1 - p} + \frac{(x - p)}{A}\left[\delta C_P - \delta p\left(\frac{1 - C_P}{1 - p}\right)\right]\right\} \tag{2.12}$$

In Eq.(2.8) to Eq.(2.12) A, B and C are constants depending only on the geometrical properties of the basis hull and can be computed by the following equations

$$\left.\begin{aligned} A &= C_P(1 - 2\overline{x}) - p(1 - C_P) \\ B &= \frac{C_P[2\overline{x} - 3k^2 - p(1 - 2\overline{x})}{A} \\ C &= \frac{B(1 - C_P) - C_P(1 - 2\overline{x})}{1 - p} \end{aligned}\right\} \tag{2.13}$$

Here $\overline{x}$ and k stand for the fractional distance (lever) of the first moment and the second moment of the half-body about midship.

2.1.3 Shape Function

During optimization, the shape function based on principle of the shifting method is introduced for generating various shapes of SAC. Specifically, some parameters in the shape function are optimized to generate the new SAC. One or more parameters are used to define the magnitude of shape function to change the cross sectional area of each station except those at ship ends and a station with the largest transverse area (usually midship) as well as at a fixed station defined by another parameters which are also to be optimized.

The shape function was firstly introduced by Kim H. et al. [7] with two parameters for optimizing only the fore body. However this function is extended in this study with several parameters for optimizing the whole body of a ship as given in Eq.(2.14), for instance with six parameters

$$
\begin{aligned}
&A_n(x) = A_0(x) + f(x) \\
&f(x) = \left\{ \begin{array}{ll}
\alpha_3 \left[0.5 \left(1 - \cos 2\pi \dfrac{x - x_1}{\alpha_1 - x_1} \right) \right]^{1/2} & , x_1 \le x \le \alpha_1 \\
\alpha_4 \left[0.5 \left(1 - \cos 2\pi \dfrac{x - \alpha_1}{\alpha_1 - x_2} \right) \right]^{1/2} & , \alpha_1 \le x \le x_2 \\
\alpha_5 \left[0.5 \left(1 - \cos 2\pi \dfrac{x - x_2}{\alpha_2 - x_2} \right) \right]^{1/2} & , x_2 \le x \le \alpha_2 \\
\alpha_6 \left[0.5 \left(1 - \cos 2\pi \dfrac{x - \alpha_2}{\alpha_2 - x_3} \right) \right]^{1/2} & , \alpha_2 \le x \le x_3
\end{array} \right\}
\end{aligned}
\tag{2.14}
$$

where $A_0(x)$ and $f(x)$ denote the original SAC and the shape function, respectively. α_3 to α_6 are the parameters used to determine the slope of SAC or magnitude of the shape function, α_1 and α_2 the parameters to control the location of fixed stations as shown in Fig. 2.2.

Specifically three among them will optimize SAC of the aft-body, with two parameters determining the slope of SAC and the remainder controlling the location of a fixed station. Another three parameters of total six parameters will optimize SAC of the fore-body with the same formation as for the aft-body. All parameters in the shape function are determined during optimization. The number of parameters can be varied to get more various shapes of SAC. Because the whole body of a ship is optimized, then the fixed stations x_1, x_2, and x_3 will be the position of the aft-end, middle (largest transverse area), and fore-end stations, respectively.

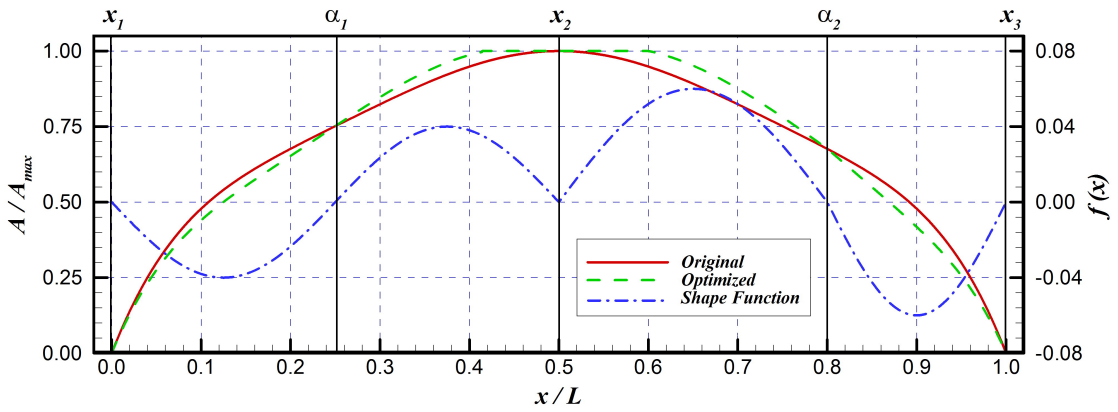

FIGURE 2.2: SAC and shape function

2.1.4 Fitness Function

In the optimization process, the objective function should be defined first whether to maximize or minimize the function. In this case the objective function is taken to minimize the added resistance. In order to understand the performance of an optimization process, it is necessary to define the fitness function or the so-called Performance Index (PI) of an individual as shown in Fig. 2.3.

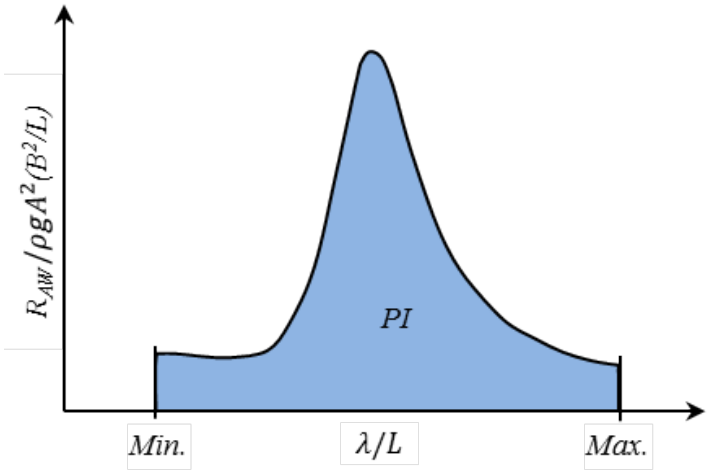

FIGURE 2.3: Performance Index (PI)

According to Fig. 2.3, the PI is defined as the area beneath the added resistance curve. It should be noted that PI itself is readily obtained by computing the blue area using a numerical integration method. Because the objective function is to minimize the added resistance, the lower a value of the PI implies the higher performance of a ship in term of the added resistance. Needless to say, the minimum and maximum wavelength ratios in Fig. 2.3 are determined according to area in which a ship being optimized will be

operated.

2.2 Theory of Water Waves

2.2.1 Governing Equations for an Inviscid Fluid

The governing equations are derived from the conservation of mass and the conservation of momentum. By defining a fluid volume under consideration as $V(t)$ and denoting the fluid density as ρ, the conservation of mass can be written in the form

$$\frac{d}{dt}\iiint_{V(t)} \rho \, dV = 0 \tag{2.15}$$

Regarding the conservation of momentum, by neglecting the viscous shear stress and considering only the normal pressure force and the gravity force, we can obtain the following relation

$$\frac{d}{dt}\iiint_{V(t)} \rho u_i \, dV = -\iint_{S(t)} p n_i \, dS + \iiint_{V(t)} \rho g \delta_{i3} \, dV \tag{2.16}$$

where S is the surface of the fluid volume and p is the pressure acting on the surface with n_i the i-th component (i=1,2,3) of the unit normal vector pointing out of fluid volume, u_i is the i-th component of the velocity vector, g and δ_{i3} denote the gravity acceleration and the Kronecker's delta, equal to 1 only for $i = 3$.

For the left-hand sides of Eqs.(2.15) and (2.16), we can apply the transport theorem [8] written in the form

$$\frac{d}{dt}\iiint_{V(t)} F_i \, dV = \iiint_{V} \frac{\partial F_i}{\partial t} \, dV + \iint_{S} F_i u_n \, dS \tag{2.17}$$

where F_i denotes the i-th component of a vector quantity or can be simply a scalar quantity.

Utilizing Gauss' theorem with understanding of $u_n = u_j n_j$, the surface integral in Eq.(2.17) can be transformed into volume integral and hence Eq.(2.15) can be expressed as

$$\frac{d}{dt}\iiint_{V} \rho \, dV = \iiint_{V} \left[\frac{\partial \rho}{\partial t} + \frac{\partial}{\partial x_j}(\rho u_j)\right] \, dV = 0 \tag{2.18}$$

Since this volume can be composed of an arbitrary group of fluid particles, the integrand itself must be equal to zero for the entire fluid. Thus the conservation of mass gives the

following continuity equation

$$\frac{\partial \rho}{\partial t} + \frac{\partial}{\partial x_j}(\rho u_j) = 0 \tag{2.19}$$

For an incompressible fluid, the density is constant, and thus the continuity equation can be given as

$$\frac{\partial u_j}{\partial x_j} = 0 \quad \text{or} \quad \nabla \cdot \boldsymbol{u} = 0 \tag{2.20}$$

Similar to the continuity equation, by applying the transport theorem as well as Gauss' theorem to the conservation of momentum, it follows that

$$\iiint_V \left[\frac{\partial}{\partial t}(\rho u_i) + \frac{\partial}{\partial x_j}(\rho u_i u_j) \right] dV = \iiint_V \left[-\frac{\partial \rho}{\partial x_i} + \rho g \delta_{i3} \right] dV \tag{2.21}$$

It is noted again that the fluid volume in question is arbitrary; hence Eq.(2.21) must hold for integrands alone. For an incompressible fluid with constant density, we can finally obtain Euler's equations in the form

$$\frac{\partial u_i}{\partial t} + u_j \frac{\partial u_i}{\partial x_j} = -\frac{1}{\rho}\frac{\partial p}{\partial x_i} + g\delta_{i3} \tag{2.22}$$

where the continuity equation Eq.(2.20) has been invoked. Equations (2.20) and (2.22) are the governing equations for an incompressible inviscid fluid.

2.2.2 Potential Flow and Velocity Potential

In most problems related to water waves, we may assume that the motion of fluid is irrotational; that is $\nabla \times \boldsymbol{u} = 0$. On the other hand, in the vector analysis, an identity of $\nabla \times \nabla \Phi = 0$ holds for an arbitrary scalar function $\Phi(\boldsymbol{x}, t)$. Combining these, we can see that velocity vector can be represented as $\boldsymbol{u} = \nabla \Phi$ in terms of scalar function which is known as the velocity potential. The flows than can be described with the velocity potential are referred to as the potential flows.

If $\boldsymbol{u} = \nabla \Phi$ is substituted in the continuity equation Eq.(2.20), it follows that

$$\frac{\partial^2 \Phi}{\partial x_j^2} = 0 \quad \text{or} \quad \nabla^2 \Phi = 0 \tag{2.23}$$

This is known as the Laplace equation and the governing equation to be solved for potential flows.

Next we consider how Euler's equations Eq.(2.22) can be transformed for the potential flow. For the case of irrotational fluid motion expressed by $\nabla \times \boldsymbol{u} = 0$, the advection

term on the left-hand side of Eq.(2.22) can be written as

$$u_j \frac{\partial u_i}{\partial x_j} = \frac{1}{2} \frac{\partial}{\partial x_i} (\nabla \Phi \cdot \nabla \Phi) \tag{2.24}$$

Therefore, by substituting $u_i = \nabla \Phi$ in Eq.(2.22), it follows that

$$\frac{\partial}{\partial x_i} \left(\frac{\partial \Phi}{\partial t} + \frac{1}{2} \nabla \Phi \cdot \nabla \Phi + \frac{p}{\rho} - gz \right) = 0 \tag{2.25}$$

and then the following equation known as Bernoulli's pressure equation can readily be obtained:

$$p - p_c = -\rho \left(\frac{\partial \Phi}{\partial t} + \frac{1}{2} \nabla \Phi \cdot \nabla \Phi - gz \right) \tag{2.26}$$

where p_c is a constant, which can be taken equal to the atmospheric pressure p_a for the case of zero forward speed and equal to $p_a + \frac{1}{2}\rho U^2$ when considered with a reference frame moving at constant speed U.

2.2.3 Boundary Conditions

In order to solve the Laplace equation, appropriate boundary conditions must be imposed on the boundaries of the fluid domain concerned. To describe those boundary conditions explicitly, we write the velocity potential as follows:

$$\Phi(\boldsymbol{x}, t) = U[\Phi_D(\boldsymbol{x}) + \phi_s(\boldsymbol{x})] + \Phi_U(\boldsymbol{x}, t) \tag{2.27}$$

$$\Phi_U(\boldsymbol{x}, t) = \Re \left[\phi(\boldsymbol{x}) e^{i\omega t} \right] \tag{2.28}$$

where Φ_D represents the steady basis flow, normally taken as the double-body flow or simply the uniform flow equal to $-x$ for the so-called Neumann-Kelvin problem. $\phi_s(\boldsymbol{x})$ denotes the steady disturbance term associated with steady waves. The unsteady velocity potential is assumed to be time-harmonic with encounter circular frequency ω, and we will consider the spatial part $\phi(\boldsymbol{x})$, with the time-dependent term $e^{i\omega t}$ factored out as in Eq.(2.28). With these expressions, first from Eq.(2.26) the pressure can be written in a decomposed form as follows:

$$P(\boldsymbol{x}, t) = \rho g z + P_S(\boldsymbol{x}) + P_U(\boldsymbol{x}, t) \tag{2.29}$$

where

$$\begin{aligned} P_S &= \frac{1}{2}\rho U^2\,(1 - \boldsymbol{V}\cdot\boldsymbol{V}) \\ &= \frac{1}{2}\rho U^2\,(1 - \nabla\Phi_D\cdot\nabla\Phi_D - 2\nabla\Phi_D\cdot\nabla\phi_s) + O(\phi_s^2) \end{aligned} \tag{2.30}$$

$$\begin{aligned} P_U &= -\rho\left(\frac{\partial}{\partial t} + U\,\boldsymbol{V}\cdot\nabla\right)\Phi_U - \frac{1}{2}\nabla\Phi_U\cdot\nabla\Phi_U \\ &= -\rho\left(\frac{\partial}{\partial t} + U\nabla\Phi_D\cdot\nabla\right)\Phi_U + O(\phi_s\Phi_U, {\Phi_U}^2) \end{aligned} \tag{2.31}$$

and $\boldsymbol{V} = \nabla(\Phi_D + \phi_s)$. In Eqs.(2.30) and (2.31), higher-order terms in ϕ_s and Φ_U are neglected. By substituting Eq.(2.28) in Eq.(2.31), the linearized unsteady pressure can be written in the form

$$\left.\begin{aligned} P_U(\boldsymbol{x},t) &= \Re\left[p(\boldsymbol{x})e^{i\omega t}\right] \\ p &= -\rho(i\omega + U\nabla\Phi_D\cdot\nabla)\phi \end{aligned}\right\} \tag{2.32}$$

Although the free-surface boundary condition can be derived by combining the kinematic and dynamic conditions, a more expedient approach is to consider the substantial derivative of the pressure equal to zero on the free surface. Namely

$$\left(\frac{\partial}{\partial t} + \nabla\Phi\cdot\nabla\right)[\rho g z + P_S(\boldsymbol{x}) + P_U(\boldsymbol{x},t)] = 0 \quad \text{on } z = \zeta \tag{2.33}$$

where $z = \zeta(x,y,t)$ denotes the wave elevation on the free surface.

Substituting Eq.(2.27) for Φ and Eqs.(2.30) and (2.32) for P_S and P_U respectively and ignoring higher-order terms in ϕ_s and ϕ as in obtaining Eqs.(2.30) and (2.31), the linearized free-surface boundary conditions for the steady and unsteady velocity potentials can be obtained. Those results may be expressed as follows:

$$\begin{aligned} &\frac{U^2}{2}\nabla\Phi_D\cdot\nabla(\nabla\Phi_D\cdot\nabla\Phi_D) + U^2\nabla\Phi_D\cdot\nabla(\nabla\Phi_D\cdot\nabla\phi_s) \\ &+\frac{U^2}{2}\nabla(\nabla\Phi_D\cdot\nabla\Phi_D)\cdot\nabla\phi_s - g\frac{\partial\phi_s}{\partial z} \quad \text{on } z = 0 \end{aligned} \tag{2.34}$$

$$\begin{aligned} &-\omega^2\phi + 2iU\omega\nabla\Phi_D\cdot\nabla\phi + U^2\nabla\Phi_D\cdot\nabla(\Phi_D\cdot\nabla\phi) \\ &+\frac{U^2}{2}\nabla(\nabla\Phi_D\cdot\nabla\Phi_D)\cdot\nabla\phi + U\nabla^2\Phi_D(i\omega + U\nabla\Phi_D\cdot\nabla)\phi - g\frac{\partial\phi}{\partial z} = 0 \quad \text{on } z = 0 \end{aligned} \tag{2.35}$$

In these boundary conditions, if only the uniform flow is considered as the steady basis flow ($\Phi_D = -x$), we can approximate as

$$\nabla \Phi_D = -\boldsymbol{e}_1 \tag{2.36}$$

where $\boldsymbol{e}_1$ denotes the unit vector along the x-axis. In this case (Neumann-Kelvin approximation), Eqs.(2.34) and (2.35) take the following forms

$$U^2 \frac{\partial^2 \phi_s}{\partial x^2} - g \frac{\partial \phi_s}{\partial z} = 0 \qquad \text{on } z = 0 \tag{2.37}$$

$$\left(i\omega - U \frac{\partial}{\partial x} \right)^2 \phi - g \frac{\partial \phi}{\partial z} = 0 \quad \text{on } z = 0 \tag{2.38}$$

Next we consider the boundary condition on the hull surface of a ship, which may be obtained also by considering the substantial derivative of the ship's hull surface equal to zero. In terms of the body-fixed coordinate system $\overline{\boldsymbol{x}} = (\overline{x}, \overline{y}, \overline{z})$, the ship's hull surface is supposed to be expressed as $F(\overline{\boldsymbol{x}}) = 0$. Then, by noting that substantial derivative should be performed with respect to the space-fixed coordinate system $\boldsymbol{x} = (x, y, z)$, the following relation holds

$$\begin{aligned} \left(\frac{\partial}{\partial t} + \nabla \Phi(\boldsymbol{x}, t) \cdot \nabla \right) F(\overline{\boldsymbol{x}}) \quad &= \quad \overline{\nabla} F \cdot \frac{\partial \overline{\boldsymbol{x}}}{\partial t} + \nabla \Phi(\boldsymbol{x}, t) \left\{ \left(\overline{\nabla} F \cdot \frac{\partial \overline{\boldsymbol{x}}}{\partial x} \right) \boldsymbol{e}_1 \right. \\ &\left. + \left(\overline{\nabla} F \cdot \frac{\partial \overline{\boldsymbol{x}}}{\partial y} \right) \boldsymbol{e}_2 + \left(\overline{\nabla} F \cdot \frac{\partial \overline{\boldsymbol{x}}}{\partial z} \right) \boldsymbol{e}_3 \right\} = 0 \end{aligned} \tag{2.39}$$

Here, $\overline{\nabla}$ denotes the differential operator with respect to the body-fixed coordinate system. With the assumption of small amplitude of unsteady ship motions, the relation between $\boldsymbol{x}$ and $\overline{\boldsymbol{x}}$ is given by

$$\boldsymbol{x} = \overline{\boldsymbol{x}} + \boldsymbol{\alpha}(t) \tag{2.40}$$

$$\boldsymbol{\alpha}(t) = \boldsymbol{\alpha}_T(t) + \boldsymbol{\alpha}_R(t) \times \overline{\boldsymbol{x}}, \quad \boldsymbol{\alpha}_T(t) = \sum_{j=1}^{3} \xi_j(t) \boldsymbol{e}_j, \quad \boldsymbol{\alpha}_R(t) = \sum_{j=1}^{3} \xi_{j+3}(t) \boldsymbol{e}_j \tag{2.41}$$

where $\xi_j(t)$ is the displacement in the j-th mode of ship motions, defined as surge, sway, heave for $j = 1, 2, 3$, and roll, pitch, yaw for $j = 4, 5, 6$, respectively.

Dividing Eq.(2.39) by $|\overline{\nabla} F|$ and noting the definition of the normal vector as $\overline{\boldsymbol{n}} = \overline{\nabla} F / |\overline{\nabla} F|$, we have from Eqs.(2.39) and (2.40) the following:

$$\nabla \Phi(\boldsymbol{x}, t) \cdot \overline{\boldsymbol{n}} = \dot{\boldsymbol{\alpha}}(t) \cdot \overline{\boldsymbol{n}} + [(\nabla \Phi(\boldsymbol{x}, t) \cdot \nabla) \boldsymbol{\alpha}(t)] \cdot \overline{\boldsymbol{n}} \tag{2.42}$$

To consider effects of the difference between $\boldsymbol{x}$ and $\overline{\boldsymbol{x}}$, the Taylor-series expansion should be applied to $\nabla\Phi(\boldsymbol{x},t)$ and the result can be written as

$$\begin{aligned}\nabla\Phi(\boldsymbol{x},t) &= U\,\boldsymbol{V}(\boldsymbol{x}) + \nabla\Phi_U(\boldsymbol{x},t) \\ &= U\,\boldsymbol{V}(\overline{\boldsymbol{x}}) + \nabla\Phi_U(\overline{\boldsymbol{x}},t) \\ &\quad +(\boldsymbol{\alpha}(t)\cdot\nabla)\left[U\,\boldsymbol{V}(\overline{\boldsymbol{x}}) + \nabla\Phi_U(\overline{\boldsymbol{x}},t)\right] + O(\boldsymbol{\alpha}^2)\end{aligned} \tag{2.43}$$

Then, substituting Eq.(2.43) in Eq.(2.42), separating into steady and unsteady terms, we can have the linearized body boundary conditions as follows

$$\boldsymbol{V}\cdot\boldsymbol{n} = \frac{\partial\Phi_D}{\partial n} + \frac{\partial\phi_s}{\partial n} = 0 \quad \text{on} \quad S_H \tag{2.44}$$

$$\nabla\Phi_U\cdot\boldsymbol{n} = \frac{\partial\Phi_U}{\partial n} = \dot{\boldsymbol{\alpha}}(t)\cdot\boldsymbol{n} + U\left[(\boldsymbol{V}\cdot\nabla)\boldsymbol{\alpha}(t) - (\boldsymbol{\alpha}(t)\cdot\nabla)\,\boldsymbol{V}\right]\cdot\boldsymbol{n} \quad \text{on} \quad S_H \tag{2.45}$$

Here S_H denotes the wetted part of hull surface of a ship, and we note that $\overline{\boldsymbol{x}}$ and $\overline{\boldsymbol{n}}$ are replaced with $\boldsymbol{x}$ and $\boldsymbol{n}$, because the effect of difference between these can be regarded as higher order and hence neglected.

Assuming time-harmonic motion, we write the unsteady displacement in the j-th mode of motion in the form

$$\xi_j(t) = \Re\left[X_j e^{i\omega t}\right] \tag{2.46}$$

where X_j is the complex amplitude. Then we can show that Eq.(2.45) can be recast in the following form

$$\frac{\partial\phi}{\partial n} = i\omega\sum_{j=1}^{6} X_j\left(n_j + \frac{U}{i\omega}m_j\right) \tag{2.47}$$

where

$$\left.\begin{aligned}(n_1,n_2,n_3) = \boldsymbol{n}, \quad (n_4,n_5,n_6) = \boldsymbol{x}\times\boldsymbol{n} \\ (m_1,m_2,m_3) = -(\boldsymbol{n}\cdot\nabla)\,\boldsymbol{V} \equiv \boldsymbol{m} \\ (m_4,m_5,m_6) = -(\boldsymbol{n}\cdot\nabla)(\boldsymbol{x}\times\boldsymbol{V}) = \boldsymbol{V}\times\boldsymbol{n} + \boldsymbol{x}\times\boldsymbol{m}\end{aligned}\right\} \tag{2.48}$$

In these body boundary conditions, if the steady basis flow is approximated with uniform flow, $\Phi_D = -x$ and thus $\boldsymbol{V} = (-1,0,0)$. Therefore Eq.(2.44) and Eq.(2.48) reduce to

$$\frac{\partial\phi_s}{\partial n} = n_1 \quad \text{on} \quad S_H \tag{2.49}$$

$$\left.\begin{aligned}(m_1,m_2,m_3) = (0,0,0) \\ (m_4,m_5,m_6) = (0,n_3,-n_2)\end{aligned}\right\} \tag{2.50}$$

Last, the radiation condition must also be imposed at a distance from the ship. This condition is physically rather complicated especially when the ship has both forward speed and harmonic oscillation. Nevertheless, mathematically, it is known that introducing the Rayleigh's artificial viscosity coefficient (denoted as μ) into the free-surface condition ensures the satisfaction of the radiation condition. Taking account of this technique, for instance, the Neumann-Kelvin type free-surface conditions, Eqs.(2.37) and (2.38), should be modified as follows:

$$U^2\frac{\partial^2\phi_s}{\partial x^2} - g\frac{\partial\phi_s}{\partial z} - \mu U\frac{\partial\phi_s}{\partial x} = 0 \qquad \text{on } z = 0 \tag{2.51}$$

$$\left(i\omega - U\frac{\partial}{\partial x}\right)^2\phi - g\frac{\partial\phi}{\partial z} + \mu\left(i\omega - U\frac{\partial}{\partial x}\right)\phi = 0 \qquad \text{on } z = 0 \tag{2.52}$$

This Rayleigh's artificial viscosity coefficient μ is supposed to be very small. Thus once a solution satisfying the radiation condition has been obtained, we may set μ equal to zero.

2.2.4 Principle of Energy Conservation

We are going to describe the principle of energy conservation which will also be used in deriving a formula of the added resistance. The conservation of energy is a fundamental concept in physics along with the conservation of mass and the conservation of momentum. In general mechanics, the total energy in the fluid is the sum of kinetic and potential energies. Mathematically it is expressed as

$$E = E_k + E_p \tag{2.53}$$

In a prescribed volume V, it is given by a volume integral

$$E = \rho\iiint_V\left(\frac{1}{2}\boldsymbol{u}^2 - gz\right)\,dV = \rho\iiint_V\left(\frac{1}{2}\nabla\Phi\cdot\nabla\Phi - gz\right)\,dV \tag{2.54}$$

where the z-axis is positive downward. Utilizing the transport theorem Eq.(2.17), the rate-of-change with respect to time of the total energy can be written as

$$\frac{dE}{dt} = \rho\iiint_V\frac{\partial}{\partial t}\left(\frac{1}{2}\nabla\Phi\cdot\nabla\Phi - gz\right)\,dV + \rho\iint_S\left(\frac{1}{2}\nabla\Phi\cdot\nabla\Phi - gz\right)u_n\,dS \tag{2.55}$$

Firstly, let us consider the integrand of the volume integral. The only contribution to this integral is from kinetic energy term which takes the form

$$\frac{\partial}{\partial t}\left(\frac{1}{2}\nabla\Phi\cdot\nabla\Phi\right)=\nabla\Phi\cdot\nabla\frac{\partial\Phi}{\partial t}=\nabla\cdot\left(\frac{\partial\Phi}{\partial t}\nabla\Phi\right) \tag{2.56}$$

Meanwhile the integrand in the second term of the right-hand side of Eq.(2.55), from Bernoulli's equation, can be given as

$$\frac{1}{2}\nabla\Phi\cdot\nabla\Phi-gz=-\left(\frac{p-p_a}{\rho}+\frac{\partial\Phi}{\partial t}\right) \tag{2.57}$$

Substituting these into Eq.(2.55), then we have

$$\frac{dE}{dt}=\rho\iiint_V\nabla\cdot\left(\frac{\partial\Phi}{\partial t}\nabla\Phi\right)\,dV-\rho\iint_S\left(\frac{p-p_a}{\rho}+\frac{\partial\Phi}{\partial t}\right)u_n\,dS \tag{2.58}$$

Lastly, by applying Gauss' theorem, the first term of the right-hand of side of Eq.(2.58) can be written as the surface integral and thus it becomes

$$\frac{dE}{dt}=\rho\iint_S\left[\frac{\partial\Phi}{\partial t}\frac{\partial\Phi}{\partial n}-\left(\frac{p-p_a}{\rho}+\frac{\partial\Phi}{\partial t}\right)u_n\right]\,dS \tag{2.59}$$

Further details about the theory of water waves in marine hydrodynamics, the reader should refer to Newman [8] and Kashiwagi [9].

2.3 Theory of the Added Resistance in Waves

2.3.1 Far-Field Asymptotic Form of the Velocity Potential

Let us introduce the velocity potential at large distance from the ship with considering a ship advancing at constant forward speed U into a plane progressive wave of amplitude A, circular frequency ω_0 and wavenumber k_0 at infinite water depth as shown in Fig. 2.4. Due to the incident wave with angle χ, the ship undergoes oscillatory motions about its mean position with the encounter frequency $\omega=\omega_0-k_0U\cos\chi$.

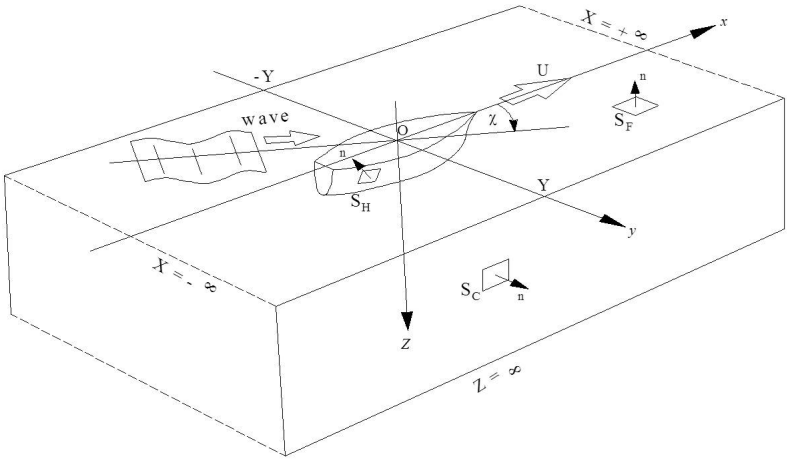

FIGURE 2.4: Coordinate system and notations

Therefore under the assumption that the fluid is inviscid and irrotational as well as the amplitude of incident wave and ship's oscillation to be small, the total velocity potential can then be written as

$$\Phi_T(x,y,z,t) = U[\Phi_D(x,y,z,t) + \phi_s(x,y,z)] + \Phi(x,y,z,t) \tag{2.60}$$

$$\Phi(x,y,z,t) = \Re[\phi(x,y,z)e^{i\omega t}] \tag{2.61}$$

where Φ_D represents the steady basis flow and in what follows for analysing the unsteady problems, the uniform flow is assumed as the basis flow; in this case $\Phi_D = -x$. U is the constant forward speed of a ship in the x-axis, ϕ_s denotes the steady disturbance potential due to steady translation of a ship in otherwise calm water. Φ is the unsteady component due to ship motions in waves given in Eq.(2.61) with $\Re$ denoting the real part is to be taken. This component consists of the diffraction and radiation potentials which can be written in the form

$$\phi(x,y,z) = \frac{gA}{i\omega_0}(\varphi_0 + \varphi) \tag{2.62}$$

where

$$\varphi_0 = e^{-k_0 z - ik_0(x\cos\chi + y\sin\chi)} \tag{2.63}$$

$$\varphi = \varphi_7 - \frac{\omega\omega_0}{g}\sum_{j=1}^{6}\frac{X_j}{A}\varphi_j \tag{2.64}$$

are the incident-wave potential and the ship-generated disturbance potential, respectively. The first term in Eq.(2.64) is the scattering wave potential (φ_7) and φ_j in the last term is the radiation potential due to ship oscillation in all six degrees of freedom

$(j = 1 \sim 6)$ with complex amplitude X_j in the j-th mode of motion. These velocity potentials must satisfy the following equations

$$[L] \qquad \nabla^2\phi = 0 \tag{2.65}$$

$$[F] \qquad \left(i\omega - U\frac{\partial}{\partial x}\right)^2 \phi - g\frac{\partial\phi}{\partial z} = 0, \quad \text{on } z = 0 \tag{2.66}$$

$$[B] \qquad \frac{\partial\phi}{\partial z} = 0, \quad \text{at } z \to \infty \tag{2.67}$$

$$[H] \qquad \frac{\partial\phi}{\partial n} = i\omega \sum_{j=1}^{6} X_j \left(n_j + \frac{U}{i\omega} m_j\right), \quad \text{on } S_H \tag{2.68}$$

where n_j and m_j are already defined in Eq.(2.48).

Applying the Green's theorem, the disturbance velocity potential satisfying the radiation condition in addition to Eqs.(2.65) $\sim$ (2.68) can take the form

$$\varphi(P) = \iint_{S_H} \left(\frac{\partial\varphi(Q)}{\partial n_Q} - \varphi(Q)\frac{\partial}{\partial n_Q}\right) G(P;Q)\; dS(Q) \tag{2.69}$$

where $P = (x, y, z)$ is the field point and $Q = (\xi, \eta, \zeta)$ is the integration point along the ship's wetted hull. With the Fourier transform technique, the Green function G appropriate for the present problem can be obtained as

$$\begin{aligned} G(P,Q) \;=\; & -\frac{1}{4\pi}\left(\frac{1}{r} - \frac{1}{r'}\right) \\ & -\frac{1}{2\pi}\int_{-\infty}^{\infty} e^{-ik(x-\xi)}\; dk \cdot \mathrm{Re}\int_0^{\infty} \frac{e^{-in(z+\zeta)-|y-\eta|\sqrt{n^2+k^2}}}{(n+i\kappa)\sqrt{n^2+k^2}} n\; dn \\ & -\frac{1}{2\pi}\left[\int_{k_1}^{k_2} + \int_{k_3}^{k_4}\right] \frac{\kappa}{\sqrt{k^2-\kappa^2}} e^{-\kappa(z+\zeta)-|y-\eta|\sqrt{k^2-\kappa^2}-ik(x-\xi)}\; dk \\ & +\frac{i}{2\pi}\left[-\int_{-\infty}^{k_1} + \int_{k_2}^{k_3} + \int_{k_4}^{\infty}\right] \frac{\kappa}{\sqrt{\kappa^2-k^2}} \\ & \qquad \times e^{-\kappa(z+\zeta)-i\varepsilon_k|y-\eta|\sqrt{\kappa^2-k^2}-ik(x-\xi)}\; dk \end{aligned} \tag{2.70}$$

where

$$\left.\begin{matrix} r \\ r' \end{matrix}\right\} = \sqrt{(x-\xi)^2+(y-\eta)^2+(z\mp\zeta)^2} \tag{2.71}$$

$$\kappa = \frac{1}{g}(\omega+kU)^2 = K+2k\tau+\frac{k^2}{K_0} \tag{2.72}$$

$$K = \frac{\omega^2}{g},\ \tau=\frac{U\omega}{g},\ K_0=\frac{g}{U^2} \tag{2.73}$$

$$\left.\begin{matrix} k_1 \\ k_2 \end{matrix}\right\} = -\frac{K_0}{2}\left[1+2\tau\pm\sqrt{1+4\tau}\ \right] \tag{2.74}$$

$$\left.\begin{matrix} k_3 \\ k_4 \end{matrix}\right\} = \frac{K_0}{2}\left[1-2\tau\mp\sqrt{1-4\tau}\ \right] \tag{2.75}$$

$$\varepsilon_k = \mathrm{sgn}(\omega+kU) = \begin{cases} -1 & \text{for } -\infty < k < k_1 \\ 1 & \text{for } k_2 < k < \infty \end{cases} \tag{2.76}$$

In the case of $\tau > 1/4$, wavenumbers k_3 and k_4 given by Eq.(2.75) are not real, and thus the limits of integration in Eq.(2.70) should be interpreted such that $k_3 = k_4$ for $\tau > 1/4$ (hereafter this convention should be understood). It should be noted for Eq.(2.69) that the so-called line integral term, contribution from the intersection line between the free surface and the ship's hull surface, is ignored for simplicity and also with the assumption of slenderness of a ship.

To obtain a far field approximation to the disturbance potential φ when the transverse distance $|y|$ is large, let us consider the asymptotic approximation of the Green function itself. It is obvious that all the terms except the last one in Eq.(2.70) vanish for large values of $|y|$. Therefore, substituting only the last term of Eq.(2.70) into Eq.(2.69), we obtain the desired approximation of the velocity potential valid at large distances from the x-axis:

$$\varphi(x,y,z) \sim \frac{i}{2\pi}\left[-\int_{-\infty}^{k_1}+\int_{k_2}^{k_3}+\int_{k_4}^{\infty}\right] H^{\pm}(k)\frac{\kappa}{\sqrt{\kappa^2-k^2}}e^{-\kappa z\mp i\varepsilon_k y\sqrt{\kappa^2-k^2}-ikx}\,dk \tag{2.77}$$

where

$$H^{\pm}(k) = \iint_{S_H}\left(\frac{\partial\varphi}{\partial n}-\varphi\frac{\partial}{\partial n}\right)e^{-\kappa\zeta\pm i\varepsilon_k\eta\sqrt{\kappa^2-k^2}+ik\xi}\,dS \tag{2.78}$$

is the Kochin function equivalent to the complex amplitude of the far field disturbance wave. The upper or lower of the complex signs in Eqs.(2.77) and (2.78) is to be taken according as the sign of y is positive or negative, respectively. With the convention that

the Kochin function is zero outside the integration range explicitly shown in Eq.(2.77), we shall write Eq.(2.77) in the form

$$\varphi(x,y,z) \sim \frac{1}{2\pi}\int_{-\infty}^{\infty} i\varepsilon_k H^{\pm}(k)\frac{\kappa}{\sqrt{\kappa^2-k^2}}e^{-\kappa z \mp i\varepsilon_k y\sqrt{\kappa^2-k^2}}e^{-ikx}\,dk \tag{2.79}$$

Up to this point, it is convenient to define the Fourier transform

$$\left.\begin{aligned}\mathcal{F}[f(x)](k) &\equiv \int_{\infty}^{\infty} f(x)e^{ikx}\,dx = F(k)\\ \mathcal{F}^{-1}[F(k)](x) &\equiv \frac{1}{2\pi}\int_{\infty}^{\infty} F(k)e^{-ikx}\,dk = f(x)\end{aligned}\right\} \tag{2.80}$$

and Dirac's delta function $\delta(x)$ which has the following property:

$$\int_{\infty}^{\infty} f(x)\delta(x-x_0)\,dx = f(x_0) \tag{2.81}$$

Different from the usual definition, here e^{ikx} is used in the Fourier transform, not in the inverse transform. By virtue of the Fourier transform, the disturbance potential in the far-field can be written as

$$\begin{aligned}\mathcal{F}[\varphi(x,y,z)] &= \int_{-\infty}^{\infty}\varphi(x,y,z)e^{ikx}\,dx\\ &= i\varepsilon_k H^{\pm}(k)\frac{\kappa}{\sqrt{\kappa^2-k^2}}e^{-\kappa z\mp i\varepsilon_k y\sqrt{\kappa^2-k^2}}\end{aligned} \tag{2.82}$$

Applying the same procedure above, the Fourier transform of incident wave potential can be given in the following expression

$$\begin{aligned}\mathcal{F}[\varphi_0(x,y,z)] &= \int_{-\infty}^{\infty}\varphi_0(x,y,z)e^{ikx}\,dx\\ &= \mathcal{F}[e^{-i(k_0\cos\chi)x}]e^{-k_0 z - ik_0 y\sin\chi}\end{aligned} \tag{2.83}$$

Making use of the property of Diract's delta function in Eq.(2.81), we may obtain the following relation

$$\left.\begin{aligned}\frac{1}{2\pi}\int_{\infty}^{\infty}\delta(k-k_0)e^{-ikx}\,dk &= \frac{1}{2\pi}e^{-ik_0x}\\ \mathcal{F}^{-1}[\delta(k-k_0)] &= \frac{1}{2\pi}e^{-ik_0x}\\ 2\pi\delta(k-k_0) &= \mathcal{F}[e^{-ik_0x}]\end{aligned}\right\} \tag{2.84}$$

where the nature of Fourier inverse transform has been used. Utilizing the relationship in Eq.(2.84), finally the desired result of incident wave potential may be written in the

following form

$$\begin{aligned} \mathcal{F}[\varphi_0(x,y,z)] &= 2\pi\delta(k-k_0\cos\chi)e^{-k_0z-ik_0y\sin\chi} \\ \varphi_0(x,y,z) &= \mathcal{F}^{-1}[2\pi\delta(k-k_0\cos\chi)e^{-k_0z-ik_0y\sin\chi}] \end{aligned} \tag{2.85}$$

2.3.2 Derivation of Added Resistance Formula

By virtue of the principle of momentum and energy conservations, a formula for the added resistance is going to be derived in this section which is the same as the one derived by Kashiwagi [10]. To this end, first let us consider the linear momentum conservation in Eq.(2.16). Applying the transport theorem to the left-hand side of this equation, the momentum conservation can be recast in the following form

$$\frac{dM_i}{dt} \equiv \frac{d}{dt}\iiint_V \rho v_i \, dV = \rho\left(\iiint_V \frac{\partial v_i}{\partial t}\, dV + \iint_S v_i u_n \, dS\right) \tag{2.86}$$

Performing the substantial derivative Eq.(**??**), the first term on the right hand side of equation above can be written as

$$\frac{\partial v_i}{\partial t} = -\frac{\partial}{\partial x_i}\left(\frac{p}{\rho} - gz\right) - v_j\partial_j v_i \tag{2.87}$$

where we note that the pressure p is measured with atmospheric pressure p_a as the reference value.

The last term of Eq.(2.87) may be written in the form

$$v_j\partial_j v_i = \partial_j(v_jv_i) - v_i\partial_j v_j \tag{2.88}$$

where the last term of this equation is the continuity equation, Eq.(2.20), that is $\partial_j v_j = \nabla\cdot\boldsymbol{v} = 0$ and another term in the right-hand side of Eq.(2.88) can be written as $\partial_j(v_jv_i) = \partial(v_jv_i)/\partial x_j$. Therefore by substituting this term into Eqs.(2.87) and (2.86) as well as applying the divergence theorem, the linear momentum conservation will be

$$\frac{dM_i}{dt} = -\rho\iint_S\left[\left(\frac{p}{\rho} - gz\right)n_i + v_i(v_n - u_n)\right]\, dS \tag{2.89}$$

Here the surface area (S) of surface integral above consists of the ship's wetted surface (S_H), the free surface (S_F) and a control surface (S_C) at a large distance from a ship as we can see in Fig. 2.4. Therefore by considering the rate of change of linear momentum conservation within the surface area and taking account of that there is no flux across

S_H and S_F as well as that the pressure on S_F is zero or

$$\left.\begin{array}{rl} v_n = u_n & \text{on } S_H \text{ and } S_F \\ u_n = 0 & \text{on } S_C^{\pm} \\ p = 0 & \text{on } S_F \end{array}\right\} \tag{2.90}$$

then we obtain the following equation

$$\frac{dM_i}{dt} = -\iint_{S_H} [(pn_i - \rho g z n_i)]\, dS - \iint_{S_C^{\pm}} [(pn_i - \rho g z n_i) + \rho v_i v_n]\, dS \tag{2.91}$$

Substituting $v_i = \nabla \Phi_T$ and $v_n = v_i \cdot n_i = \nabla \Phi_T \cdot \boldsymbol{n}$ and considering only the forces in the transverse plane ($g z n_i = 0$), the linear momentum conservation is to be

$$\frac{d\boldsymbol{M}}{dt} = -\iint_{S_H} p\boldsymbol{n}\, dS - \iint_{S_C^{\pm}} [p\boldsymbol{n} + \rho \nabla \Phi_T (\nabla \Phi_T \cdot \boldsymbol{n})]\, dS \tag{2.92}$$

From the equation above, we may obtain the force acting on the ship. Substituting the velocity potential, Eq.(2.60), into the linear momentum conservation and taking only the x-component as well as neglecting steady disturbance potential, the force may be written in the following equation

$$F_x \equiv \iint_{S_H} p n_x\, dS = -\frac{dM_x}{dt} - \iint_{S_C^{\pm}} \left[p n_x + \rho \left(\frac{\partial \Phi}{\partial x} - U \right) \left(\frac{\partial \Phi}{\partial n} - U n_x \right) \right] dS \tag{2.93}$$

Taking time average of above equation dM_x/dt will vanish due to the periodicity of fluid motions. It means that there can be no net increase of momentum in the whole volume of fluid from one cycle to another. Defining a resistance as the force in the negative x-axis, the added resistance may be computed as

$$\overline{R} = \iint_{S_C^{\pm}} \overline{\left[p n_x + \rho \left(\frac{\partial \Phi}{\partial x} - U \right) \left(\frac{\partial \Phi}{\partial n} - U n_x \right) \right]}\, dS \tag{2.94}$$

In the present analysis the control surface (S_C) will be considered as two flat plates instead of the usual circular cylinder control surface as shown in Fig. 2.4. In this case, the two flat plates are located at $y = \pm Y$ and extend from $x = -\infty$ to $x = \infty$ as well as free surface down to $z = +\infty$. Considering the normal vector in the x component is zero ($n_x = 0$) on $S_C^{\pm}$, the added resistance can be expressed in the following form

$$\overline{R} = \iint_{S_C} \overline{\left[\frac{\partial \Phi}{\partial x} \frac{\partial \Phi}{\partial y} \right]_{-Y}^{Y}}\, dS \tag{2.95}$$

where $[\quad]_{-Y}^{Y}$ means the difference between the values of the quantity in brackets at $y = Y$ and $y = -Y$.

Here on the present control surface, the local wave near the x-axis can be neglected due to the assumption that Y is large. It means that the local waves will be zero at $x = \pm\infty$ in the three dimensional case. Meanwhile the disturbance waves radiating away from the x-axis are exactly taken into account. By this control surface, the surface integral, Eq.(2.95), can be transformed as below, if the free surface elevation is denoted as $z = \zeta_F$.

$$\begin{aligned} \iint_{S_C} dS &= \int_{\zeta_F}^{\infty} dz \int_{-\infty}^{\infty} dx \\ &= \left[\int_{\zeta_F}^{0} + \int_{0}^{\infty}\right] dz \int_{-\infty}^{\infty} dx \end{aligned} \tag{2.96}$$

In the integral range above, contribution from $(\zeta_F, 0)$ is of higer order than $O(\Phi^3)$ because the integrand is already of order $O(\Phi^2)$ and thus should be neglected. Then Eq.(2.96) can be rewritten as

$$\iint_{S_C} dS = \int_{0}^{\infty} dz \int_{-\infty}^{\infty} dx \tag{2.97}$$

Utilizing this equation, the surface integral in Eq.(2.95) can be written in the form

$$\overline{R} = \rho \int_{0}^{\infty} dz \int_{-\infty}^{\infty} \overline{\left[\frac{\partial \Phi}{\partial x}\frac{\partial \Phi}{\partial y}\right]_{-Y}^{Y}} dx \tag{2.98}$$

Now let us substitute Φ in Eq.(2.61) into this equation as follows

$$\overline{R} = \rho \int_{0}^{\infty} dz \int_{-\infty}^{\infty} \overline{\Re\left[\left(\frac{\partial \phi}{\partial x}e^{i\omega t}\right)\left(\frac{\partial \phi}{\partial y}e^{i\omega t}\right)\right]_{-Y}^{Y}} dx \tag{2.99}$$

Considering time-average calculation by using the relation

$$\overline{\Re[Ae^{i\omega t}]\Re[Be^{i\omega t}]} = \frac{1}{2}\Re[AB^*] \tag{2.100}$$

where the asterisk denotes the complex conjugate. Therefore the added resistance, Eq.(2.99), can then be written as follows

$$\overline{R} = \frac{1}{2}\rho\,\Re \int_{0}^{\infty} dz \int_{-\infty}^{\infty} \left[\frac{\partial \phi}{\partial x}\frac{\partial \phi^*}{\partial y}\right]_{-Y}^{Y} dx \tag{2.101}$$

Next we substitute the velocity potential in Eq.(2.61) into Eq.(2.101). It follows that

$$\overline{R} = \frac{1}{2}\rho\left(\frac{gA}{\omega_0}\right)^2 \Re\int_0^\infty dz \int_{-\infty}^{\infty}\left[\left(\frac{\partial\varphi_0}{\partial x}+\frac{\partial\varphi}{\partial x}\right)\left(\frac{\partial\varphi_0^*}{\partial y}+\frac{\partial\varphi^*}{\partial y}\right)\right]_{-Y}^{Y} dx \quad (2.102)$$

As we already assumed that the water depth is infinite ($k_0 = \omega_0^2/g$) and also in Eq.(2.102) the contribution of φ_0 alone is zero because there can be no force associated with the undisturbed incident wave system, therefore the added resistance can be written in the form

$$\begin{aligned}\overline{R} &= \frac{\rho g A^2}{k_0}\frac{1}{2}\Re\int_0^\infty dz \int_{-\infty}^{\infty}\left[\frac{\partial\varphi}{\partial x}\frac{\partial\varphi^*}{\partial y}+\frac{\partial\varphi_0}{\partial x}\frac{\partial\varphi^*}{\partial y}+\frac{\partial\varphi}{\partial x}\frac{\partial\varphi_0^*}{\partial y}\right]_{-Y}^{Y} dx \\ &= \frac{\rho g A^2}{k_0}\left[\overline{R_1}+\overline{R_2}\right] \end{aligned} \quad (2.103)$$

where

$$\overline{R_1} = \frac{1}{2}\Re\int_0^\infty dz \int_{-\infty}^{\infty}\left[\frac{\partial\varphi}{\partial x}\frac{\partial\varphi^*}{\partial y}\right]_{-Y}^{Y} dx \quad (2.104)$$

$$\overline{R_2} = \frac{1}{2}\Re\int_0^\infty dz \int_{-\infty}^{\infty}\left[\frac{\partial\varphi_0}{\partial x}\frac{\partial\varphi^*}{\partial y}+\frac{\partial\varphi}{\partial x}\frac{\partial\varphi_0^*}{\partial y}\right]_{-Y}^{Y} dx \quad (2.105)$$

As we can see in the equation above, the integration with respect to x allows us to apply the Fourier-transform theorem *(Parseval's theorem)* which can be written as

$$\int_{-\infty}^{\infty} f(x)g(x)\,dx = \frac{1}{2\pi}\int_{-\infty}^{\infty} F(k)G^*(k)\,dk \quad (2.106)$$

where $F(k)$ and $G(k)$ are the Fourier transforms of $f(x)$ and $g(x)$ respectively, which may be calculated from the definition of the Fourier transform itself as Eq.(2.80), expressed as

$$\left.\begin{aligned} F(k) &= \mathcal{F}[f(x)] \text{ or } f(x) = \mathcal{F}^{-1}[F(k)] \\ G(k) &= \mathcal{F}[g(x)] \text{ or } g(x) = \mathcal{F}^{-1}[G(k)] \end{aligned}\right\} \quad (2.107)$$

At first, let us consider $\overline{R_1}$ given in Eq.(2.104). Here we have only the disturbance potential (φ) defined in Eq.(2.79). Differentiating φ with respect to x and y, then we have

$$\begin{aligned}\frac{\partial\varphi}{\partial x} &= \frac{1}{2\pi}\int_{-\infty}^{\infty} k\varepsilon_k H^{\pm}(k)\frac{\kappa e^{-\kappa z \mp i\varepsilon_k y\sqrt{\kappa^2-k^2}}}{\sqrt{\kappa^2-k^2}}e^{-ikx}\,dk \\ &= \mathcal{F}^{-1}\left[k\varepsilon_k H^{\pm}(k)\frac{\kappa e^{-\kappa z \mp i\varepsilon_k y\sqrt{\kappa^2-k^2}}}{\sqrt{\kappa^2-k^2}}\right] \end{aligned} \quad (2.108)$$

$$\begin{aligned}\frac{\partial\varphi}{\partial y} &= \frac{1}{2\pi}\int_{-\infty}^{\infty} \pm\varepsilon_k^2 H^{\pm}(k)\kappa e^{-\kappa z \mp i\varepsilon_k y\sqrt{\kappa^2-k^2}} e^{-ikx}\, dk \\ &= \mathcal{F}^{-1}\left[\pm H^{\pm}(k)\kappa e^{-\kappa z \mp i\varepsilon_k y\sqrt{\kappa^2-k^2}}\right] \end{aligned} \tag{2.109}$$

where the nature of $\varepsilon_k^2 = 1$ has been used and $\pm$ sign just before the Kochin funtion depends on whether $y = Y$ and $y = -Y$. Substituting Eq.(2.108) and Eq.(2.109) and applying Parseval's theorem into Eq.(2.104), $\overline{R_1}$ can then be written as follows

$$\overline{R_1} = \frac{1}{4\pi}\Re\int_{-\infty}^{\infty}\left[\pm k\varepsilon_k |H^{\pm}(k)|^2 \frac{\kappa^2}{\sqrt{\kappa^2-k^2}}\int_0^{\infty} e^{-2\kappa z}\, dz\right]_{-Y}^{Y} dk \tag{2.110}$$

Solving the integral equation with respect to z in Eq.(2.109) and following the nature of ε_k as well as the integraton range, leads $\overline{R_1}$ to the following expression

$$\begin{aligned}\overline{R_1} &= \frac{1}{8\pi}\int_{-\infty}^{\infty}\varepsilon_k(|H^+(k)|^2 + |H^-(k)|^2)\frac{\kappa}{\sqrt{\kappa^2-k^2}}k\, dk \\ &= \frac{1}{8\pi}\left[-\int_{-\infty}^{k_1} + \int_{k_2}^{k_3} + \int_{k_4}^{\infty}\right](|H^+(k)|^2 + |H^-(k)|^2)\frac{\kappa}{\sqrt{\kappa^2-k^2}}k\, dk \end{aligned} \tag{2.111}$$

Note that $k_3 = k_4$ in case of $\tau > 1/4$.

Next, we consider $\overline{R_2}$ as in Eq.(2.105). Here we have not only disturbance potential (φ) but also the incident wave potential (φ_0) as defined in Eq.(2.85). Differentiating φ_0 with respect to x and y, the results are

$$\begin{aligned}\mathcal{F}^1\left[\frac{\partial\varphi_0}{\partial x}\right] &= \int_{-\infty}^{\infty}\left[(-ik_0\cos\chi)\, e^{-k_0 z - ik_0(x\cos\chi + y\sin\chi)}\right] e^{ikx} dx \\ &= -2\pi i k_0\cos\chi e^{-k_0 z - ik_0 y\sin\chi}\delta\left(k - k_0\cos\chi\right) \\ \frac{\partial\varphi_0}{\partial x} &= \mathcal{F}^{-1}\left[-2\pi i k_0\cos\chi\delta\left(k - k_0\cos\chi\right) e^{-k_0 z - ik_0 y\sin\chi}\right] \end{aligned} \tag{2.112}$$

$$\begin{aligned}\mathcal{F}^1\left[\frac{\partial\varphi_0}{\partial y}\right] &= \int_{-\infty}^{\infty}\left[(-ik_0\sin\chi)\, e^{-k_0 z - ik_0(x\cos\chi + y\sin\chi)}\right] e^{ikx} dx \\ &= -2\pi i k_0\sin\chi e^{-k_0 z - ik_0 y\sin\chi}\delta\left(k - k_0\cos\chi\right) \\ \frac{\partial\varphi_0}{\partial y} &= \mathcal{F}^{-1}\left[-2\pi i k_0\sin\chi\delta\left(k - k_0\cos\chi\right) e^{-k_0 z - ik_0 y\sin\chi}\right] \end{aligned} \tag{2.113}$$

where the relationship in Eq.(2.84) has been used in the equations above. Substituting Eq.(2.108) and Eq.(2.109) as well as Eq.(2.112) and Eq.(2.113) and applying Parseval's

theorem into Eq.(2.105), then $\overline{R_2}$ can be recast in the following form

$$\begin{aligned}
\overline{R_2} &= \Re\left[\frac{1}{2}\int_0^\infty dz\int_{-\infty}^{\infty}\left[\frac{\partial\varphi_0}{\partial x}\frac{\partial\varphi^*}{\partial y}+\frac{\partial\varphi^*}{\partial x}\frac{\partial\varphi_0^*}{\partial y}\right]_{-Y}^{Y}dx\right] \\
&= \Re\left[\frac{1}{2}\int_0^\infty dz\frac{1}{2\pi}\int_{-\infty}^{\infty}\left[\left(-2\pi ik_0\cos\chi\delta\left(k-k_0\cos\chi\right)e^{-k_0z-ik_0y\sin\chi}\right)\right.\right. \\
&\quad\times\left(\pm H^{\pm}(k)\kappa e^{-\kappa z\mp i\varepsilon_k y\sqrt{\kappa^2-k^2}}\right)^* \\
&\quad+\left(k\varepsilon_k H^{\pm}(k)\frac{\kappa}{\sqrt{\kappa^2-k^2}}e^{-\kappa z\mp i\varepsilon_k y\sqrt{\kappa^2-k^2}}\right) \\
&\quad\left.\left.\times\left(-2\pi ik_0\sin\chi\delta\left(k-k_0\cos\chi\right)e^{-k_0z-ik_0y\sin\chi}\right)^*\right]_{-Y}^{Y}dk\right] \\
&= \Re\left[\frac{i\kappa k_0\cos\chi}{2}\int_0^\infty e^{-(\kappa+k_0)z}dz\right. \\
&\quad\times\left[\left(\mp H^{\pm}(k_0\cos\chi)^*e^{-iy\left(k_0\sin\chi\mp i\varepsilon_k\sqrt{\kappa^2-(k_0\cos\chi)^2}\right)}\right)\right. \\
&\quad\left.\left.+\left(\varepsilon_k H^{\pm}(k_0\cos\chi)\frac{k_0\sin\chi e^{iy\left(k_0\sin\chi\mp i\varepsilon_k\sqrt{\kappa^2-(k_0\cos\chi)^2}\right)}}{\sqrt{\kappa^2-(k_0\cos\chi)^2}}\right)\right]_{-Y}^{Y}\right]
\end{aligned} \tag{2.114}$$

where the relationship in Eq.(2.84) again has been used in the last expression.

According to the theory of hyper function, sinusoidal terms will vanish when taking the limit of $Y\to\infty$ after performing the x and z integrations. It means that it is sufficient to retain only terms which are independent of the y-axis in the equation above. Therefore our consideration here is only for the two cases namely $k_0\sin\chi=+\varepsilon_k\sqrt{\kappa^2-(k_0\cos\chi)^2}$ and $k_0\sin\chi=-\varepsilon_k\sqrt{\kappa^2-(k_0\cos\chi)^2}$. If we solve them as a quadratic equation, we will have

$$(k_0\sin\chi)^2=\left(\pm\varepsilon_k\sqrt{\kappa^2-(k_0\cos\chi)^2}\right)^2 \tag{2.115}$$

By using the nature of $\pm\varepsilon_k=1$, then we have the relation between κ and k_0 as below

$$\begin{aligned}
\kappa^2 &= k_0^2\left(\sin^2\chi+\cos^2\chi\right) \\
\kappa &= k_0
\end{aligned} \tag{2.116}$$

Performing integral equation with respect to z of Eq.(2.114), the result is

$$\begin{aligned}
\int_0^\infty e^{-(\kappa+k_0)z}\,dz &= \left[-\frac{1}{(\kappa+k_0)}e^{-(\kappa+k_0)z}\right]_0^\infty \\
&= \frac{1}{(\kappa+k_0)} \\
&= \frac{1}{2\kappa}
\end{aligned} \tag{2.117}$$

Further, noting that $\varepsilon_k = 1$ when the sign in $H^{\pm}$ is positive and $\varepsilon_k = -1$ when the sign in $H^{\pm}$ is negative and substituting $k = k_0 \cos\chi$, the Kochin function Eq.(2.78) can be recast in the form

$$\begin{aligned} H^{\pm}(k_0\cos\chi) &= \iint_{S_H}\left(\frac{\partial\varphi}{\partial n} - \varphi\frac{\partial}{\partial n}\right) e^{-\kappa\zeta \pm i\varepsilon_k\eta\sqrt{\kappa^2-(k_0\cos\chi)^2}+i(k_0\cos\chi)\xi} dS \\ &= \iint_{S_H}\left(\frac{\partial\varphi}{\partial n} - \varphi\frac{\partial}{\partial n}\right) e^{-\kappa\zeta+ik_0(\eta\sin\chi+\xi\cos\chi)} dS \\ &\equiv H(k_0,\chi) \end{aligned} \tag{2.118}$$

Note that for each case of $y = Y$, $y = -Y$, the exponential function in Eq.(2.114), will be

$$e^{\mp iy\left(k_0\sin\chi \mp \varepsilon_k\sqrt{\kappa^2-(k_0\cos\chi)^2}\right)} \to 1 \tag{2.119}$$

Taking the result of Eq.(2.115) to Eq.(2.119) into account, $\overline{R_2}$ in Eq.(2.114) can be written as follows

$$\begin{aligned} \overline{R_2} &= \Re\left[\frac{i\kappa k_0\cos\chi}{2}\left[\mp H(k_0,\chi)^* + \varepsilon_k H(k_0,\chi)\frac{k_0\sin\chi}{k_0\sin\chi/\varepsilon_k}\right]_{-Y}^{Y}\frac{1}{2\kappa}\right] \\ &= \Re\left[\frac{ik_0\cos\chi}{4}\left[\mp H(k_0,\chi)^* + H(k_0,\chi)\right]_{-Y}^{Y}\right] \end{aligned} \tag{2.120}$$

Utilizing the relation below

$$\Re[iz_a] = -\Im[z_a] = \Im[z_a^*] \tag{2.121}$$

finally the last result of $\overline{R_2}$ can be obtained as follows

$$\begin{aligned} \overline{R_2} &= -\frac{k_0\cos\chi}{4}\left[\Im\left[\mp H(k_0,\chi)^* + H(k_0,\chi)\right]_{-Y}^{Y}\right] \\ &= -\frac{k_0\cos\chi}{4}\Im\left[-H(k_0,\chi)^* + H(k_0,\chi) - \{H(k_0,\chi)^* + H(k_0,\chi)\}\right] \\ &= \frac{k_0\cos\chi}{2}\Im\left[H(k_0,\chi)^*\right] \\ &= -\frac{k_0\cos\chi}{2}\Im\left[H(k_0,\chi)\right] \end{aligned} \tag{2.122}$$

where symbol $\Im$ denotes the imaginary part.

Therefore, the total added resistance can be rewritten by substituting $\overline{R_1}$ and $\overline{R_2}$ into Eq.(2.103)

$$\begin{aligned} \frac{\overline{R}}{\rho g A^2} &= \frac{1}{8\pi k_0}\left[-\int_{-\infty}^{k_1} + \int_{k_2}^{k_3} + \int_{k_4}^{\infty}\right]\left\{\left|H^+(k)\right|^2 + \left|H^-(k)\right|^2\right\}\frac{\kappa}{\sqrt{\kappa^2-k^2}}kdk \\ &\quad -\frac{1}{2}\cos\chi\,\Im\left[H(k_0,\chi)\right] \end{aligned} \tag{2.123}$$

After considering the principle of linear momentum conservation, to get the expected result of the added resistance as obtained by Maruo [11], let us consider the principle of energy conservation Eq.(2.59). Considering the boundary condition of each control surface in Eq.(2.90), Eq.(2.59) may be written in the form

$$\frac{dE}{dt} = -\iint_{S_H} (p - p_a) v_n \, dS + \iint_{S_C} \frac{\partial \Phi}{\partial t} \frac{\partial \Phi}{\partial n} \, dS \tag{2.124}$$

Taking time average of Eq.(2.59), $\overline{dE/dt}$ will be zero due to periodicity of fluid motions. Here we have no work done or no dissipation energy by the floating ship because there is no external force except the constant towing force and gravitational force keeping the equilibrium position of the ship in space. It means that

$$\iint_{S_H} \overline{(p - p_a) v_n} \, dS = 0 \tag{2.125}$$

Thus the only contribution from taking time average of Eq.(2.124) is

$$\iint_{S_C} \overline{\frac{\partial \Phi}{\partial t} \frac{\partial \Phi}{\partial n}} \, dS = 0 \tag{2.126}$$

Substituting the velocity potential Eq.(2.60) into above and considering that the normal vector of x and z components on S_C are equal to zero, then we can write equation below

$$\iint_{S_C} \overline{\frac{\partial \Phi}{\partial t} \frac{\partial \Phi}{\partial y}} \, dS = 0 \tag{2.127}$$

In order to treat the surface integral of Eq.(2.127), Eq.(2.97) may be used instead and yields the following equation

$$\int_0^\infty dz \int_{-\infty}^{\infty} \overline{\left[\frac{\partial \Phi}{\partial t} \frac{\partial \Phi}{\partial y} \right]_{-Y}^{Y}} \, dx = 0 \tag{2.128}$$

Making use of taking time average relation in Eq.(2.100) and substituting Eq.(2.61), the transformation result of Eq.(2.128) will be

$$\begin{aligned} \int_0^\infty dz \int_{-\infty}^{\infty} \overline{\left[\frac{\partial \Phi}{\partial t} \frac{\partial \Phi}{\partial y} \right]_{-Y}^{Y}} \, dx &= \int_0^\infty dz \int_{-\infty}^{\infty} \overline{\left[\Re(i\omega\phi e^{i\omega t}) \Re\left(\frac{\partial \phi}{\partial y} e^{i\omega t} \right) \right]_{-Y}^{Y}} \, dx \\ &= \frac{1}{2} \Re \int_0^\infty dz \int_{-\infty}^{\infty} \left[i\omega\phi \frac{\partial \phi^*}{\partial y} \right]_{-Y}^{Y} dx \end{aligned} \tag{2.129}$$

By substituting Eq.(2.62), utilizing relation in Eq.(2.121) and decomposing the result above into two parts, then we have

$$\frac{1}{2}\omega\left(\frac{gA}{\omega_0}\right)^2 \Re\int_0^\infty dz\int_{-\infty}^{\infty}\left[i(\varphi_0+\varphi)\frac{\partial(\varphi_0^*+\varphi^*)}{\partial y}\right]_{-Y}^{Y} dx$$
$$= -\frac{1}{2}\omega\left(\frac{gA}{\omega_0}\right)^2 \Im\int_0^\infty dz\int_{-\infty}^{\infty}\left[\varphi_0\frac{\partial\varphi_0^*}{\partial y}+\varphi_0\frac{\partial\varphi^*}{\partial y}+\varphi\frac{\partial\varphi_0^*}{\partial y}+\varphi\frac{\partial\varphi^*}{\partial y}\right]_{-Y}^{Y} dx \quad (2.130)$$

The first term in brackets of the right-hand side has no effect because there can be no force associated with the undisturbed incident wave system as already explained before. Therefore, Eq.(2.130) will be

$$\frac{1}{2}\Im\int_0^\infty dz\int_{-\infty}^{\infty}\left[\varphi\frac{\partial\varphi^*}{\partial y}\right]_{-Y}^{Y} dx = -\frac{1}{2}\Im\int_0^\infty dz\int_{-\infty}^{\infty}\left[\varphi_0\frac{\partial\varphi^*}{\partial y}+\varphi\frac{\partial\varphi_0^*}{\partial y}\right]_{-Y}^{Y} dx \quad (2.131)$$

The procedure of performing these integrations with respect to x and z is the same as that for Eq.(2.104) and Eq.(2.105); that is, to apply Parseval's theorem given in Eq.(2.107) with the Fourier transforms of φ and φ_0. Substituting Eq.(2.82), Eq.(2.109) and utilizing Eq.(2.117) to solve integral equation with respect to z, the left-hand side of Eq.(2.131) (which is denoted as $\mathcal{L}$) is written as

$$\begin{aligned}
\mathcal{L} &= \frac{1}{2}\Im\left[\int_0^\infty dz\frac{1}{2\pi}\int_{-\infty}^{\infty}\left[\left(i\varepsilon_k H^{\pm}(k)\frac{\kappa}{\sqrt{\kappa^2-k^2}}e^{-\kappa z\mp i\varepsilon_k y\sqrt{\kappa^2-k^2}}\right)\right.\right.\\
&\quad\left.\left.\times\left(\pm H^{\pm}(k)\kappa e^{-\kappa z\mp i\varepsilon_k y\sqrt{\kappa^2-k^2}}\right)^*\right]_{-Y}^{Y} dk\right]\\
&= \frac{1}{8\pi}\Im\left[\int_{-\infty}^{\infty}\left[\pm i\varepsilon_k\left|H^{\pm}(k)\right|^2\frac{\kappa}{\sqrt{\kappa^2-k^2}}\right]_{-Y}^{Y} dk\right]\\
&= \frac{1}{8\pi}\Im\left[i\int_{-\infty}^{\infty}\varepsilon_k\left\{\left|H^{+}(k)\right|^2+\left|H^{-}(k)\right|^2\right\}\frac{\kappa}{\sqrt{\kappa^2-k^2}}dk\right]\\
&= \frac{1}{8\pi}\int_{-\infty}^{\infty}\varepsilon_k\left\{\left|H^{+}(k)\right|^2+\left|H^{-}(k)\right|^2\right\}\frac{\kappa}{\sqrt{\kappa^2-k^2}}dk\\
&= \frac{1}{8\pi}\left[-\int_{-\infty}^{k_1}+\int_{k_2}^{k_3}+\int_{k_4}^{\infty}\right]\left\{\left|H^{+}(k)\right|^2+\left|H^{-}(k)\right|^2\right\}\frac{\kappa}{\sqrt{\kappa^2-k^2}}dk \quad (2.132)
\end{aligned}$$

Similarly, the right-hand side of Eq.(2.131) (which is denoted as $\mathcal{R}$) is obtained by substituting Eqs.(2.82), (2.85), (2.109) and Eq.(2.113) as follows

$$\begin{aligned}
\mathcal{R} &= -\frac{1}{2}\Im\left[\int_0^\infty dz \int_{-\infty}^\infty \left[\left(-2\pi i k_0 \sin\chi \delta\left(k - k_0\cos\chi\right) e^{-k_0 z - i k_0 y \sin\chi}\right)^* \right.\right. \\
&\quad \times \left(i\varepsilon_k H^{\pm}(k) \frac{\kappa}{\sqrt{\kappa^2 - k^2}} e^{-\kappa z \mp i\varepsilon_k y\sqrt{\kappa^2-k^2}}\right) \\
&\quad \left.\left. + \left(\pm H^{\pm}(k)\kappa e^{-\kappa z \mp i\varepsilon_k y\sqrt{\kappa^2-k^2}}\right)^* \left(2\pi\delta\left(k - k_0\cos\chi\right) e^{-k_0 z - i k_0 y\sin\chi}\right)\right]_{-Y}^{Y} dk\right] \\
&= \frac{1}{4}\Im\left[\left[H\left(k_0,\chi\right) \mp H\left(k_0,\chi\right)^*\right]_{-Y}^{Y}\right] \\
&= \frac{1}{4}\Im\left[-2H\left(k_0,\chi\right)^*\right] \\
&= \frac{1}{2}\Im\left[H\left(k_0,\chi\right)\right] \qquad (2.133)
\end{aligned}$$

where several relationships such as $k_0 \sin\chi = \pm\varepsilon_k\sqrt{\kappa^2 - \left(k_0\cos\chi\right)^2}$ and Eq.(2.115) through Eq.(2.119) are used in obtaining Eq.(2.133). Thus Eq.(2.131) takes the following expression

$$\frac{1}{8\pi}\left[-\int_{-\infty}^{k_1} + \int_{k_2}^{k_3} + \int_{k_4}^{\infty}\right]\left\{\left|H^+(k)\right|^2 + \left|H^-(k)\right|^2\right\}\frac{\kappa}{\sqrt{\kappa^2-k^2}}dk = \frac{1}{2}\Im\left[H\left(k_0,\chi\right)\right] \qquad (2.134)$$

Substituting this result into Eq.(2.123), the added resistance can be recast in the form

$$\frac{\overline{R}}{\rho g A^2} = \frac{1}{8\pi k_0}\left[-\int_{-\infty}^{k_1} + \int_{k_2}^{k_3} + \int_{k_4}^{\infty}\right]\left\{\left|H^+(k)\right|^2 + \left|H^-(k)\right|^2\right\}\frac{\kappa\left(k - k_0\cos\chi\right)}{\sqrt{\kappa^2-k^2}}dk \qquad (2.135)$$

If we decompose the Kochin function in the symmetric $C(k)$ and anti-symmetric $S(k)$ components with respect to the center plane of a ship symmetrical about $y = 0$ as

$$H^{\pm}(k) = C(k) \pm i\varepsilon_k S(k) \qquad (2.136)$$

where

$$\begin{aligned}
C(k) &= \frac{1}{2}\left\{H^{\pm}(k;\eta=\eta) + H^{\pm}(k;\eta=-\eta)\right\} \\
&= \frac{1}{2}\iint_{S_H}\left(\frac{\partial\varphi}{\partial n} - \varphi\frac{\partial}{\partial n}\right)e^{-\kappa\zeta}e^{ik\xi}\left(e^{\pm i\varepsilon_k\eta\sqrt{\kappa^2-k^2}} + e^{\mp i\varepsilon_k\eta\sqrt{\kappa^2-k^2}}\right)dS \\
&= \iint_{S_H}\left(\frac{\partial\varphi}{\partial n} - \varphi\frac{\partial}{\partial n}\right)e^{-\kappa\zeta}e^{ik\xi}\cos\left(\varepsilon_k\eta\sqrt{\kappa^2-k^2}\right)dS \\
&= \iint_{S_H}\left(\frac{\partial\varphi}{\partial n} - \varphi\frac{\partial}{\partial n}\right)e^{-\kappa\zeta + ik\xi}\cos\left(\eta\sqrt{\kappa^2-k^2}\right)dS \qquad (2.137)
\end{aligned}$$

and

$$\begin{aligned}
\pm i\varepsilon_k S(k) &= \frac{1}{2}\left\{H^{\pm}(k;\eta=\eta) - H^{\pm}(k;\eta=-\eta)\right\} \\
&= \frac{1}{2}\iint_{S_H}\left(\frac{\partial\varphi}{\partial n} - \varphi\frac{\partial}{\partial n}\right)e^{-\kappa\zeta}e^{ik\xi}\left(e^{\pm i\varepsilon_k\eta\sqrt{\kappa^2-k^2}} - e^{\mp i\varepsilon_k\eta\sqrt{\kappa^2-k^2}}\right)dS \\
&= \iint_{S_H}\left(\frac{\partial\varphi}{\partial n} - \varphi\frac{\partial}{\partial n}\right)e^{-\kappa\zeta}e^{ik\xi}\left\{\pm i\sin\left(\varepsilon_k\eta\sqrt{\kappa^2-k^2}\right)\right\}dS \\
&= \pm i\varepsilon_k\iint_{S_H}\left(\frac{\partial\varphi}{\partial n} - \varphi\frac{\partial}{\partial n}\right)e^{-\kappa\zeta+ik\xi}\sin\left(\eta\sqrt{\kappa^2-k^2}\right)dS \qquad (2.138)
\end{aligned}$$

Finally the added resistance in Eq.(2.135) can be recast and given in the form

$$\frac{\overline{R}}{\rho g A^2} = \frac{1}{4\pi k_0}\left[-\int_{-\infty}^{k_1} + \int_{k_2}^{k_3} + \int_{k_4}^{\infty}\right]\left\{|C(k)|^2 + |S(k)|^2\right\}\frac{\kappa\left(k - k_0\cos\chi\right)}{\sqrt{\kappa^2-k^2}}dk \qquad (2.139)$$

From this equation we can see that no contribution to the added resistance exists from the interaction between symmetric waves $C(k)$ and anti-symmetric wave $S(k)$. They give only independent contributions.

2.4 Enhanced Unified Theory (EUT)

In order to compute the added resistance, the unsteady velocity potential given in Eq.(2.61) must be sought to satisfy the Laplace equation, appropriate boundary conditions on the free surface and ship's hull surface, and the radiation condition. In the slender-ship theory, these governing equations and boundary conditions may be simplified further by introducing the slenderness parameter ε, which is usually taken as B/L or d/L (B, d, L being ship's breadth, draft, and length, respectively).

In the outer region far from the ship, when the limit of $\varepsilon \to 0$, the ship will be viewed as a segment along the x axis and then the body boundary condition cannot be imposed; which is called the outer problem. By the variable transformation of $y = \varepsilon Y$ and $z = \varepsilon Z$, the y and z axes may be stretched to zoom in the body surface. Therefore the body boundary condition can be satisfied in the magnified Y-Z plane.

On the other hand, the far-field behavior of ship-generated waves cannot be perceived in the near field close to the ship, and thus the radiation condition cannot be imposed; which is called the inner problem. In what follows, only the symmetric mode of motions in the radiation problem (surge, heave, and pitch corresponding to j= 1, 3, and 5, respectively) and the symmetric component in the diffraction problem with respect to the vertical x-z plane ($j = 7$) are to be considered.

2.4.1 Radiation Problem

In the inner region close to the ship hull, the gradient of the flow velocity along the x-axis is small compared to that in transverse sections and the radiation condition cannot be imposed. Therefore the unsteady velocity potential in radiation problem must satisfy the following boundary conditions

$$\frac{\partial^2\phi_j}{\partial y^2} + \frac{\partial^2\phi_j}{\partial z^2} = 0 \qquad \text{for } z \geq 0 \tag{2.140}$$

$$\frac{\partial\phi_j}{\partial z} + K\phi_j = 0 \qquad \text{on } z \geq 0 \tag{2.141}$$

$$\frac{\partial\phi_j}{\partial n} = n_j + \frac{U}{i\omega}m_j \qquad \text{on } C_H(x) \tag{2.142}$$

where $K = \omega^2/g, n_j$ denotes the j-th components of the unit normal vector positive pointing out of fluid domain

$$\left.\begin{array}{c} \boldsymbol{n} = (n_1, n_2, n_3) \\ (\boldsymbol{x} \times \boldsymbol{n}) = (n_4, n_5, n_6) \\ \boldsymbol{x} = (x, y, z) \end{array}\right\} \tag{2.143}$$

and m_j is the j-th components of the so-called m-term, speed-dependent term which represents interactions with steady flow

$$\left.\begin{array}{c} -(\boldsymbol{n}\cdot\nabla)\,\boldsymbol{V} = (m_1, m_2, m_3) \\ -(\boldsymbol{n}\cdot\nabla)(\boldsymbol{x} \times \boldsymbol{V}) = (m_4, m_5, m_6) \\ \boldsymbol{V} = \nabla[-x + \phi_s(x, y, z)] \end{array}\right\} \tag{2.144}$$

These are considered on the contour $C_H(x)$ of the transverse section at position x over the ship's length. It should be noted here that the contributions from the steady disturbance potential (ϕ_s) for computing the m-term are neglected in this paper and thus $m_j = 0$ for $j = 1, 3; m_5 = n_3$ and $n_5 = -xn_3$. Note that only the symmetric mode of motion ($j = 1, 3, 5$) in the radiation problem is considered.

Due to lack of the radiation condition, a homogeneous solution may be allowed to construct the general inner solution satsifying the boundary conditions in the following form

$$\phi_j(x; y, z) = \phi_j^P(y, z) + C_j(x)\phi^H(y, z) \tag{2.145}$$

$$\phi_j^P(y, z) = \varphi_j(y, z) + \frac{U}{i\omega}\hat{\varphi}_j(y, z) \tag{2.146}$$

$$\phi_j^H(y, z) = \{\varphi_3(y, z) - \varphi_3^*(y, z)\} \tag{2.147}$$

where ϕ_j^P denotes the particular solutions with φ_j and φ_j are solutions corresponding to the first and the second terms on the right-hand side of Eq.(2.142) respectively. ϕ_j^H is a homogeneous solution with $C_j(x)$ being the unknown coefficient and the asterisk denotes the complex conjugate.

In the outer region far away from the ship, the body boundary condition cannot be imposed. Thus the outer solution can be provided by a line distribution of the 3D source along the x-axis and expressed in the form

$$\phi_j(x,y,z) = \int_L Q_j(\xi) G(x-\xi,y,z) d\xi \tag{2.148}$$

where G is the $3D$ Green function given by Eq.(2.70) for the translating and oscillating problems, and Q_j is its unknown strength. By matching the outer expansion of the inner solution and the inner expansion of the outer solution in an overlap region, the unknown $C_j(x)$ in Eq.(2.146) and $Q_j(x)$ in Eq.(2.148) can be obtained and given as follows

$$\phi_j(x) + \frac{i}{2\pi}\left(1 - \frac{\sigma_3}{\sigma_3^*}\right) = \int_L Q_j(\xi) f(x-\xi) d\xi = \sigma_j + \frac{U}{i\omega}\hat{\sigma_j} \tag{2.149}$$

$$C_j(x)\left\{\sigma_3 - \sigma_3^*\right\} = Q_j - \left\{\sigma_j + \frac{U}{i\omega}\hat{\sigma_j}\right\} \tag{2.150}$$

where $f(x-\xi)$ is the kernel function representing the $3D$ and forward-speed effects; its explicit expression is given in the original unified theory developed by Newman & Sclavounos [12]. σ_j and $\hat{\sigma_j}$ denote the $2D$ Kochin function to be computed from φ_j and $\hat{\varphi_j}$, respectively.

2.4.2 Diffraction Problem

With assumption that the rapidly-varying part of the scattering potential along the ship's length is of the same form as the incident wave, the scattering potential may be sought in the form

$$\phi_7(x;y,z) = \psi_7(x;,y,z)e^{ilx}; \;\; l = -k_0\cos\chi \tag{2.151}$$

where ψ_7 is the slowly-varying part of the inner solution satisfying the following boundary conditions

$$\frac{\partial^2\psi_7}{\partial y^2} + \frac{\partial^2\psi_7}{\partial z^2} - l^2\psi_7 = 0 \quad \text{on } z \geq 0 \tag{2.152}$$

$$\frac{\partial\psi_7}{\partial z} + k_0\psi_7 = 0 \quad \text{on } z = 0 \tag{2.153}$$

$$\frac{\partial\psi_7}{\partial n} = k_0 e^{-k_0 z}\{(n_3 + in_1\cos\chi)\cos(k_0 y\sin\chi) + n_2\sin\chi\sin(k_0 y\sin\chi)\} \quad \text{on } C_H(x) \tag{2.154}$$

Therefore in the same fashion as in the radiation problem, the general inner solution for the diffraction problem can be given as follows

$$\psi_7(x;y,z) = \psi_7^P(y,z) + C_7(x)\psi_7^H(y,z) \tag{2.155}$$

$$\psi_7^P(y,z) = -e^{-k_0 z}\cos(k_0 y\sin\chi) \tag{2.156}$$

$$\psi_7^H(y,z) = \left\{\psi_{2D}(x;y,z) + e^{-k_0 z}\cos k_0 y\sin\chi\right\} \tag{2.157}$$

where ψ_{2D} denotes the numerical solution satisfying the body boundary condition which includes the contribution of x-component of the normal vector in Eq.(2.154). Using the same procedure for obtaining the unknown coefficient in the radiation problem, the unknown in the diffraction problem $C_7(x)$ can also be obtained by matching the inner and outer solutions. Therefore by solving an integral equation of the source strength in the outer solution, the unknown coefficient $C_7(x)$ can be determined from the followings:

$$Q_7(x) + \frac{1}{\pi}\sigma_7\left\{Q_7(x)h_1(\chi) - \int_L Q_7(\xi)f(x-\xi)d\xi\right\} = \sigma_7 e^{ilx} \tag{2.158}$$

$$C_7(x)\sigma_7 e^{ilx} = Q_7(x) \tag{2.159}$$

where

$$h_1(x) = \csc\chi\cosh^{-1}(|\sec\chi|) - ln(2|\sec\chi|) \tag{2.160}$$

Fore more details about radiation and diffraction problems in the EUT, the reader should refer to Kashiwagi [13] and Kashiwagi [14]

2.4.3 Hydrodynamic Forces

In order to obtain hydrodynamic forces, let us first consider the pressure. In the linear theory, the spatial part of the unsteady pressure can be obtained by discarding the

higher order terms in Bernoulli's pressure equation and given as

$$p = -\rho(i\omega + U\,\boldsymbol{V}\cdot\nabla)\phi + \rho g(X_3 + X_4 y - X_5 x) \tag{2.161}$$

where the first term on the right-hand side represents the hydrodynamic pressure, with $\boldsymbol{V}$ defined as in Eq.(2.144) and the second term is the hydrostatic pressure due to ship motions from its equilibrium position and has nothing to do with the velocity potential. Neglecting the contribution from ϕ_s in $\boldsymbol{V}$, Eq.(2.161) can be rewritten as

$$p = -\rho\left(i\omega - U\frac{\partial}{\partial x}\right)\phi + \rho g(X_3 + X_4 y - X_5 x) \tag{2.162}$$

Substituting ϕ in Eq.(2.162), then the total oscillating pressure acting on the ship can be divided into three components; radiation pressure p_R, diffraction pressure p_D and the variance of hydrostatic pressure p_S, respectively, and expressed as

$$p(\boldsymbol{x}) = p_R(\boldsymbol{x}) + p_D(\boldsymbol{x}) + p_S(\boldsymbol{x}) \tag{2.163}$$

where

$$p_R(\boldsymbol{x}) = \rho\omega^2\left(1 - \frac{U}{i\omega}\frac{\partial}{\partial x}\right)\sum_{j=1,3,5} X_j\phi_j \tag{2.164}$$

$$p_D(\boldsymbol{x}) = -\rho g A\frac{\omega}{\omega_0}\left(1 - \frac{U}{i\omega}\frac{\partial}{\partial x}\right)\phi_D \tag{2.165}$$

$$p_S(\boldsymbol{x}) = \rho g(X_3 + X_4 y + X_5 x) \tag{2.166}$$

and ϕ_D in Eq.(2.165) is the diffraction potential that is the sum of the incident wave potential and scattering potential.

After introducing the pressures, now let us consider the hydrodynamic forces. These forces can be obtained by integrating the pressures as in Eqs.(2.164) to (2.166) on the wetted surface of the ship S_H. The first one from Eq.(2.164), the radiation force acting in the i-th direction is written as

$$\begin{aligned} F_i &= -\iint_{S_H} p_R(\boldsymbol{x}) n_i dS \\ &= -(i\omega)^2 \sum_{j=1,3,5}\left[A_{ij} + \frac{B_{ij}}{i\omega}\right] X_j \end{aligned} \tag{2.167}$$

where

$$\begin{aligned} A_{ij} + \frac{B_{ij}}{i\omega} &= -\rho \int_L dx \int_{C_H} \left(n_i - \frac{U}{i\omega} m_i \right) \left(\varphi_j + \frac{U}{i\omega} \hat{\varphi}_j \right) \\ &\quad -\rho \int_L dx C_j(x) \int_{C_H} \left(n_i - \frac{U}{i\omega} m_i \right) \phi_j^H dS \end{aligned} \tag{2.168}$$

and Tuck's theorem [15] has been applied in obtaining the final result. A_{ij} and B_{ij} denote the added mass and the damping coefficients in the i-th direction due to the j-th mode of motion. The second one is the resulting force from diffraction pressure Eq.(2.165) which is the wave exciting force, given in the following result

$$\begin{aligned} E_i &= -\iint_{S_H} p_D(\boldsymbol{x}) n_i dS \\ &= \rho g A \int_L dx C_7(x) e^{ilx} \int_{C_H} \left\{ \psi_{2D} + e^{-k_0 z} \cos(k_0 y \sin\chi) \right\} n_i dS \end{aligned} \tag{2.169}$$

The last one is the contribution from the hydrostatic pressure that is the restoring force, which can be expressed as

$$\begin{aligned} S_i &= -\iint_{S_H} p_S(\boldsymbol{x}) n_i dS \\ &= -\rho g \iint_{S_H} (X_3 + X_4 y - X_5 x) n_i dS \end{aligned} \tag{2.170}$$

The existence of this force may cause resonance in the direction of heave and also in pitch as well as in roll as the moment due to couple of vertical forces.

2.4.4 Ship Motions

It has been mentioned before that only symmetric modes of motion are considered here, then the motion equations for surge, heave and pitch motions can be computed by the following equation

$$\sum_{j=1,3,5} [-\omega^2 (M_{ij} + A_{ij}) + i\omega B_{ij} + C_{ij}] X_j = E_i \quad (i = 1, 3, 5) \tag{2.171}$$

where M_{ij} is the generalized mass matrix and C_{ij} the restoring force matrix. The resulting nonzero terms from these matrices are

$$\left.\begin{aligned} &M_{11} = M_{33}, \quad M_{55} = I_{55} = \rho\nabla\kappa_{yy}^2 \\ &C_{33} = \rho g A_w, \quad C_{35} = C_{53} = -\rho g A_w x_w \\ &C_{55} = \rho g \nabla \overline{GM_L} \end{aligned}\right\} \tag{2.172}$$

where ∇ denotes the displacement volume, κ_{yy} is the gyrational radius in pitch. A_w is the waterplane area with x_w as its center in x-axis and $\overline{GM_L}$ is a distance from the center of gravity to the longitudinal metacenter.

Once the linearized boundary-value problems for the unsteady velocity potentials have been solved, the added resistance in waves, which is a time-averaged quantity of second order with respect to the incident-wave amplitude, can be computed with Eq.(2.139) known as Maruo's [11] formula. Note that the added resistance can be computed only from the symmetric components of the Kochin function when considering only the head waves, hence it can be given as

$$\frac{\overline{R}}{\rho g A^2} = \frac{1}{4\pi k_0}\left[-\int_{-\infty}^{k_1} + \int_{k_2}^{k_3} + \int_{k_4}^{\infty}\right] |H(k)|^2 \frac{\kappa}{\sqrt{\kappa^2 - k^2}}(k + k_0)dk \tag{2.173}$$

where $H(k)$ denotes the symmetric component of the Kochin function given in the form of superposition of ship-generated progressive waves and can be written specifically in the following expression

$$H(k) = H_7(k) - \sqrt{k_0 K} \sum_{j=1,3,5} \frac{X_j}{A} H_j(k) \tag{2.174}$$

$$|H(k)|^2 = |H_7(k)|^2 + k_0 K |\xi_j H_j(k)|^2 - 2\sqrt{k_0 K}\Re[H_7(k)\{\xi_j H_j(k)\}^*] \tag{2.175}$$

For simplicity X_j/A in Eq.(2.174) is denoted by ξ_j in Eq.(2.175), where asterisk means the complex conjugate and summation convention is applied in Eq.(2.175) instead of summation sign in Eq.(2.174), subscript $j = 1, 3, 5$ denotes the Kochin function of surge, heave and pitch motions respectively, for the radiation problem and $j = 7$ for diffraction problem. In the EUT, the Kochin function can be computed from

$$H_j(k) = \int_L Q_j(x) e^{ikx} dx \tag{2.176}$$

Each term on the right-hand side of Eq.(2.175) denotes the contribution from the diffraction wave, the radiation wave, and the cross terms between the diffraction and radiation waves. Thus in accordance with each term in Eq.(2.175), it might be useful to write the

added resistance as a summation of the following three components:

$$R_{AW} = R_{AW}^{(DD)} + R_{AW}^{(RR)} + R_{AW}^{(DR)} \tag{2.177}$$

where

$$R_{AW}^{(DD)} = \frac{1}{4\pi k_0}\left[-\int_{-\infty}^{k_1}+\int_{k_2}^{k_3}+\int_{k_4}^{\infty}\right]|H_7(k)|^2\,\frac{\kappa}{\sqrt{\kappa^2-k^2}}(k+k_0)dk \tag{2.178}$$

$$R_{AW}^{(RR)} = \frac{K}{4\pi}\left[-\int_{-\infty}^{k_1}+\int_{k_2}^{k_3}+\int_{k_4}^{\infty}\right]|\xi_j H_j(k)|^2\,\frac{\kappa}{\sqrt{\kappa^2-k^2}}(k+k_0)dk \tag{2.179}$$

$$R_{AW}^{(DR)} = -\frac{\sqrt{K}}{2\pi\sqrt{k_0}}\left[-\int_{-\infty}^{k_1}+\int_{k_2}^{k_3}+\int_{k_4}^{\infty}\right]\Re[H_7(k)\,\{\xi_j H_j(k)\}^*]\frac{\kappa(k+k_0)}{\sqrt{\kappa^2-k^2}}dk \tag{2.180}$$

2.5 Steady Wave Resistance

In order to confirm the amount of reduction of the total wave resistance, the steady wave resistance should also be computed. In the Holtrop & Mennen [16] method, the wave resistance is formulated in the form

$$R_W = c_1 c_2 c_5 \nabla\rho g \exp\left\{m_1 + F_n^{-0.9} + m_2\cos(\lambda F_n^{-2})\right\} \tag{2.181}$$

where

$$c_1 = 2223105\, c_7^{3.78613}(d/B)^{1.07961}(90-i_E)^{-1.37565} \tag{2.182}$$

$$c_7 = \begin{cases} 0.229577(B/L)^{1/3} & \text{for } B/L < 0.11 \\ B/L & \text{for } 0.11 < B/L < 0.25 \\ 0.5 - 0.0625L/B & \text{for } B/L > 0.25 \end{cases} \tag{2.183}$$

$$c_2 = \exp(-1.89\sqrt{c_3}) \tag{2.184}$$

$$c_3 = \frac{0.56A_{Bd}^{1.5}}{\left\{Bd(0.31\sqrt{A_{BT}}+d-h_B)\right\}} \tag{2.185}$$

c_2 is a parameter which accounts for the reduction of the wave resistance due to the bulbous bow and c_3 the coefficient that determines the influence of the bulbous bow on the wave resistance with h_B is the center position of the transverse area of the bulb A_{BT}

above the keel line. Another coefficient in Eq.(2.181) is c_5 which can be given as follows

$$c_5 = 1 - 0.8A_T/(BdC_M) \tag{2.186}$$

where A_T represents the immersed part of the transverse area of the transom at zero speed and C_M the coefficient of midship. The other parameters in Eq.(2.181) can be computed as follow

$$\lambda = \begin{cases} 1.446C_P - 0.03L/B & \text{for } B/L < 12 \\ 1.446C_P - 0.36 & \text{for } B/L > 12 \end{cases} \tag{2.187}$$

$$m_1 = 0.0140407L/d - 1.75254\nabla^{1/3}/L - 4.79323B/L - c_{16} \tag{2.188}$$

$$c_{16} = \begin{cases} 8.07981C_P - 13.8673C_P^2 + 6.984388C_P^3 & \text{for } C_P < 0.80 \\ 1.73014 - 0.7067C_P & \text{for } C_P > 0.80 \end{cases} \tag{2.189}$$

$$m_2 = c_{15}C_P^2 \exp(-0.1F_n^{-2}) \tag{2.190}$$

$$c_{15} = \begin{cases} -1.69385 & \text{for } L^3/\nabla < 512 \\ -1.69385 + (L/\nabla^{1/3} - 8.0)/2.36 & \text{for } 512 < L^3/\nabla < 1727 \\ 0 & \text{for } L^3/\nabla > 1727 \end{cases} \tag{2.191}$$

In Eq.(2.182), i_E denotes the half angle of entrance of the waterline in degrees measured at the bow with reference to the ship center plane. ∇ appearing above is the ship displacement and C_P the coefficient of prismatic. Hence the steady wave-making coefficient can be obtained and given in a nondimensional form as

$$C_W = \frac{R_W}{\frac{1}{2}\rho S U^2} \tag{2.192}$$

with S indicates the wetted surface area of a ship.

Chapter 3

Computed Models

3.1 Modified Wigley Model

For the purpose of establishing a new BCGA and to examine its performance in connection with the EUT, a modified Wigley model with blunt-bow coefficients is employed in this optimization as a basis ship geometry. The hull geometry of this model can be expressed mathematically in the form

$$\left.\begin{aligned} \eta = (1-\zeta^2)(1-\xi^2)(1+0.6\xi^2+\xi^4) + \zeta^2(1-\zeta^8)(1-\xi^2)^4 \\ \xi = \frac{x}{(L/2)}, \quad \eta = \frac{y}{B/2}, \quad \zeta = \frac{z}{d} \end{aligned}\right\} \tag{3.1}$$

The computation is performed at $Fn = 0.20$ in the range of wavelength ratio of incident wave, $\lambda/L = 0.3 \sim 2.0$. Furthermore, the main dimensions of the ship model and the parameters used in the computation are given in Table 3.1 below.

TABLE 3.1: Principal particular of modified Wigley model

Item	**Value**	**Unit**
Length (L)	2.500	m
Breadth (B)	0.500	m
Draft (d)	0.175	m
Block coefficient (C_B)	0.6342	-
Midship coefficient (C_M)	0.9088	-
Prismatic coefficient (C_P)	0.6979	-
Waterplane coefficient (C_{WP})	0.8038	-
Displacement (∇)	0.1388	m^3
Center of gravity (OG)	0.031	m
Pitch gyrational radius (K_{yy}/L)	0.236	-
Froude Number (Fn)	0.20	-
Wavelength ratio (λ/L)	$0.30 \sim 2.00$	-

Because this optimization is dealing with the Sectional Area Curve (SAC), it is necessary to show SAC of modified Wigley model as depicted in Fig. 3.1. The body plan and perspective view of this model are also shown in Fig. 3.2 and Fig. 3.3, respectively.

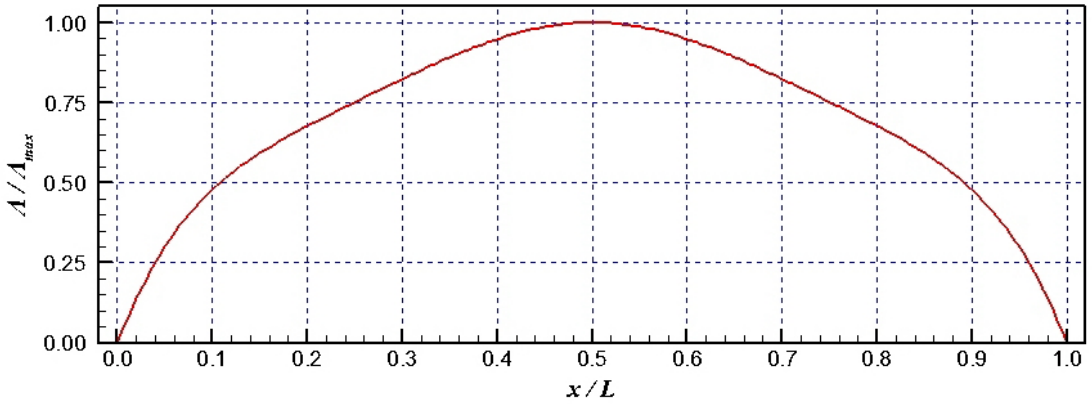

FIGURE 3.1: SAC of modified Wigley model

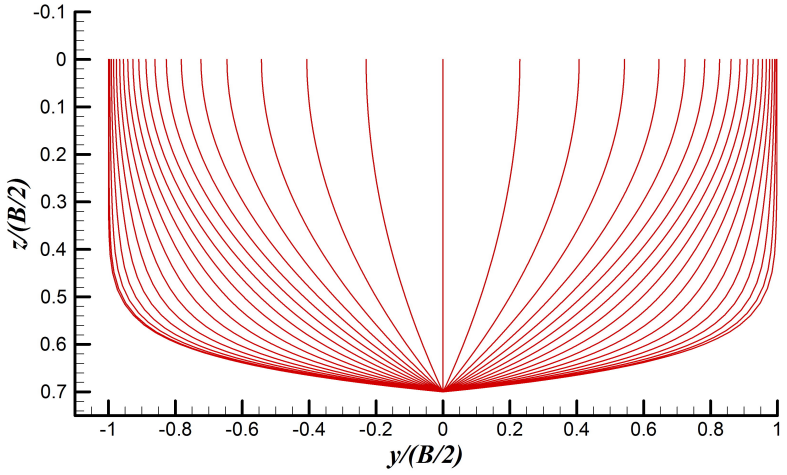

FIGURE 3.2: Body plan of modified Wigley model

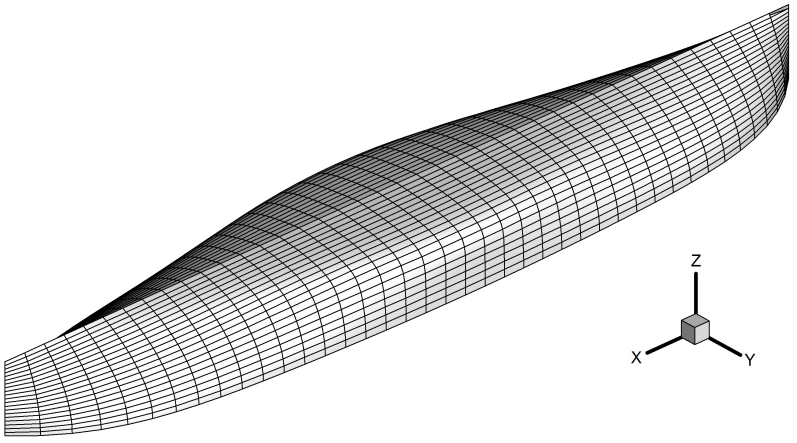

FIGURE 3.3: Perspective view of modified Wigley model

From Figs.3.1 and 3.2, we are able to see that this modified Wigley model is symmetric with respect to both $x = 0$ and $y = 0$. Because of its symmetricity with respect to $x = 0$, contribution from restoring coefficient of coupled motions between heave and pitch in Eq.(2.172) is equal to zero.

3.2 Container Ship SR-108

In addition to the modified Wigley model, a real container ship SR-108 will also be optimized in order to confirm and illustrate the effectiveness and efficiency of the present practical integrated optimization method. The principal dimensions of SR-108 are given in the following Table 3.2.

TABLE 3.2: Principal particular of SR-108

Item	**Value**	**Unit**
Length (L_{PP})	175.00	m
Breadth (B)	25.400	m
Draft (d)	9.5000	m
Block coefficient (C_B)	0.5719	-
Midship coefficient (C_M)	0.9700	-
Prismatic coefficient (C_P)	0.5895	-
Waterplane coefficient (C_{WP})	0.7111	-
Displacement (∇)	24149.907	m^3
Froude number (Fn)	0.20	-
Incident wave angle (χ)	180	degree

The perspective view of SR-108 is depicted in the following Fig. 3.4.

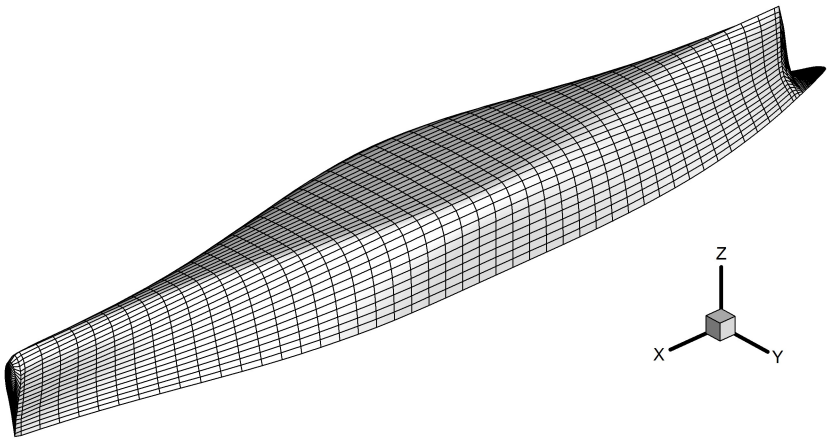

FIGURE 3.4: Perspective view of SR-108

The body plan and SAC of SR-108 are also given in the following Fig. 3.5 and Fig. 3.6.

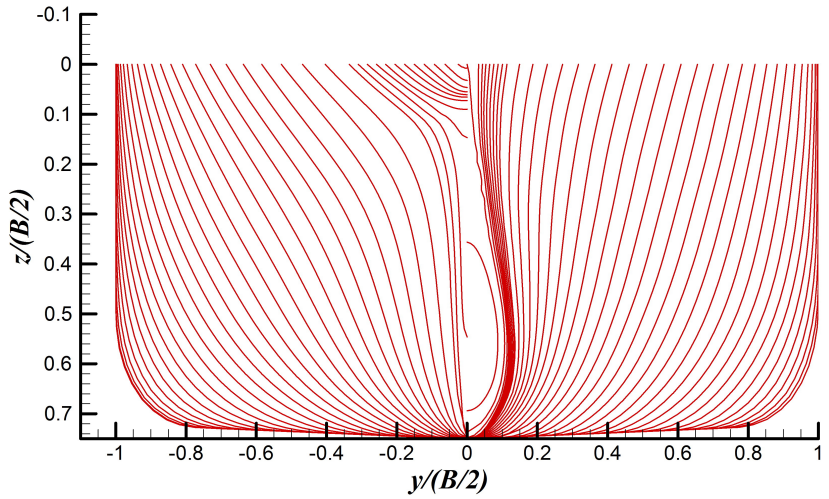

FIGURE 3.5: Body plan of SR-108

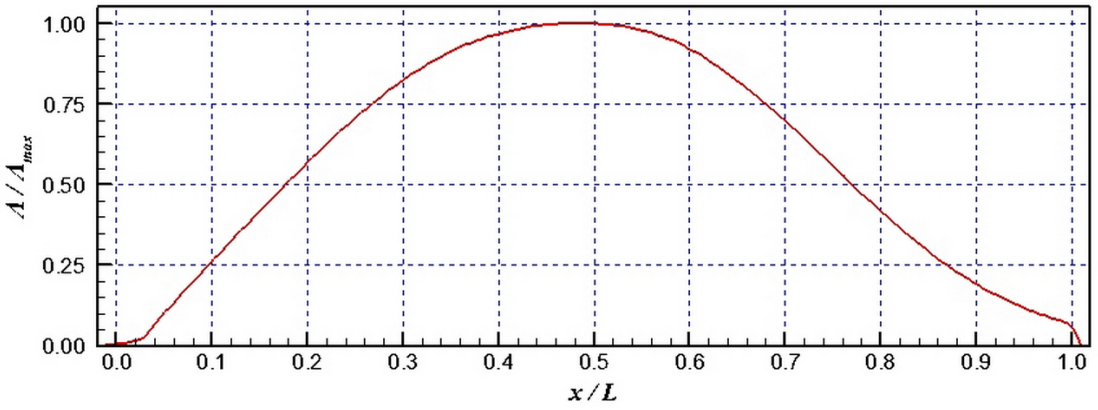

FIGURE 3.6: SAC of SR-108

Needless to say that in this optimization the principal dimensions of ship are kept constant. Therefore the shifting method used in this optimization will only shift the stations between after peak and fore peak stations, excluding a station in which the sectional area becomes maximum.

Chapter 4

Study on Added Resistance

4.1 Sensitivity of a Peak Value of the Added Resistance

In order to reduce the added resistance in waves, it is necessary to understand its sensitivity to the ship motions, particularly the peak value of the added resistance. In sensitivity study, we check sensitivity of the peak value of the added resistance to the amplitude and phase difference of ship motions [1]. To this end, a calculation of the added resistance by using measured (experiment) data will be performed. In this case, experiment data which can be only the amplitude or only the phase or both of them for each mode of ship motions will be used in computing the added resistance.

Because the added resistance in head waves can be computed only from symmetric modes of motion (surge, heave and pitch), only these modes will be considered. In order to realize sensitivity of the peak value of the added resistance to the ship motions, it is necessary to show discrepancy between experiment data and computed one by EUT for the amplitude and phase of ship motions as shown in Figs. 4.1, 4.2 and 4.3.

Considering only the wavelength where the added resistance becomes maximum that is at the middle wavelength region around $\lambda/L = 1.1$, then we can see the amount of discrepancy between those data for ship motions. However the phase difference in pitch motion between experiment and computed data is almost zero. Corresponding to those figures, the resulting added resistance can be depicted in Fig. 4.4 through Fig. 4.6. At those figures, blue square, green triangle and orange gradient represent the value of the added resistance computed from the experiment data in both amplitude and phase difference, only amplitude and only phase difference, respectively. Meanwhile red line represents the added resistance computed from numerical result (computed data) of ship motions.

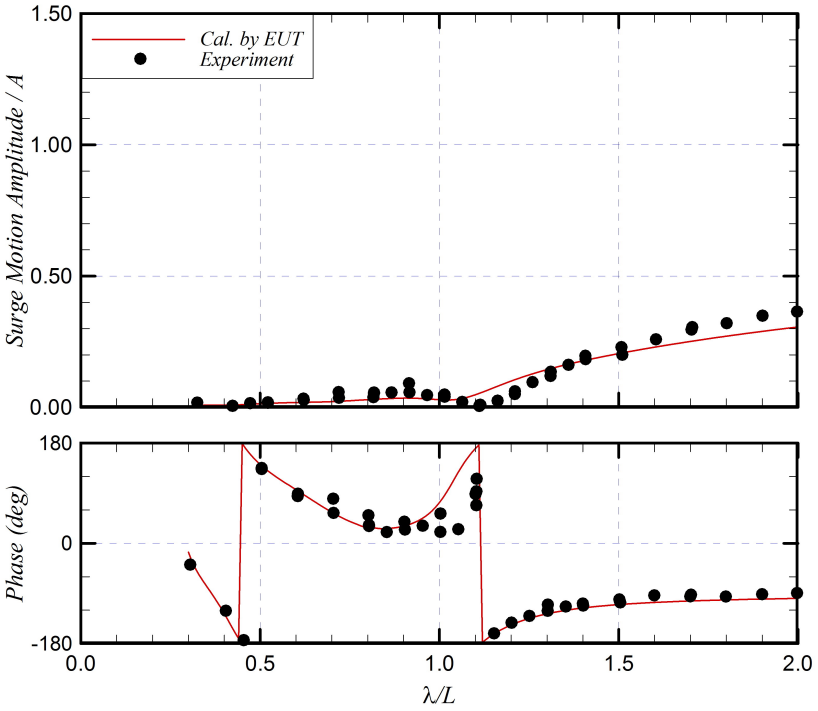

FIGURE 4.1: Amplitude and phase of surge motion

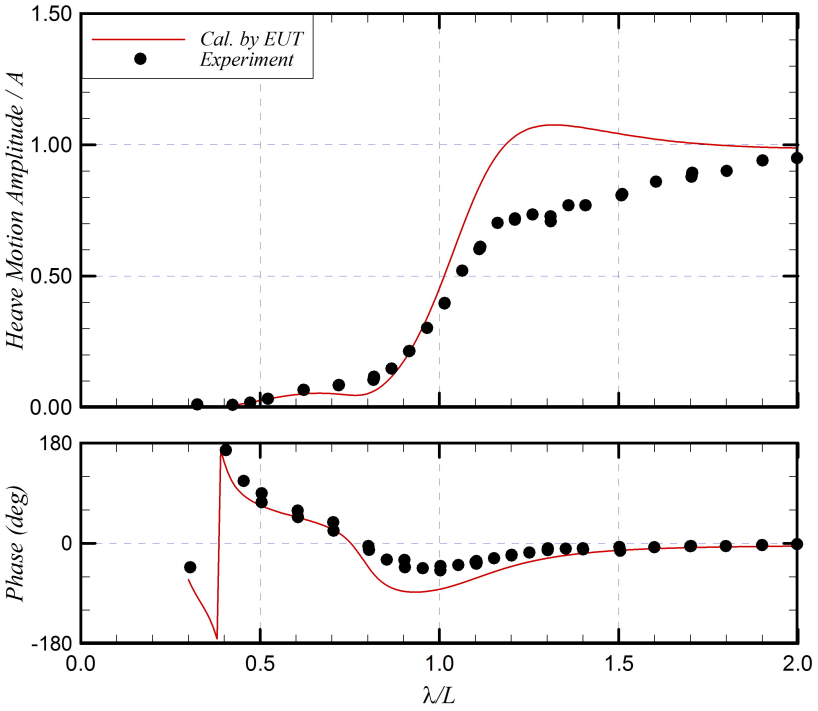

FIGURE 4.2: Amplitude and phase of heave motion

Figure 4.1 shows the differences between measured data and computed result of surge motion for both amplitude and phase difference. Although these discrepancies can be observed, all corresponding results of the added resistance are almost the same as shown in Fig. 4.4. It means that the peak value of added resistance is not sensitive to the

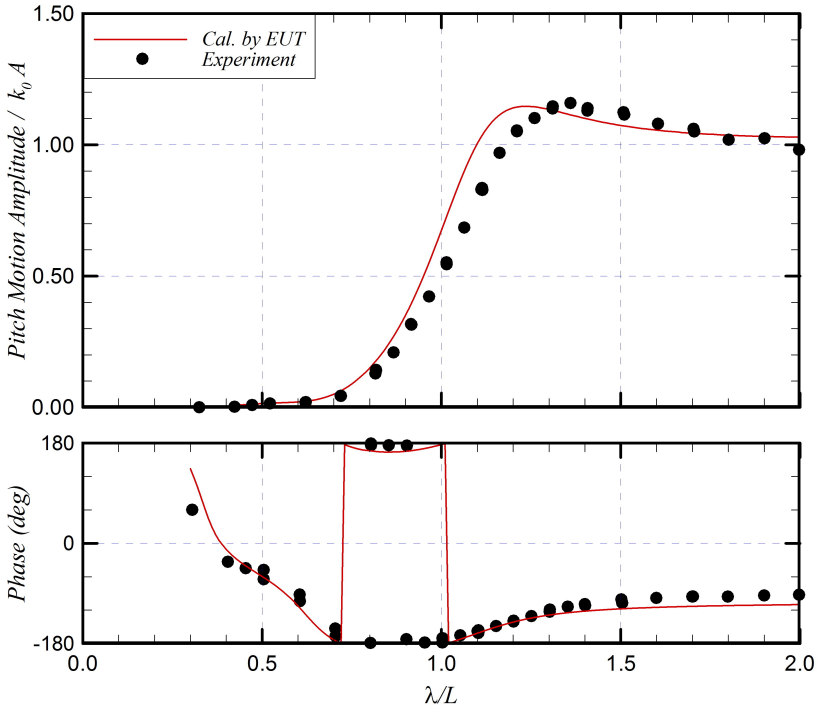

FIGURE 4.3: Amplitude and phase of pitch motion

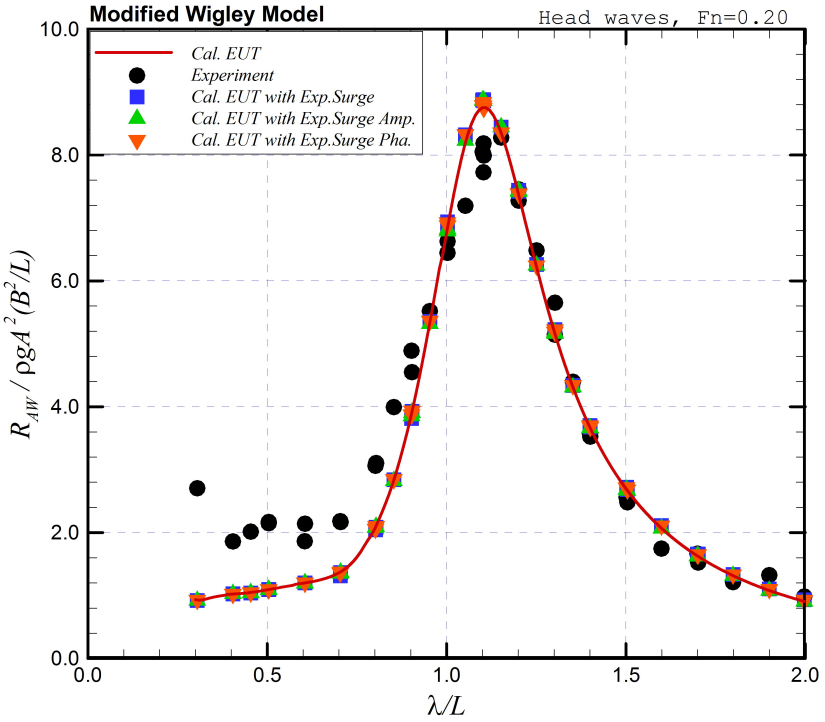

FIGURE 4.4: Added resistance from measured and computed data of surge motion

surge motion in both amplitude and phase difference and hence it can be neglected. In case of heave motion, discrepancy of amplitude and phase difference between measured and computed data is shown in Fig. 4.2. Using measured data, the peak value of added

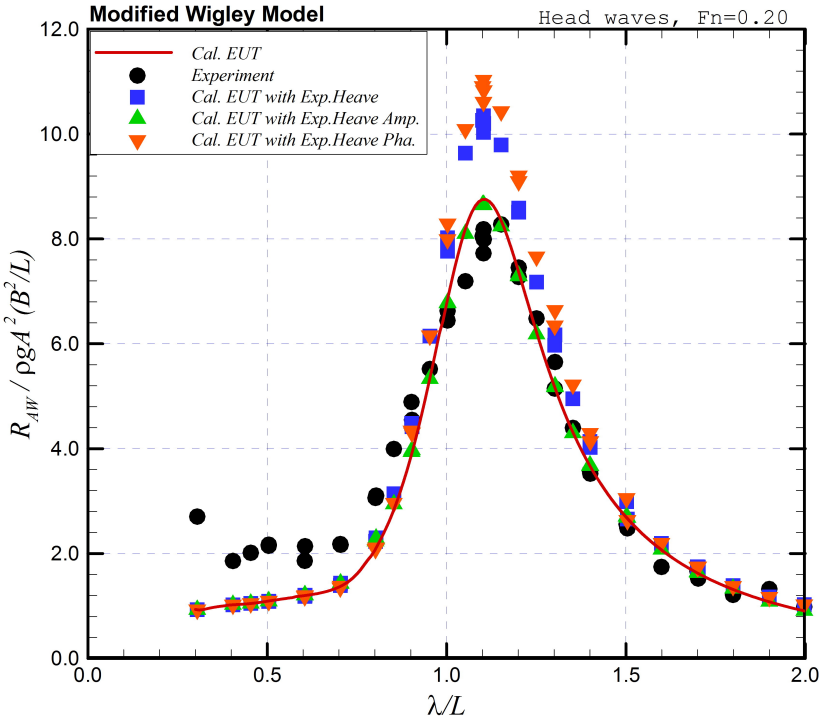

FIGURE 4.5: Added resistance from measured and computed data of heave motion

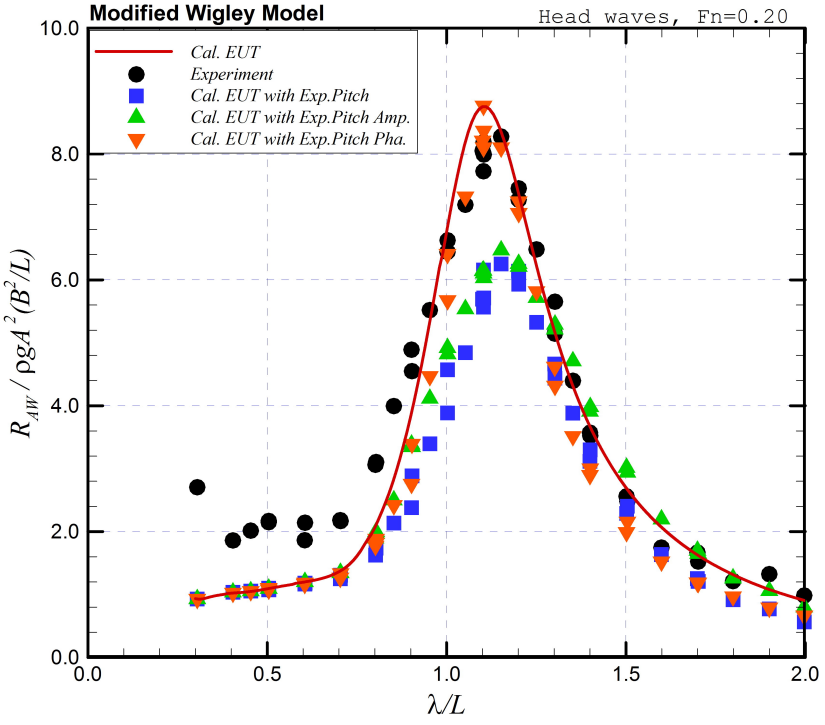

FIGURE 4.6: Added resistance from measured and computed data of pitch motion

resistance changes drastically compared to the original one (computed data) as depicted by blue square in Fig. 4.5. Thus it allows us to say that the peak value of added resistance is sensitive to the heave motion. However green triangle and orange gradient

reveal that the peak value of added resistance is only sensitive to the phase difference of heave motion.

In Fig. 4.3, it is shown that the pitch amplitude of measured data is different from computed one; however discrepancy in phase difference cannot be observed. Computing the added resistance using measured data makes aware that its peak value decreases significantly which is shown as blue square in Fig. 4.6. Even only using the amplitude of measured data, the corresponding added resistance is also changed which is similar when using both amplitude and phase difference of pitch motion of measured data. Thus we may say that the peak value of added resistance is sensitive to the amplitude of pitch motion.

4.2 Relative Importance of Each Term in Added Resistance

Apart from previous investigations, now let us investigate the contribution from each term of the Kochin function in the equation of added resistance as in Eq.(2.175) or Eq.(2.177). As we can see in this equation, the added resistance consists of three terms that are diffraction term, radiation term and cross-term between diffraction and radiation. According to the sensitivity study, the surge motion is not influential in determination of the peak value of added resistance. Thus in the following investigation, the contribution from this term can be neglected. The corresponding results of the added resistance from each term of the Kochin function is shown in Fig. 4.7.

It is well-known that the most important component in the added resistance in the short wavelength region is the contribution from diffraction component. However in the subsequent wavelength, the radiation component becomes important and gives the largest contribution to the added resistance as well as the cross-term between diffraction and radiation waves which is in opposite sign as clearly shown also in Fig. 4.7.

In order to realize which motion is the most important in the radiation waves, this term may be decomposed further for each mode of motion or combination between them. These decompositions can be written as follow

$$R_{AW}^{(HH)} = \frac{K}{4\pi}\left[-\int_{-\infty}^{k_1}+\int_{k_2}^{k_3}+\int_{k_4}^{\infty}\right]|\xi_3 H_3(k)|^2\,\frac{\kappa}{\sqrt{\kappa^2-k^2}}(k+k_0)dk \tag{4.1}$$

$$R_{AW}^{(PP)} = \frac{K}{4\pi}\left[-\int_{-\infty}^{k_1}+\int_{k_2}^{k_3}+\int_{k_4}^{\infty}\right]|\xi_5 H_5(k)|^2\,\frac{\kappa}{\sqrt{\kappa^2-k^2}}(k+k_0)dk \tag{4.2}$$

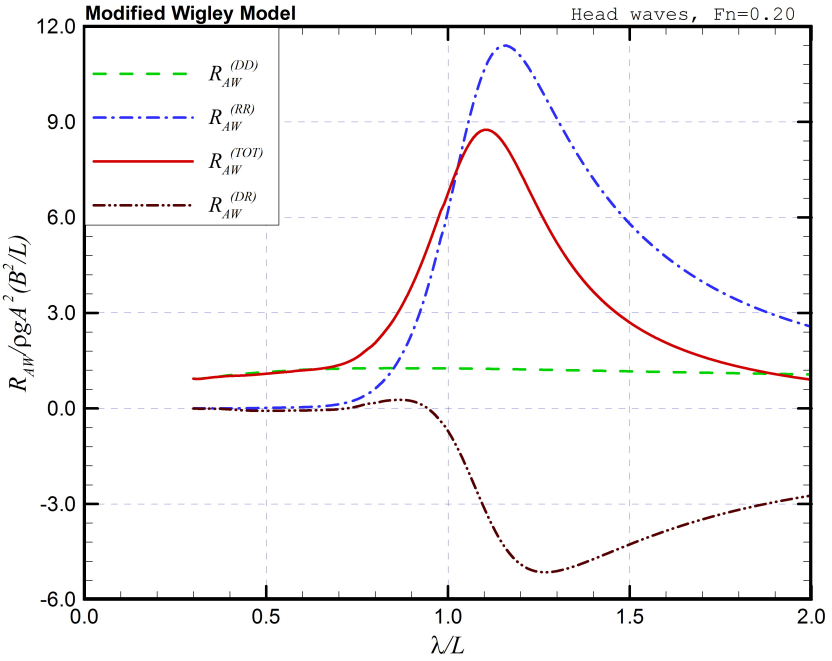

FIGURE 4.7: Relative importance of each term in added resistance

The added resistance due to these decompositions can be seen in Fig. 4.8. Meanwhile the cross-term can also be decomposed for combination between diffraction and radiation terms as shown in Fig. 4.9 which can be given in the following equations.

$$R_{AW}^{(DH)} = -\frac{\sqrt{K}}{2\pi\sqrt{k_0}}\left[-\int_{-\infty}^{k_1}+\int_{k_2}^{k_3}+\int_{k_4}^{\infty}\right]\Re[H_7(k)\{\xi_3 H_3(k)\}^*]\frac{\kappa(k+k_0)}{\sqrt{\kappa^2-k^2}}dk \quad (4.3)$$

$$R_{AW}^{(DP)} = -\frac{\sqrt{K}}{2\pi\sqrt{k_0}}\left[-\int_{-\infty}^{k_1}+\int_{k_2}^{k_3}+\int_{k_4}^{\infty}\right]\Re[H_7(k)\{\xi_5 H_5(k)\}^*]\frac{\kappa(k+k_0)}{\sqrt{\kappa^2-k^2}}dk \quad (4.4)$$

$$R_{AW}^{(HP)} = -\frac{\sqrt{K}}{2\pi\sqrt{k_0}}\left[-\int_{-\infty}^{k_1}+\int_{k_2}^{k_3}+\int_{k_4}^{\infty}\right]\Re[\xi_3 H_3(k)\{\xi_5 H_5(k)\}^*]\frac{\kappa(k+k_0)}{\sqrt{\kappa^2-k^2}}dk \quad (4.5)$$

According to Fig. 4.8, the largest contribution to the peak value of added resistance arises from the Kochin function of pitch motion. A reason for this might be due to the sensitivity of the peak value of added resistance to the pitch motion in both amplitude and phase difference. Besides that, this figure also shows that the wavelength where the added resistance in terms of pitch motion (brown dashed-double-dotted line) takes its maximum coincides with the wavelength where the added resistance due to radiation component (blue dashe-dotted line) becomes maximum. It means that the pitch motion also plays an important role in determining the peak frequency of added resistance due to radiation and even in determination of the peak frequency of total added resistance (red solid line).

Nevertheless the peak frequency of added resistance due to pitch motion is slightly different with the peak frequency of total added resistance. It might be mainly attributed

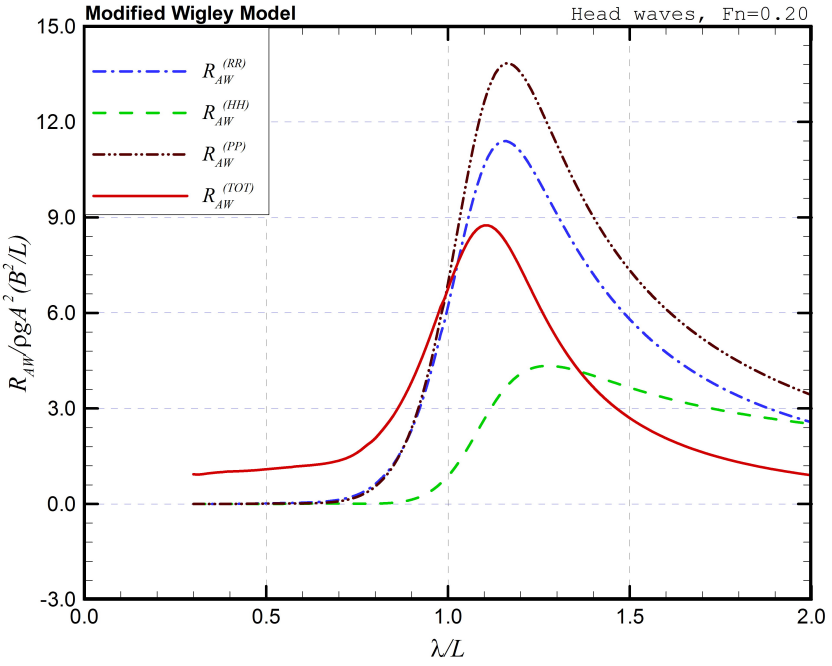

FIGURE 4.8: Relative importance of each term in radiation waves

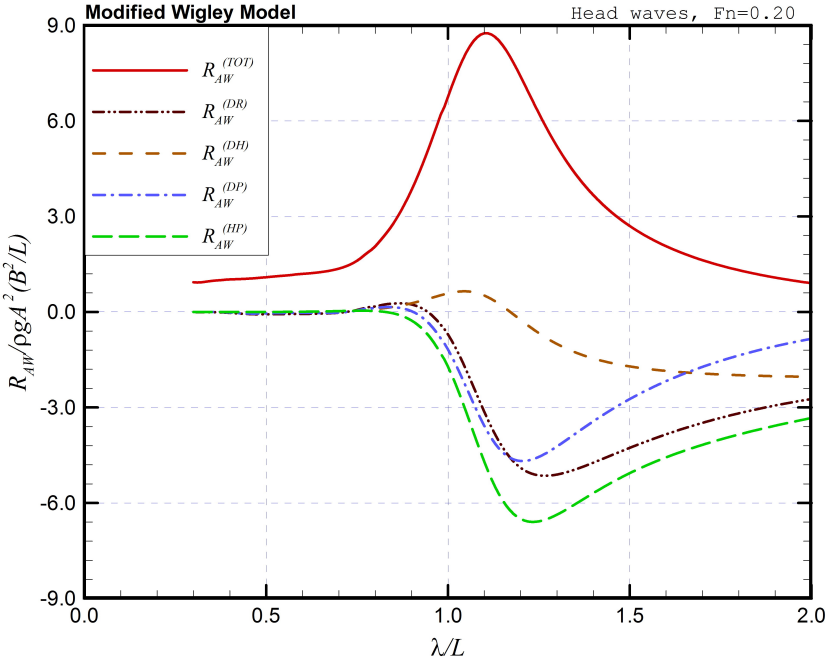

FIGURE 4.9: Relative importance of each term in cross-terms between scattered and radiation waves

to the effects of damping coefficients and coupled motions in Eq.(2.171). Based on these results, it can be concluded that the pitch motion is the most important part in determining the peak value of the added resistance. Thus it will be used as primary fitness function in addition to the total added resistance as a secondary fitness function during optimization process, particularly in optimizing the SR-108 at middle wavelengths.

On the other hand, the cross term between heave and pitch motions represented as green long-dashed line in Fig. 4.9 gives the largest reduction to the added resistance, especially near the peak. In addition, the cross term contribution of diffraction and pitch motion also reduces the added resistance around its peak given as blue dashed-dotted line on the same figure. Having a close look to Fig. 4.9, then we could realize that all of the cross terms become negative before $\lambda/L = 1.0$, except that of a cross term between diffraction and heave motion (light brown dashed line). It becomes negative after the total added resistance reaches its maximum, thus it implies that this cross term increases the peak value of the added resistance in reverse with other cross terms.

Chapter 5

Variation of Ship Hull Geometry by Shifting Method

Because the principle of the shifting method is adopted during optimization, it might be useful to understand the characteristics of SAC of the new ship hull geometry directly generated by this method. It should be noted here that in the shifting method, a new ship hull geometry may be derived from the following three cases [17]:

- Varying the block coefficient (C_B)
- Shifting the longitudinal center of buoyancy (L_{CB})
- Introducing the parallel middle body (P_{MB})

In this chapter, the above three cases will be discussed in details. The effect of changing those three parameters will also be investigated.

5.1 Varying the Block Coefficient (C_B)

Let us begin to derive a new hull geometry of ship by changing its C_B. In this case C_B of a basis hull geometry, namely the modified Wigley model is set to $C_B = 0.60$ and $C_B = 0.70$ from its original value as shown in Table 3.1. By using the Lackenby's transformation given in Eq.(2.8) to Eq.(2.12), the necessary shift (δx) in the x-axis can be obtained. Thus the corresponding sectional area curve resulting from change in C_B is given in Fig. 5.1. Due to variation of C_B in Fig. 5.1, the ship displacement (∇) will change to $\nabla = 0.13125$ (m^3) and $\nabla = 0.15313$ (m^3) for $C_B = 0.60$ and $C_B = 0.70$,

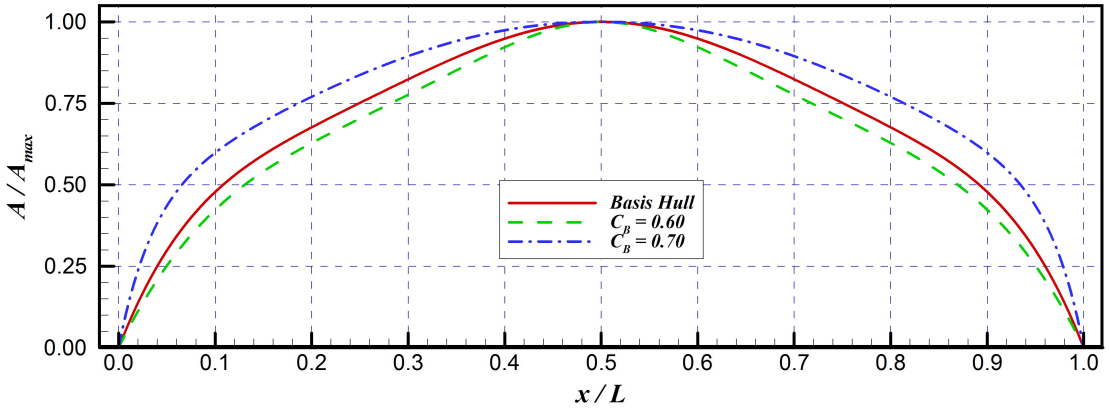

FIGURE 5.1: SAC of varying C_B

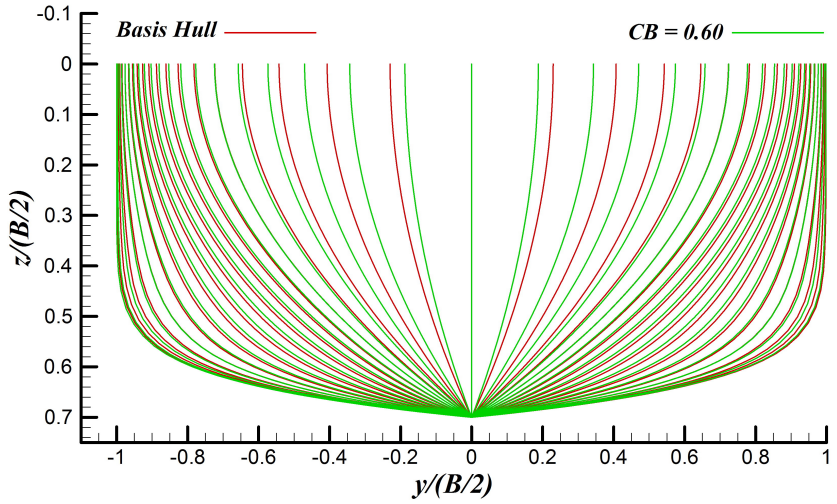

(a) Body plan

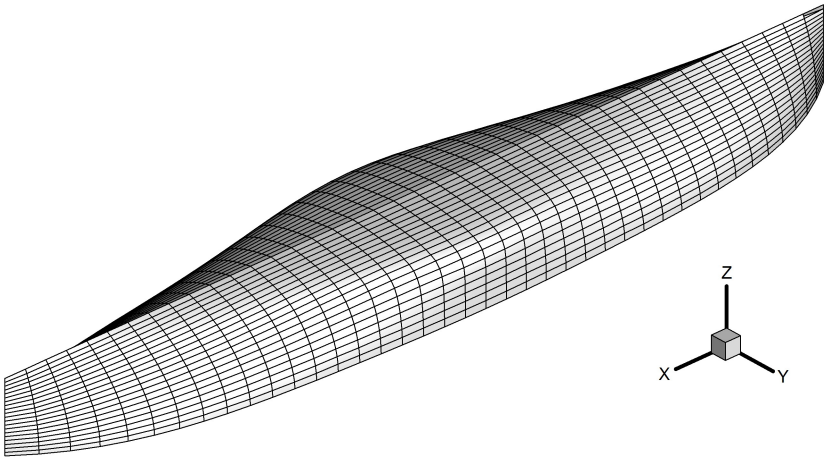

(b) Perspective view

FIGURE 5.2: Body plan and perspective view of $C_B = 0.60$

respectively. The body plan and perspective view of both of them are shown in Figs.5.2 and 5.3 for $C_B = 0.60$ and $C_B = 0.70$, respectively.

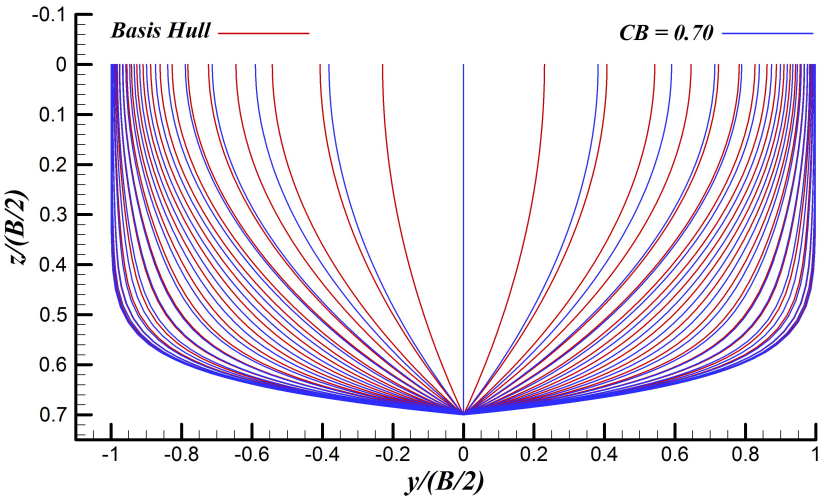

(a) Body plan

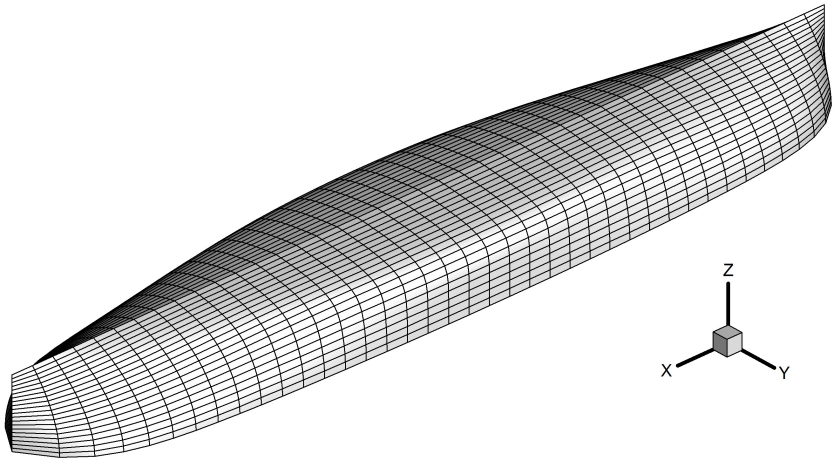

(b) Perspective view

FIGURE 5.3: Body plan and perspective view of $C_B = 0.70$

The corresponding results of comparisons for surge, heave and pitch motions at $Fn = 0.20$ between basis hull and derived hull forms are presented in Fig. 5.4 through Fig. 5.6. In Fig. 5.4 for the surge motion, we can see that decreasing the block coefficient tends to increase the surge motion. In another word, a large C_B will decrease this motion. This trend can also be observed for the case of heave and pitch motions as shown in Figs. 5.5 and 5.6. It means that increasing C_B will decrease the amplitude of symmetric mode of motions. The corresponding results of the added resistance resulting from this case is depicted in Fig. 5.7

In the previous chapter, we confirmed that the amplitude of pitch motion as well as the phase difference of heave and pitch motions are sensitive to the peak value of the added resistance. Thus judging from Figs. 5.5 and 5.6, one may envisage that the resulting added resistance will reduce relatively largely. However, in this case it is clearly shown in Fig. 5.7 that only small quantity of the added resistance diminishes about its peak

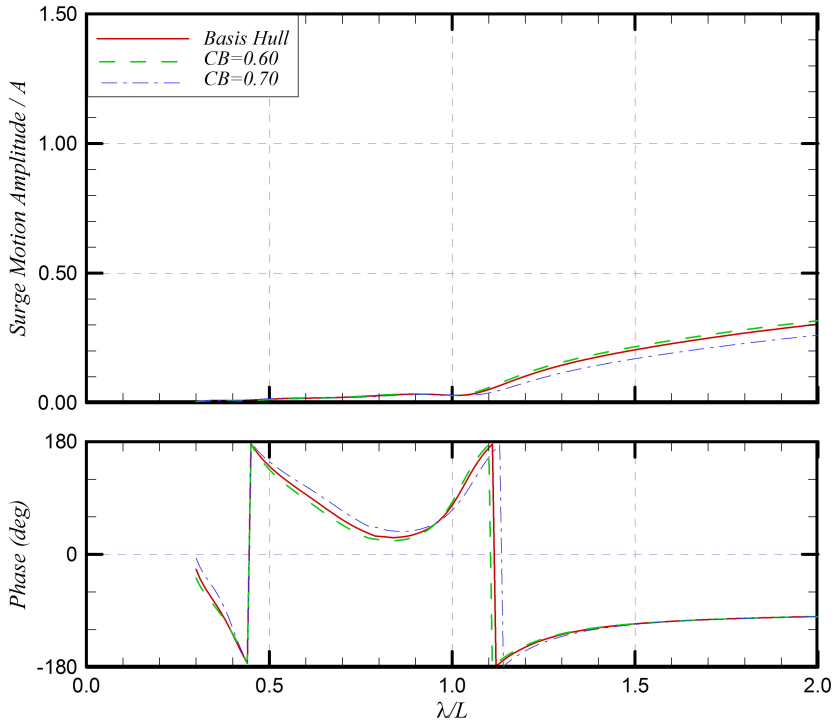

FIGURE 5.4: Surge motion of varying C_B

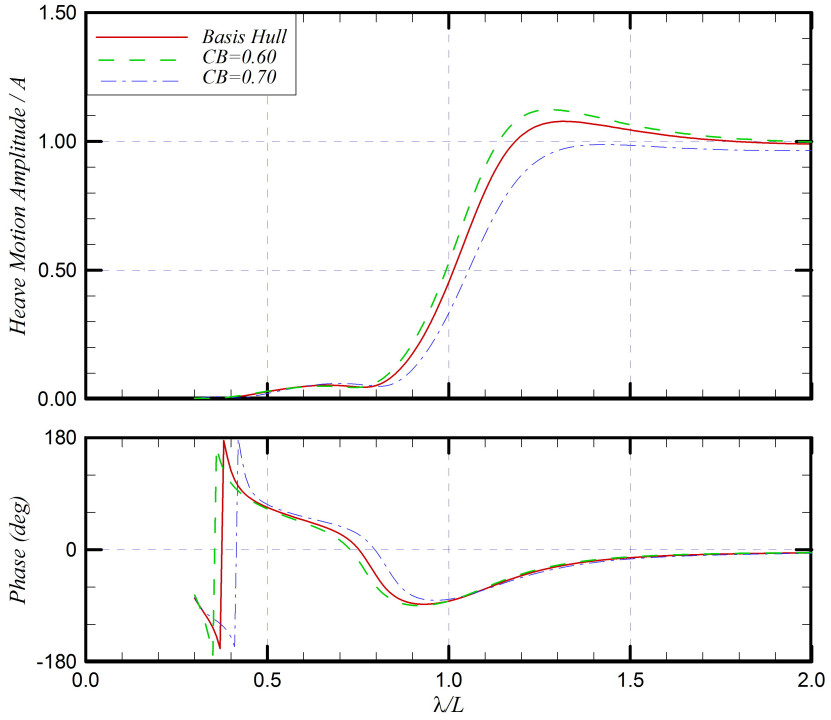

FIGURE 5.5: Heave motion of varying C_B

although the amplitude of heave and pitch motions decrease fairly large with similar phase difference of both of them. It implies that only the pitch amplitude gives a large contribution to such reduction. It is also observed in the same figure that the added resistance in the shorter wavelengths region increases for the case of $C_B = 0.70$. It

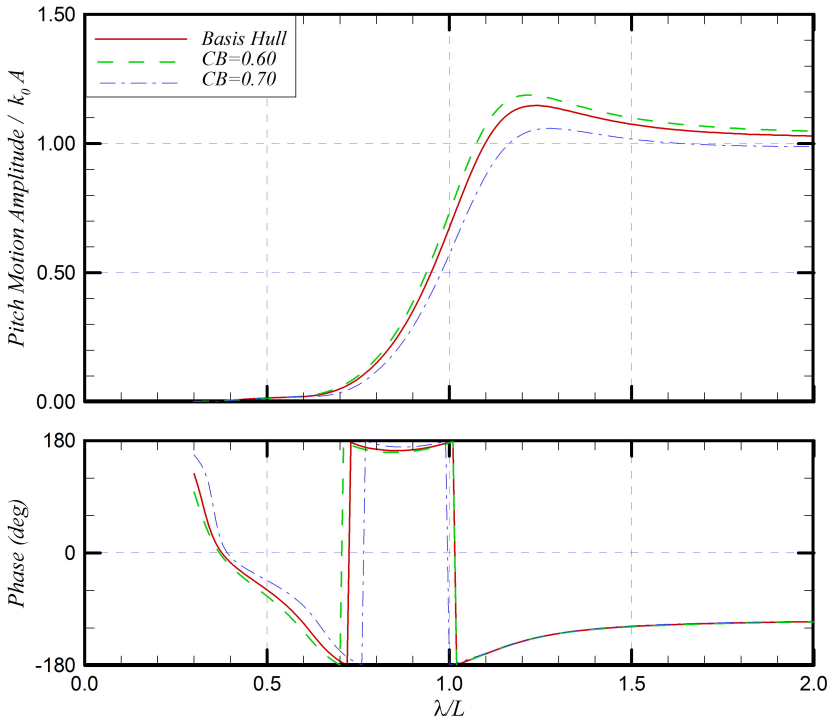

FIGURE 5.6: Pitch motion of varying C_B

might be attributed to the larger amplitude of Kochin function at transverse section, especially in the diffraction problem; that is, this increase might be induced by numerical irregularity and hence probably not real.

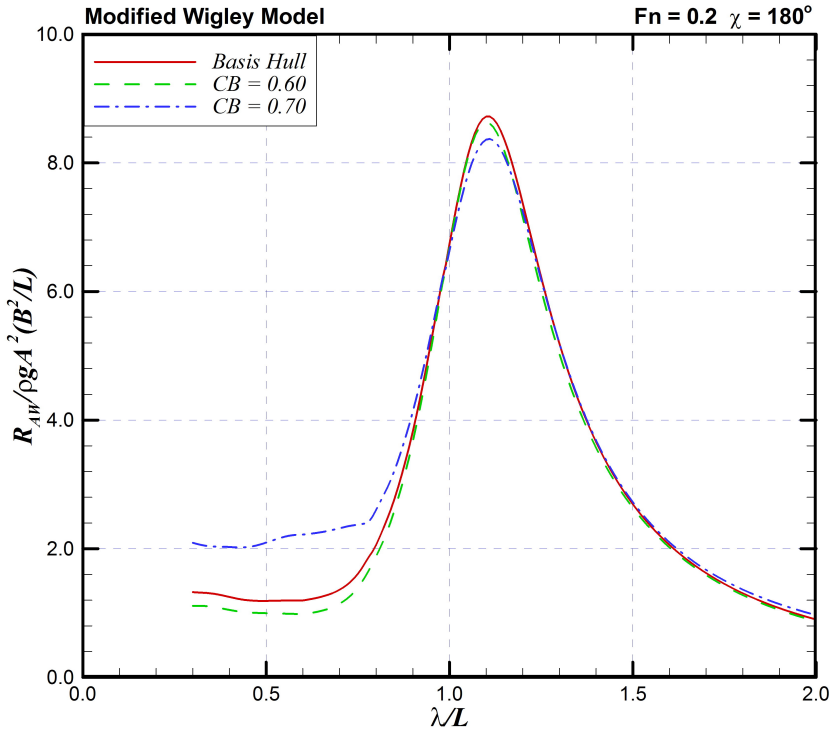

FIGURE 5.7: Added resistance of varying C_B

5.2 Shifting the Longitudinal Center of Buoyancy (L_{CB})

In this case, the longitudinal center of buoyancy is shifted about 0.05 (m) towards ship's stern and bow without changing the principal particulars of a ship, including its C_B. For the case of shifting L_{CB} towards ship's stern, the stern part becomes blunter and fore part finer. It can be seen clearly through its body plan and perspective view as given in Fig. 5.8. The body plan and perspective view of shifting L_{CB} towards ship's bow are elucidated in Fig. 5.9. The comparison of SAC among them is shown in Fig. 5.10.

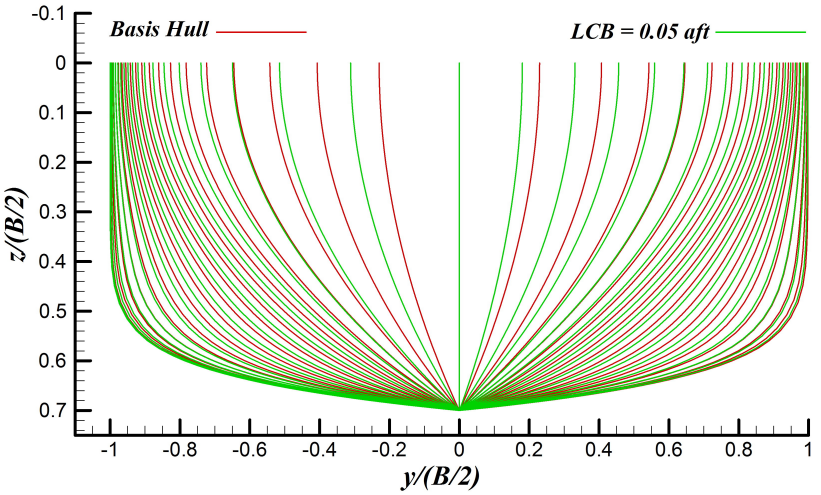

(a) Body plan

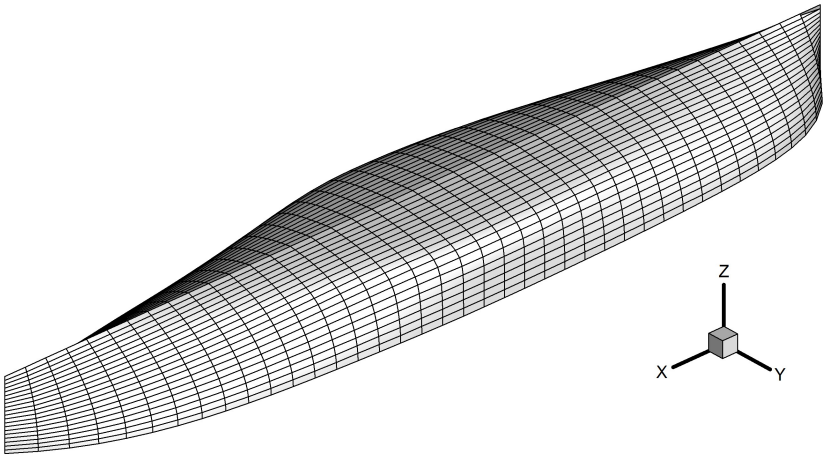

(b) Perspective view

FIGURE 5.8: Body plan and perspective view of shifting $L_{CB} = 0.05$ aft

The symmetric modes of ship motions resulting from this case are shown in Fig. 5.11 through Fig. 5.13. Figure 5.11 reveals that the effect of shifting L_{CB} for surge motion is very small. For heave motion, shifting the L_{CB} affects the heave motion which increases its amplitude as L_{CB} shifted towards ship's bow as shown in Fig. 5.12. Different with

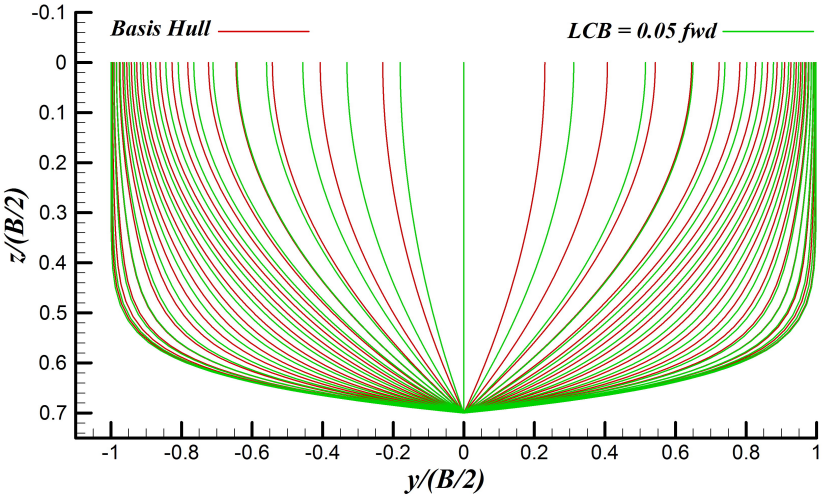

(a) Body plan

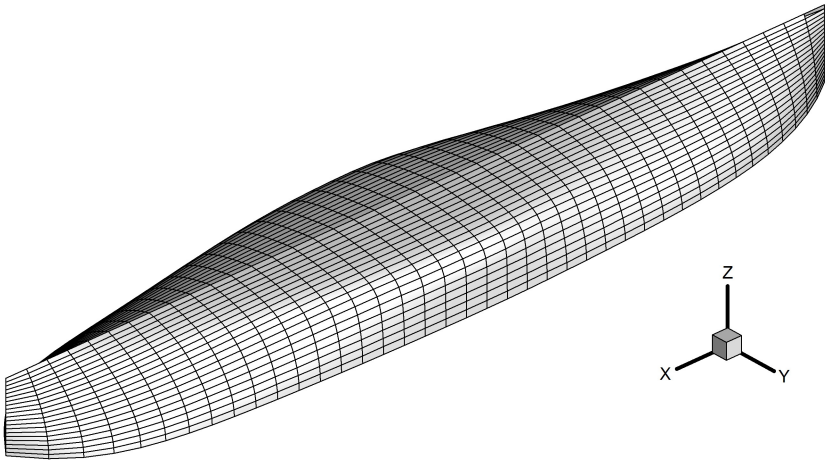

(b) Perspective view

FIGURE 5.9: Body plan and perspective view of shifting $L_{CB} = 0.05$ fwd

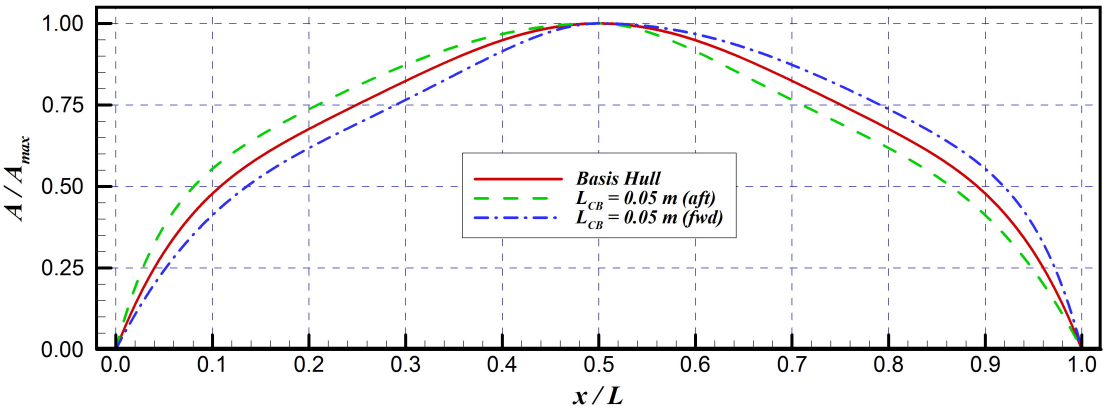

FIGURE 5.10: SAC of shifting L_{CB}

heave motion, the amplitude of pitch motion decreases as the L_{CB} shifted forward and its phase also changes to some little extent which is depicted in Fig. 5.13.

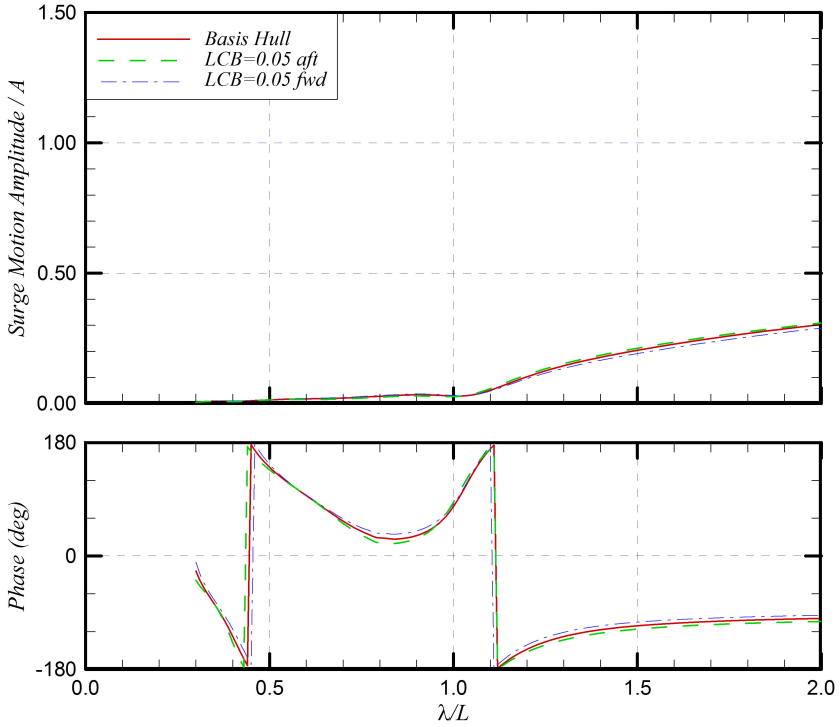

FIGURE 5.11: Surge motion of shifting L_{CB}

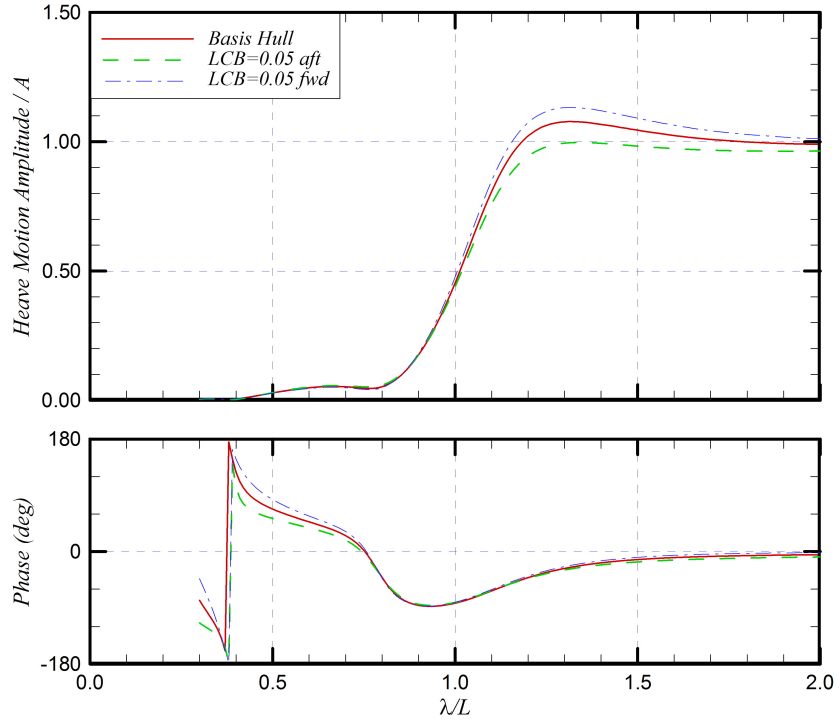

FIGURE 5.12: Heave motion of shifting L_{CB}

As a consequence, the added resistance changes depending on the direction where L_{CB} moves. This change in the added resistance is shown in Fig. 5.14. From this figure, we could observe that shifting L_{CB} towards ship's bow reduces the added resistance, particularly around its peak to longer waves due to the sensitivity of the pitch motion

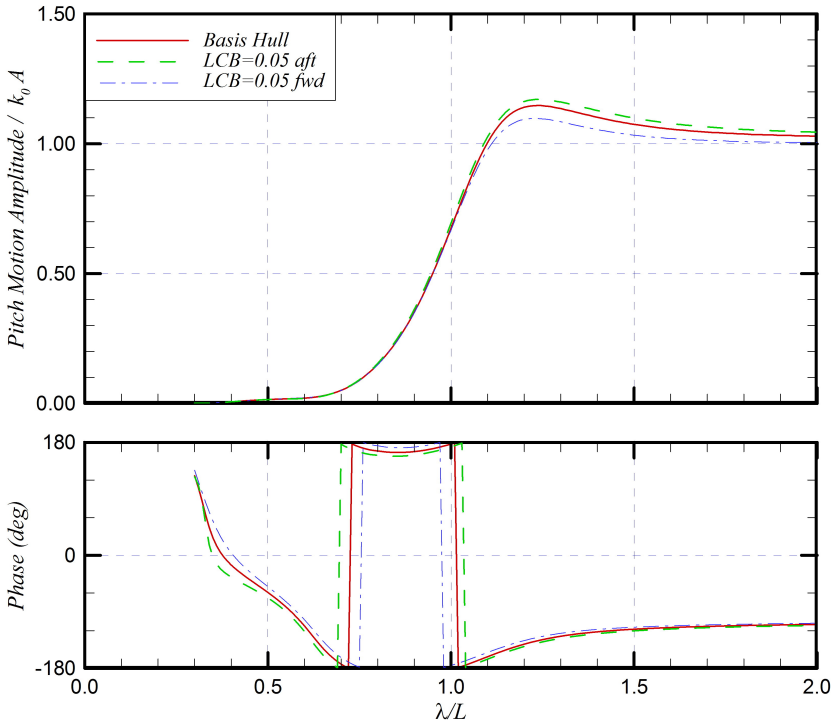

FIGURE 5.13: Pitch motion of shifting L_{CB}

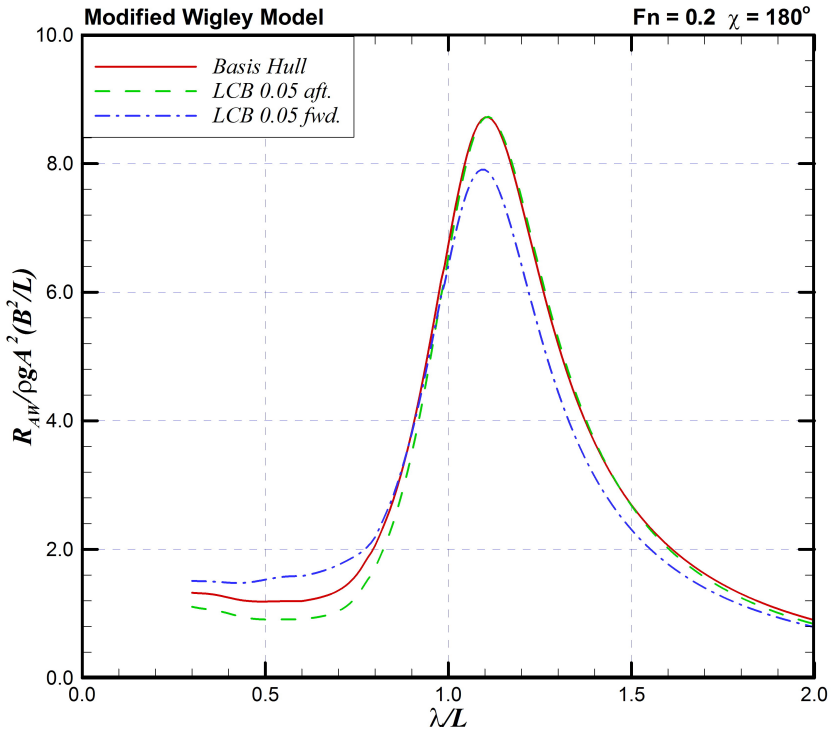

FIGURE 5.14: Added resistance of shifting L_{CB}

in both amplitude and phase difference to the peak of added resistance. However, the added resistance increases at the shorter wavelengths region. The reason for this is owing to the larger amplitude of Kochin function at transverse section near the bow

in the diffraction problem as its bow shape becomes blunter. On the other hand, the bow shape becomes finer as L_{CB} shifted towards ship's stern; hence diffracts less waves than that of the basis hull. Therefore the corresponding results of the added resistance decreases around shorter wavelengths region which is also shown in Fig. 5.14.

5.3 Introducing the Parallel Middle Body (P_{MB})

In case of introducing the parallel middle body (P_{MB}), we insert the P_{MB} to the basis hull without increasing C_B. In this case we insert P_{MB} to aft- and fore-bodies with length of 0.15 (m), respectively and to the middle body with equal distance. For the case of inserting P_{MB} to the aft- and fore-bodies, the body plan and perspective view of them are given in Fig. 5.15 and Fig. 5.16, respectively.

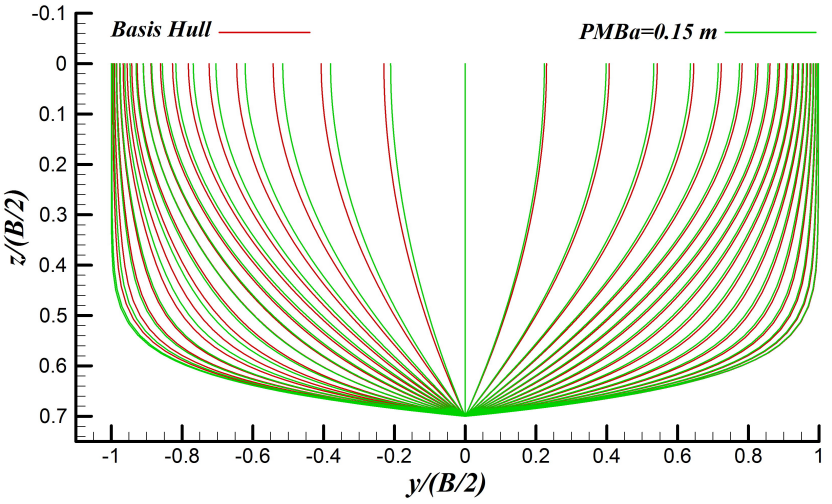

(a) Body plan

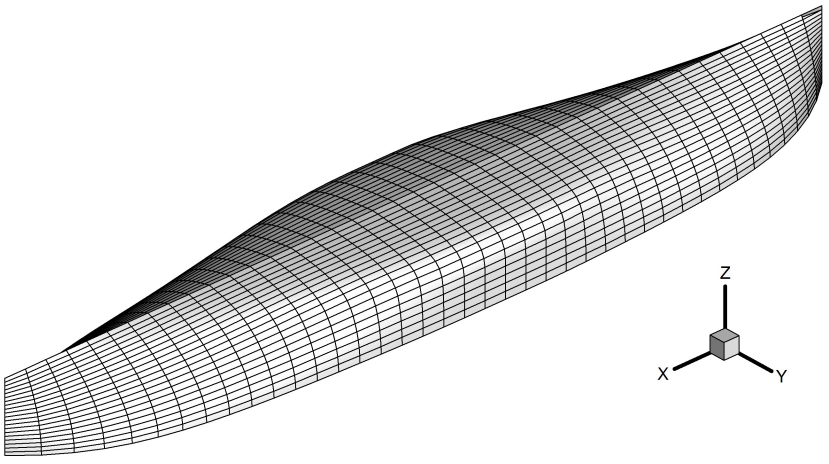

(b) Perspective view

FIGURE 5.15: Body plan and perspective view of introducing $P_{MB} = 0.15$ m aft

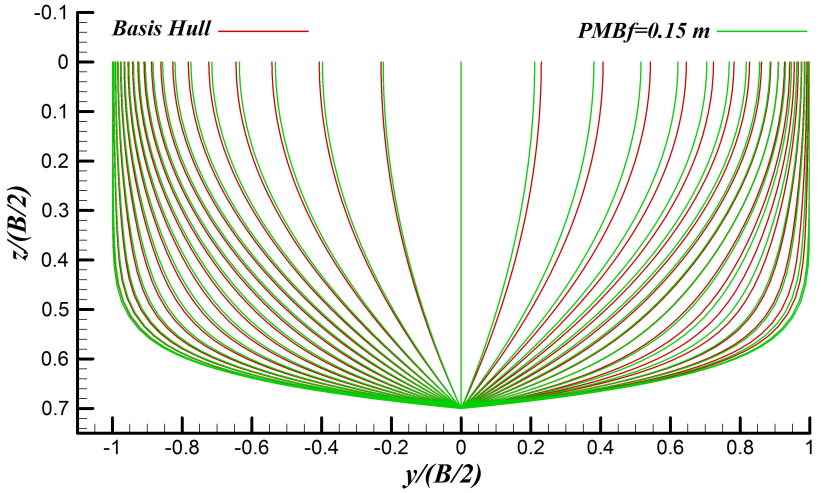

(a) Body plan

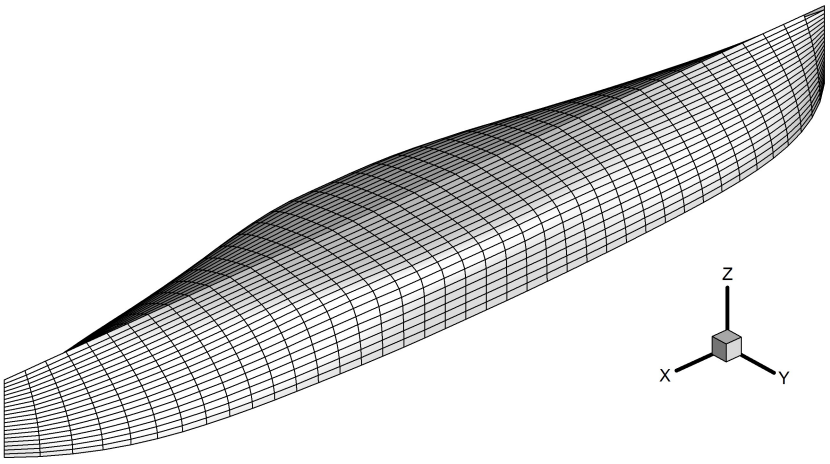

(b) Perspective view

FIGURE 5.16: Body plan and perspective view of introducing $P_{MB} = 0.15$ m fwd

Meanwhile the body plan and perspective view of inserting P_{MB} to the middle body is depicted in Fig. 5.17. The comparison of SAC among them can be observed in Fig. 5.18. The ship motions resulting from introducing P_{MB} are shown in Fig. 5.19 to Fig. 5.21 for surge, heave, and pitch motions, respectively. It is obviously shown in Fig. 5.19 that inserting P_{MB} to the aft- and fore-bodies as well as to the middle body does not affect the surge motion and hence it becomes negligible. Figures 5.20 and 5.21 show the amplitude and phase difference of heave and pitch motions, respectively. Introducing the P_{MB} to the fore body and to the middle body increases the amplitude of both heave and pitch motions. However inserting P_{MB} to the aft body increases only the amplitude of pitch motion.

Figure 5.22 shows the resulting added resistance due to introducing of the P_{MB} to the basis hull. Although inserting the P_{MB} at the aft body affects only the pitch motion, the resulting added resistance due to this change increases relatively largely at its peak

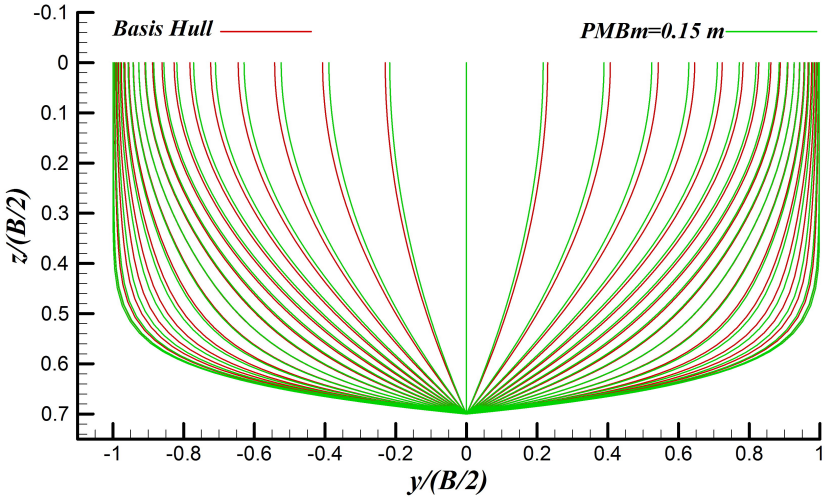

(a) Body plan

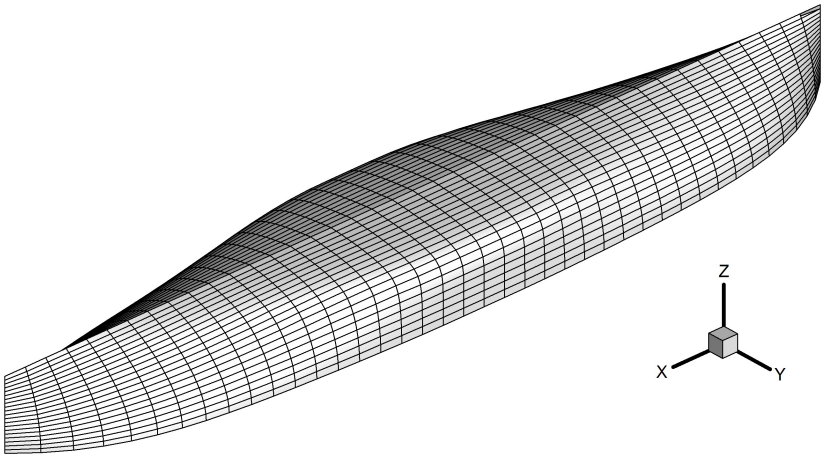

(b) Perspective view

FIGURE 5.17: Body plan and perspective view of introducing P_{MB} = 0.15 m middle

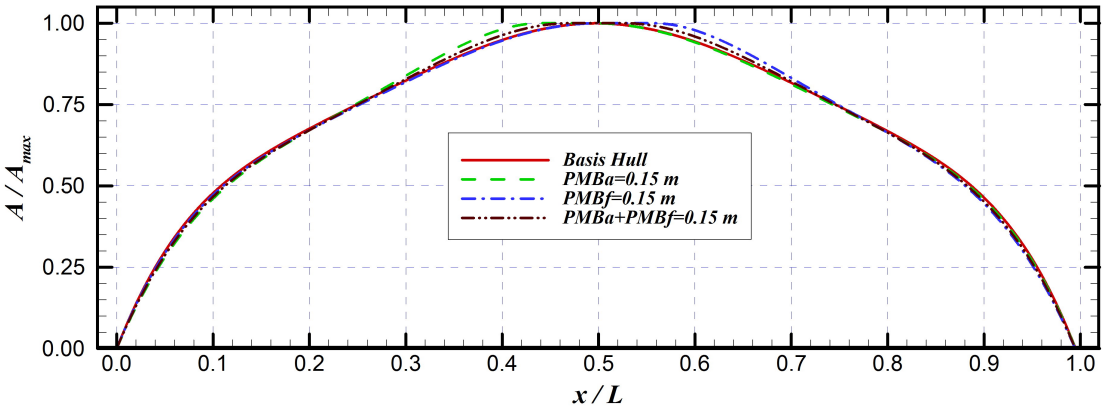

FIGURE 5.18: SAC of introducing P_{MB}

compared to the case of inserting P_{MB} at the fore body and the middle body. Conversely, the effects of inserting the P_{MB} at the fore body to the peak value of the added resistance

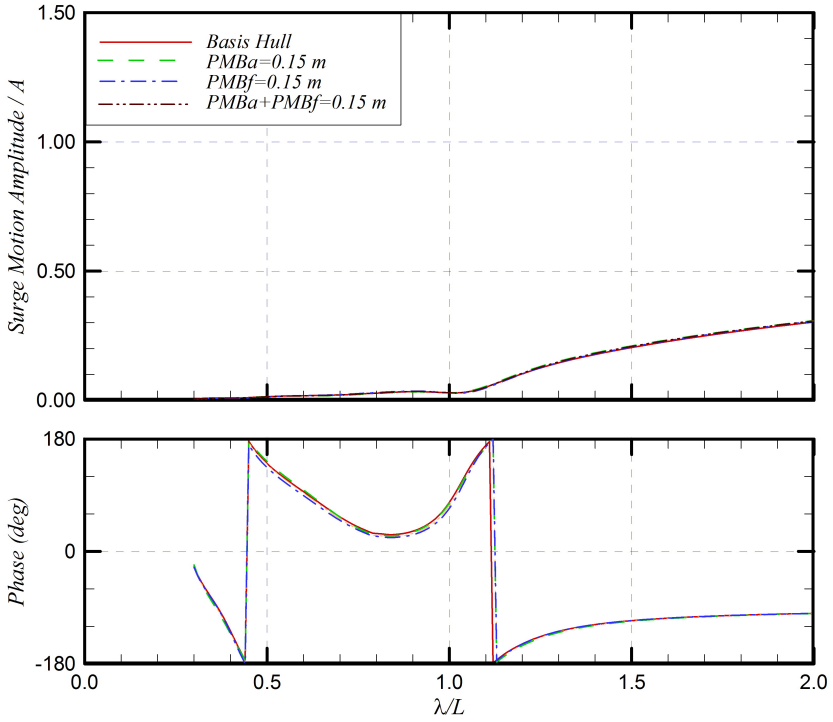

FIGURE 5.19: Surge motion of introducing P_{MB}

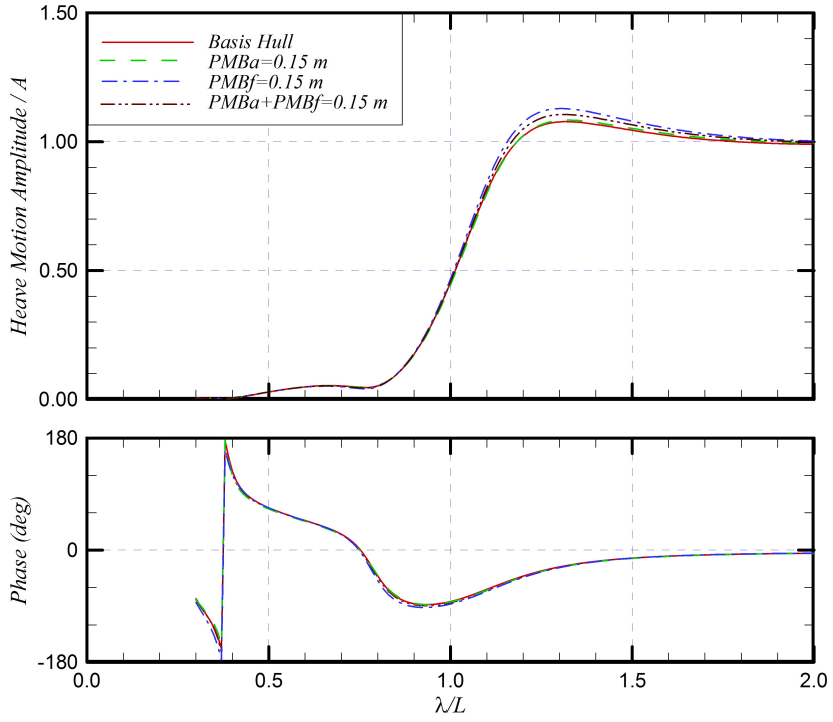

FIGURE 5.20: Heave motion of introducing P_{MB}

is negligible even though it increases the amplitude of both heave and pitch motions. It might be due to slight change in phase difference of pitch motion. Meanwhile the effects of combination between these two given as brown (dashed and double-dotted) line can be observed in Fig. 5.19 through Fig. 5.22.

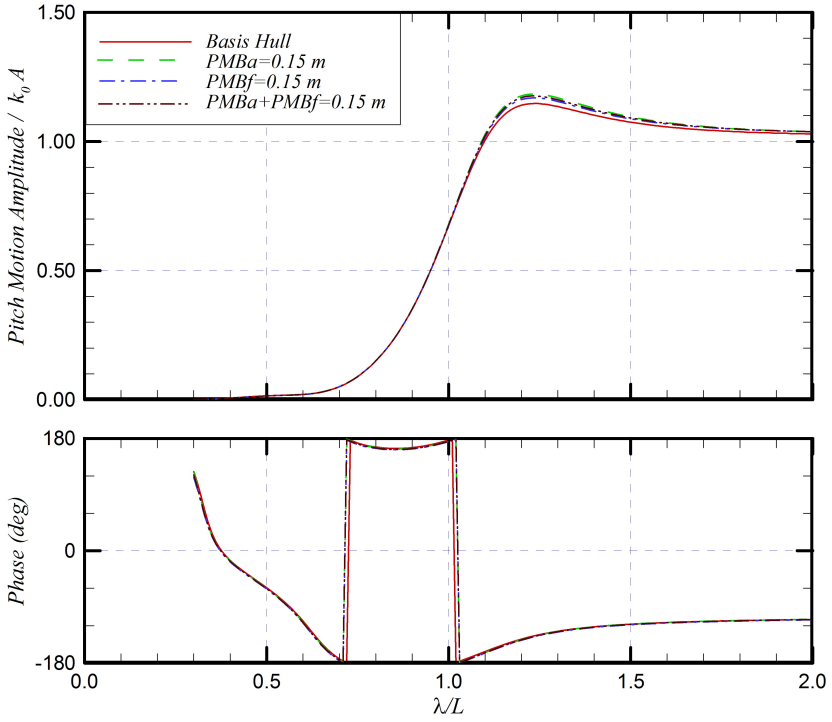

FIGURE 5.21: Pitch motion of introducing P_{MB}

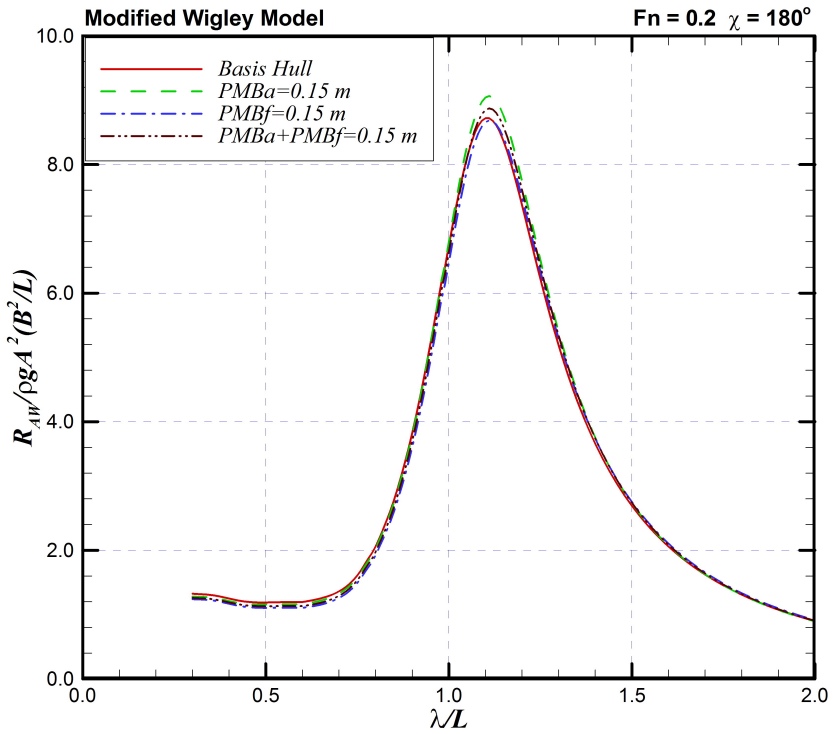

FIGURE 5.22: Added resistance of introducing P_{MB}

Chapter 6

Optimization Results and Discussions

6.1 Preliminary and Validation of Computation

Because the most important part of a genetic algorithm is the genetic operations, thus it is necessary to determine the genetic operators themselves first whether suitable or not to reach the goal of this study as a preliminary computation. Therefore some computations with a modified Wigley model employed as a basis hull are performed with different genetic operators. At the beginning, let us consider the selection operator,

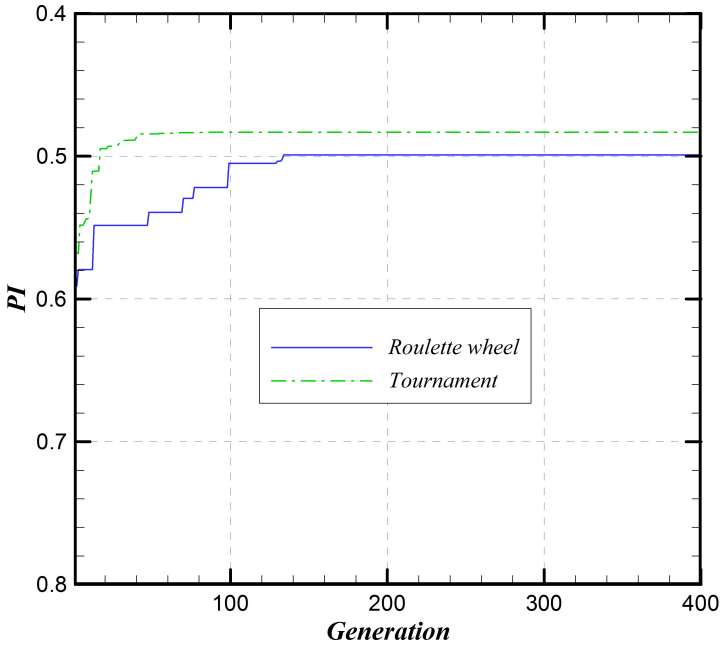

FIGURE 6.1: PI of selection operator

namely roulette wheel and tournament selection operators. The Performance Index (PI) depicting the comparison between them is shown in Fig. 6.1. It is obviously shown on this figure that for the case of adopting the tournament selection, particularly for the short wavelength region ($\lambda/L = 0.30 \sim 0.80$), the PI converges before 100^{th} generation. Meanwhile for roulette wheel selection, it converges after 130^{th} generation. Besides that, it is also noticed that the PI of tournament selection has higher performance than the PI of roulette wheel selection.

As the main search tool of the BCGA relies on the crossover operator, it is also necessary to define this operator. The commonly used methods for crossover are single-point, uniform, and k-point crossovers. Fig. 6.2 shows the PI of those crossovers. As can be seen in Fig. 6.2, the single-point crossover gives the best performance followed by the uniform crossover and the k-point (in this case $k = 3$) crossover, respectively.

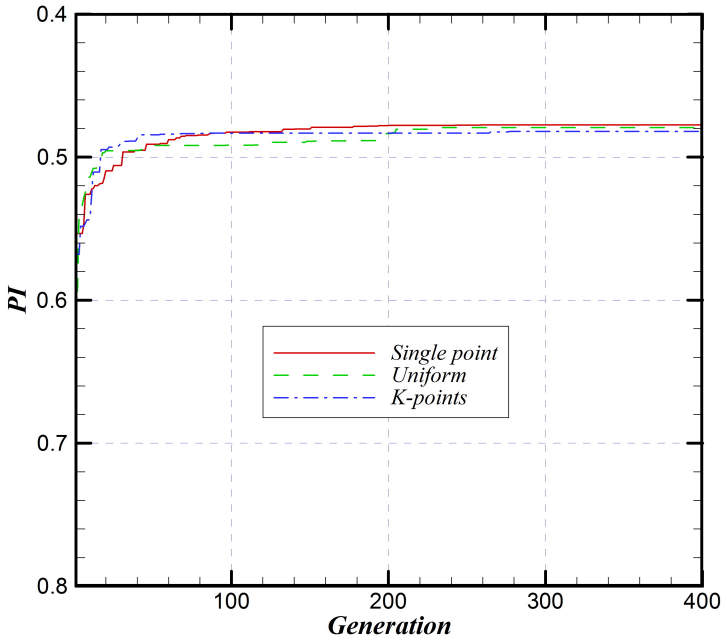

FIGURE 6.2: PI of crossover operator

The remaining operator is the mutation operator. There are indeed several kinds of mutation operator, however only flip-bit mutation is available for binary string which is used in this study. The same preliminary computation is also done for the middle wavelength region ($\lambda/L = 0.80 \sim 1.30$) to confirm its suitable genetic operators. Therefore from these preliminary computations, the genetic operators for both short and middle wavelength cases have been determined and are summarized in Table 6.1 together with another parameters used in the optimization [2].

It is noted here again that a modified Wigley model is employed on this preliminary computation with tweenty (20) population numbers for each generation. Needless to say that the genetic operators shown in Table 6.1 may change depending on the problem

TABLE 6.1: Parameter used for Wigley optimization

Parameters	**Short wavelength**	**Middle wavelength**
Minimum wavelength	0.30	0.80
Maximum wavelength	0.80	1.30
Population number	20	20
Selection operator	Tournament	Roulette
Crossover operator	Single point	3-points
Mutation operator	Flipping	Flipping
Crossover probability (P_c)	0.8	0.8
Mutation probability (P_m)	0.0156	0.0156
Another operator	Elitism	Elitism
PI of basis hull	0.6132	2.9693

encountered. However for selection and crossover operators, the tournament and single point operators are generally used for all cases in order to acquire the best optimized model with faster convergence.

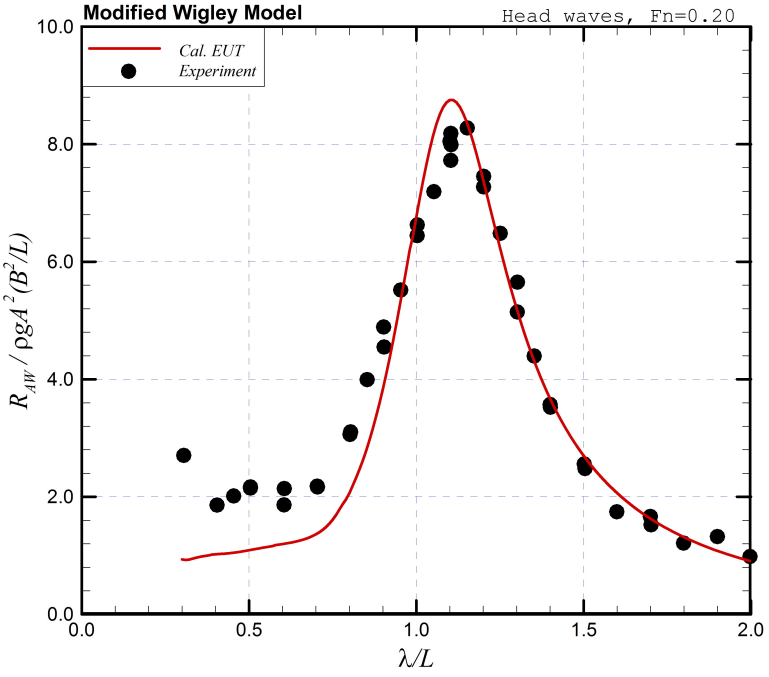

FIGURE 6.3: Comparison of EUT and experimental results

In an optimization problem, besides the optimization algorithm itself, the most important thing is that a reliability of a method used for computing the objective function. Hence, in this chapter, a validation of the Enhanced Unified Theory (EUT) as a core method of computation should be given. For this purpose, a comparison of the added resistance of a modified Wigley model between the results of experiment conducted by Kashiwag [18] and the one computed by EUT is depicted in Fig. 6.3 which was already described explicitly in Chapter 4.

From this figure, we could observe a favorable agreement between the results of basis hull computed by the EUT and ones by experiment for almost all wavelengths, except around short wavelengths in which the EUT underestimates the experimental results. Nonetheless a correction formula for that discrepancy is also given on that paper (Kashiwagi [18]) which can be applied in this study. Therefore the combination between the BCGA and EUT can be relied on in obtaining the best optimized hull geometry of a ship in reducing the added resistance, especially around its peak.

6.2 Optimization of Modified Wigley Model

After obtaining the suitable genetic operators described in the preceding section, the optimization with a modified Wigley model by BCGA via shape function is going to be performed. In this case the optimization is performed for two operational regions of a ship, namely short and middle wavelength regions. Short and middle wavelength regions are defined as λ/L varied between $0.30 \sim 0.80$ and $0.80 \sim 1.30$, respectively. It should be noted here that the objective function of this optimization is to minimize the added resistance at those wavelength regions.

Now let us consider the PI both of them as shown in Fig. 6.4. From this figure, it can be seen that the best optimized hull geometry for the case of short wavelengths region is obtained at 259^{th} generation as its PI converges from this generation; meanwhile the PI for the case of middle wavelengths region converges at 302^{th} generation.

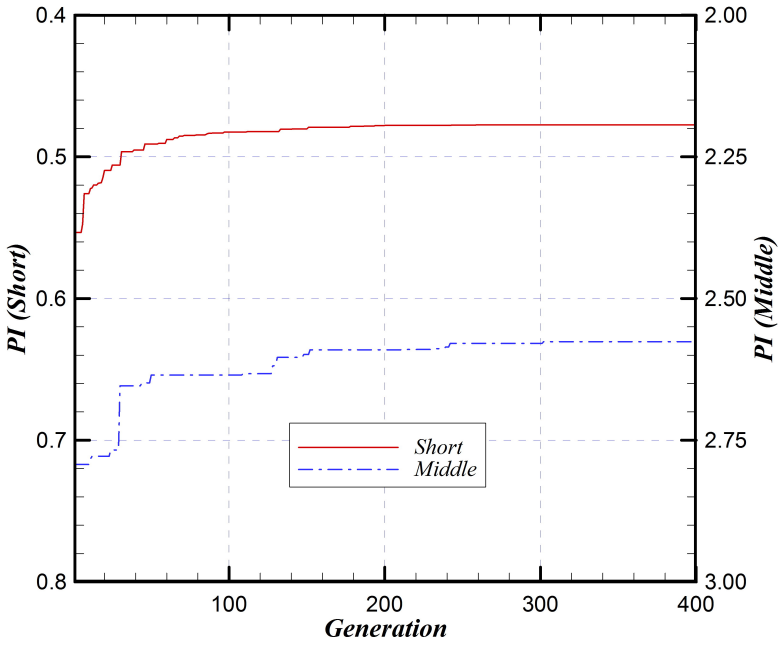

FIGURE 6.4: PI of short and middle wavelength regions

Case of Short Wavelength Region

The optimization for short wavelength region is considered first. From Fig. 6.4 the corresponding sectional area curve (SAC) of the best optimized hull geometry together with SAC of the basis hull geometry and its shape function can be depicted in Fig. 6.5. In this figure, it can be observed that the fore-front part of the best optimized hull geometry is finer than the basis hull geometry. This is due to the fact that the magnitude of the shape function becomes negative at bow part and thus diminishes the sectional area of some sections around this part. It can also be illustrated clearly at the comparison of their body plans shown in Fig. 6.6. The perspective view of this best optimized geometry is also depicted in the same figure.

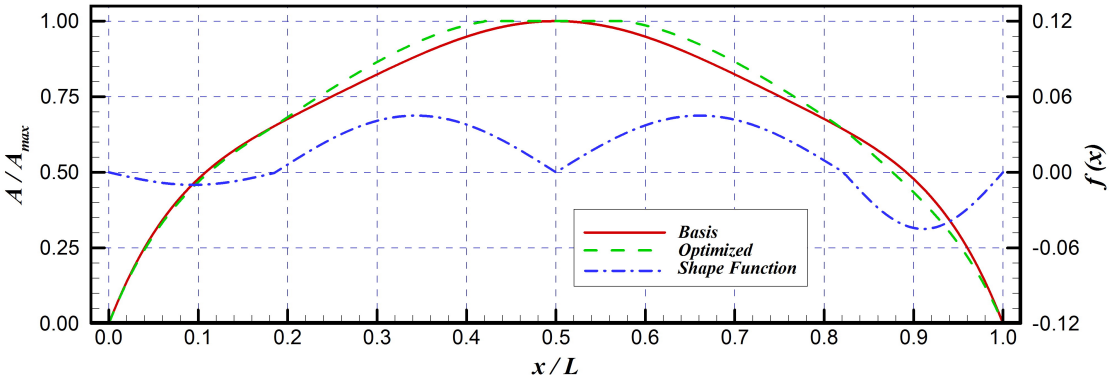

FIGURE 6.5: SAC and shape function for short wavelength region

In the preceding chapter, it was found that introducing the parallel middle body (P_{MB}) to the SAC of aft- and fore-bodies and reducing the sectional area of the end-parts of them could reduce the added resistance, especially at short wavelengths region. A similar shape of SAC is obtained as the best optimized shape during optimization which can obviously be observed in Fig. 6.5. Hence, it is expected that the corresponding added resistance resulting from this optimization decreases at short wavelength region.

It is well known that the most important component in determining the added resistance at short wavelength region is the diffraction component in which the incident waves are diffracted mainly near the ship's bow. Fortunately, the EUT used to obtain the fitness function, namely the added resistance in this optimization, takes account of the effect of wave diffraction through the retention of n_1-term in the body boundary condition for the diffraction problem as shown in Eq.(2.154).

Therefore judging from Figs. 6.5 and 6.6, we may say that the amount of incident waves diffracted by the finer bow shape of the best optimized hull form tends to become small compared to that of the basis hull form does. This phenomenon can be observed from the resulting added resistance obtained in this optimization as shown in Fig. 6.7. Although the ship-ends become finer, due to the insertion of P_{MB} to the middle body, the block

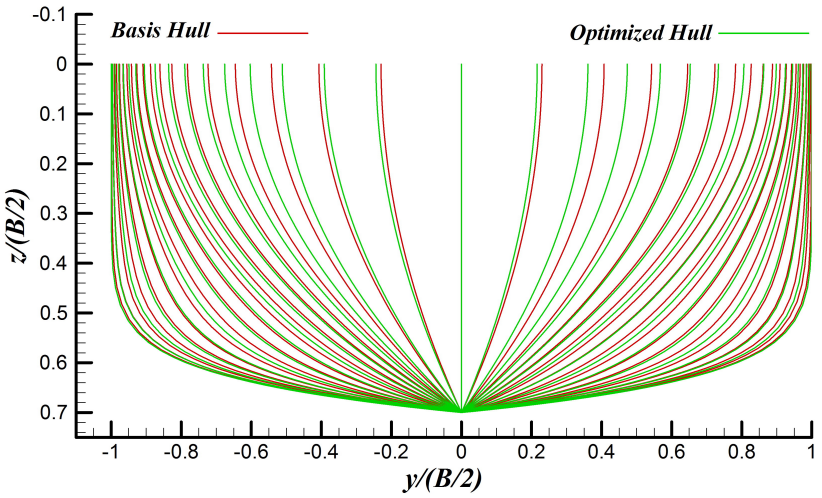

(a) Body plan

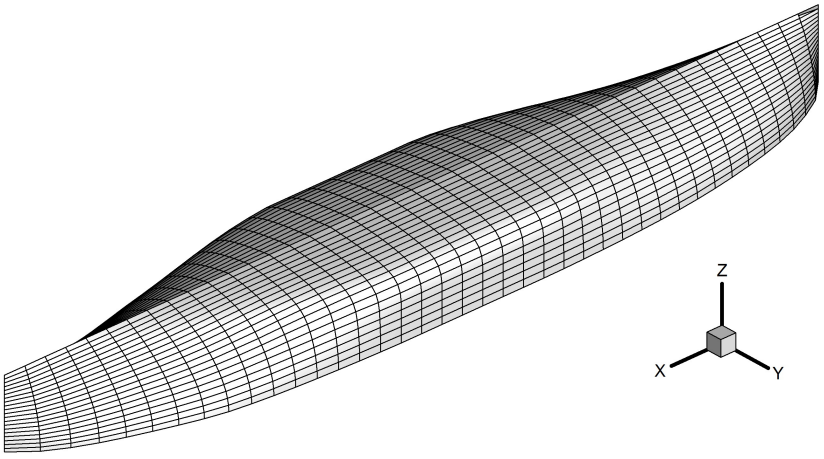

(b) Perspective view

FIGURE 6.6: Body plan and perspective view for short wavelength region

coefficient of the best optimized hull form slightly increases to 0.6441 and hence the prismatic coefficient becomes 0.7086.

As can be seen in Fig. 6.7, even though the basis hull form is only optimized at $\lambda/L = 0.30 \sim 0.80$, the obtained added resistance decreases until λ/L about 1.10 which means that the added resistance can be optimized until around its peak by only considering some wavelengths at shorter wavelength region and hence reducing the computation time. On the other hand, it is found that the separation distance between longitudinal center of buoyancy (L_{CB}) and longitudinal center of floatation (L_{CF}) of the best optimized hull form becomes positive from its original zero value. It implies that the resonance frequency in ship motion shifts to longer waves and consequently the added resistance in longer waves increases. For further details about the separation distance between L_{CB} and L_{CF}, the readers are advised to read Kashiwagi and Sumi [19].

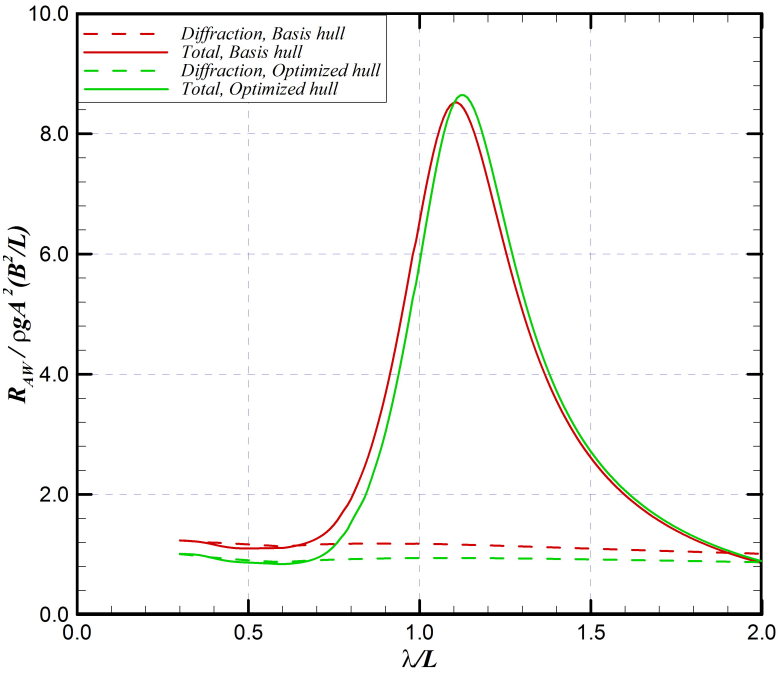

FIGURE 6.7: Added resistance for short wavelength region

Case of Middle Wavelength Region

Unlike for short wavelength region, the shape of SAC obtained from Fig. 6.4 for middle wavelength region is slightly blunter than the original shape at its bow and stern which is illustrated in Fig. 6.8 together with its shape function. The shape function shown in this figure, particularly around $x/L = 0.98$ becomes positive and returns to exactly zero at fore-end station ($x/L = 1.00$) which is a constraint described on the related chapter. It is observable in Fig. 6.8 that the P_{MB} is also inserted to the original SAC but only to the fore body and thus the block coefficient somewhat rises to 0.6385. This can also be observed in Fig. 6.9.

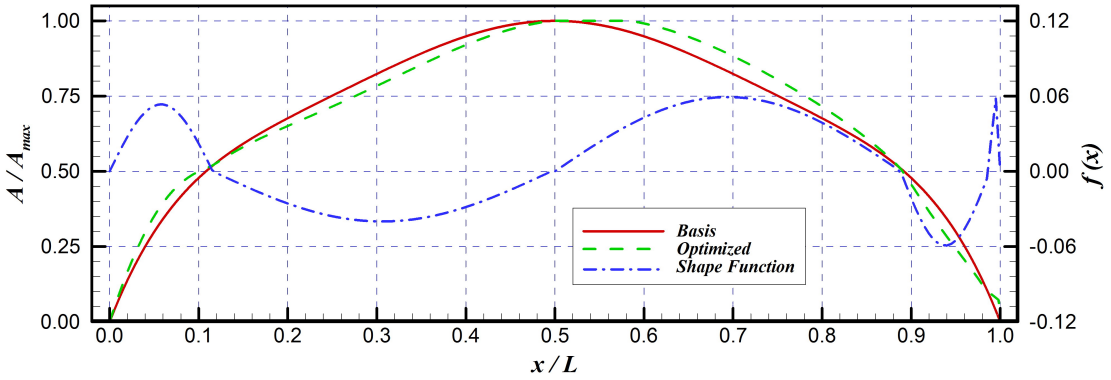

FIGURE 6.8: SAC and shape function for middle wavelength region

Figure 6.10 illustrates the results of the added resistance for optimization at middle wavelength region, in which the obtained added resistance for the best optimized hull

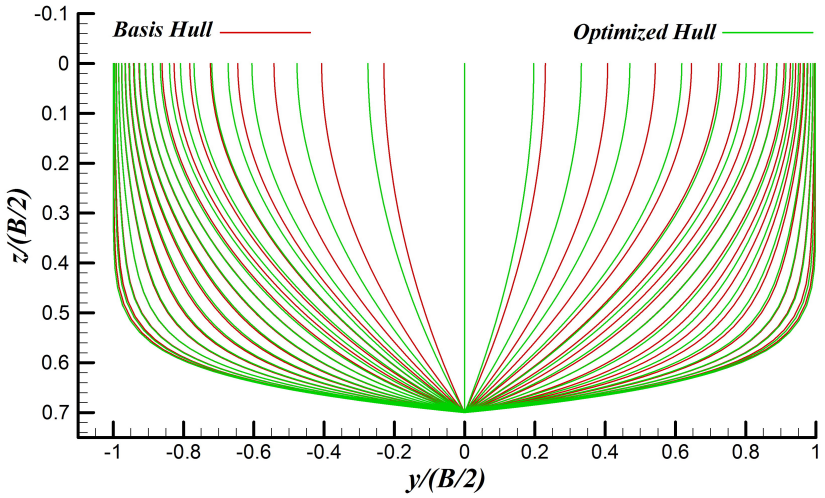

(a) Body plan

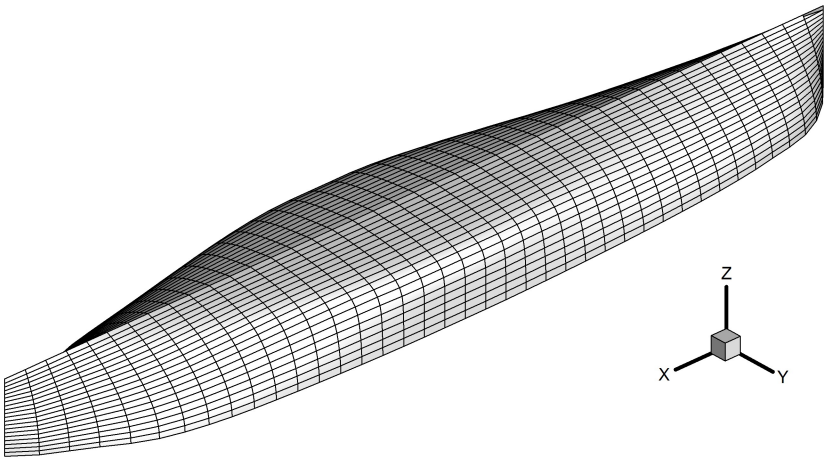

(b) Perspective view

FIGURE 6.9: Body plan and perspective view for middle wavelength region

geometry reduces relatively largely at concerned wavelengths, especially at its peak. It might be attributed to the radiation component, namely ship motion which is the most important component in the added resistance to determine its peak, especially pitch motion. Nonetheless, the obtained results of the added resistance somewhat increase at short wavelengths due to an increase of sectional area of few sections at the most-front part of the fore body which is marked by positive value of the shape function at those sections shown in Fig. 6.8.

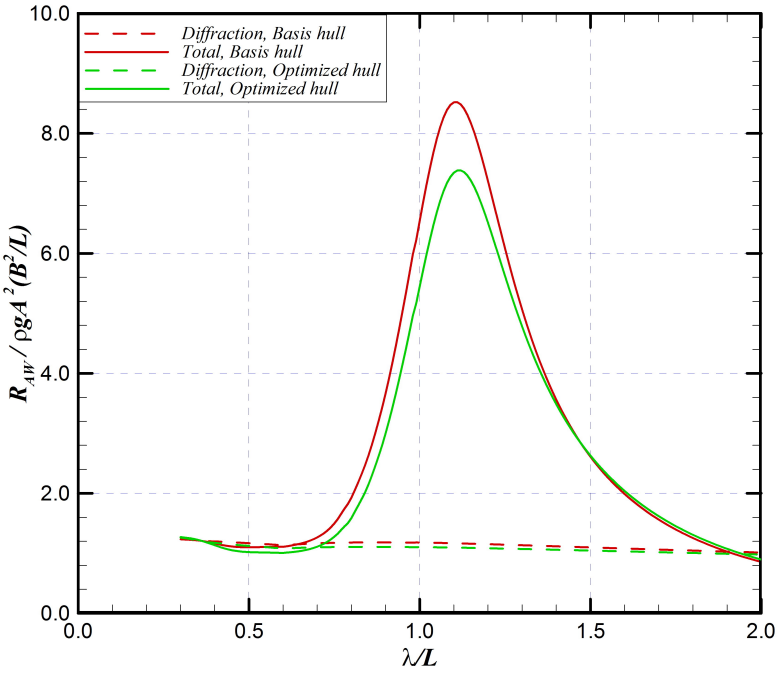

FIGURE 6.10: Added resistance for middle wavelength region

6.3 Optimization of SR-108 Container Ship

An optimization method based on natural selection, namely the genetic algorithm with binary encoding or so-called the Binary-Coded Genetic Algorithm (BCGA), has been developed and utilized in the previous section to find out the best optimized hull geometry of a parent hull, i.e. modified Wigley model. The results of optimization were favorable in which the added resistance decreased relatively largely at concerned wavelengths regions. However an optimization only with modified Wigley model is not sufficient to prove the reliability of the present method. For that reason, therefore, an optimization with the actual ship is going to be performed. In this case, an actual ship e.g. SR-108 is employed as a basis hull geometry. The SAC and body plan of SR-108 together with its perspective view could be seen in Chapter 3. In addition, the steady wave resistance is also computed by Holtrop & Mennen method [16] to confirm reduction of the total resistance of a ship being optimized.

According to sensitivity study of the peak value of the added resistance described in Chapter 4, it was found that both amplitude and phase of pitch motion gives the largest contribution to the peak value of the added resistance, especially at its peak. Thus in this optimization, the primary objective function is to reduce the pitch motion and the secondary one is to reduce the added resistance. Besides that, the peak value of the added resistance and the added resistance due to diffraction are also included in the primary fitness function as a summation of them.

It has been explained before that the number of parameters being optimized (genes) in the shape function could be increased to generate more various shapes of SAC, but it does not mean that the best optimized hull cannot be obtained with less number of these parameters. Since the whole body is going to be optimized, at least four genes should be involved. The following parameters are used in this optimization as shown in Table 6.2.

TABLE 6.2: Parameter used for SR-108 optimization

Parameters	**Value**
Population number	20
Selection operator	Tournament
Crossover operator	Single point
Mutation operator	Flipping
Crossover probability (P_c)	0.8
Mutation probability (P_m)	0.0125
Another operator	Elitism
Minimum wavelength	0.80
Maximum wavelength	1.30

In Table 6.2, we could see that the tournament selection combined with single-point crossover operators are obtained as the most suitable operators for SR-108 in middle wavelength region which are different with the case of optimizing the modified Wigley model.

Optimization with Four Genes

For the purpose of optimization of the whole body, firstly four genes for each chromosome are used with the range of amplitude set to be ± 0.10 (aft) and ± 0.12 (fore). For the fixed stations, the range varies from AP station to the station with the largest transverse area and from this station to FP station for aft and fore body respectively with a condition that these genes should not be the same of the position of those three stations.

The results of optimization with four genes for each chromosome can be seen in the following Figs. 6.11 to 6.16. The body plan and perspective view resulting from this optimization is depicted in Fig. 6.11. In Fig. 6.12, it is clearly shown that both aft and fore bodies become blunter and the parallel middle body is introduced at fore body. This means that the centroid of the SAC or so-called the longitudinal center of buoyancy (L_{CB}) shifts toward fore body. The ship motions resulting from this optimization are shown in Figs. 6.13, 6.14 and 6.15 for surge, heave and pitch motions, respectively.

In Fig. 6.15 the pitch motion as the primary fitness function decreases in large quantity, especially at the wavelength ratio ($\lambda/L = 0.80 \sim 1.30$) in which the optimization is performed. Although the heave motion is not included directly to the primary fitness

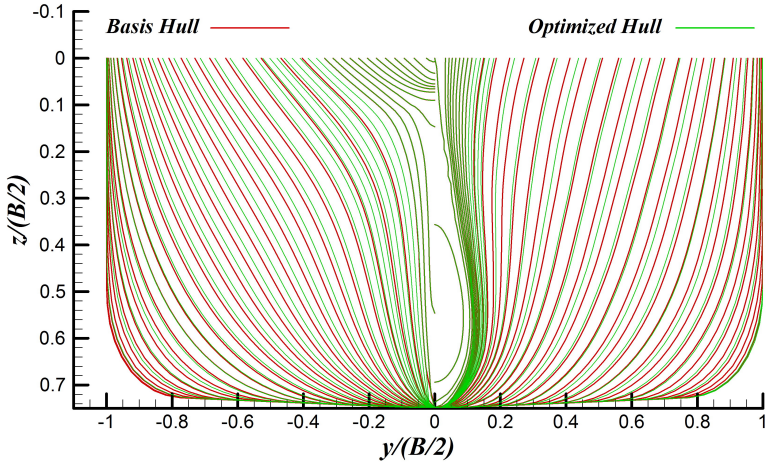

(a) Body plan

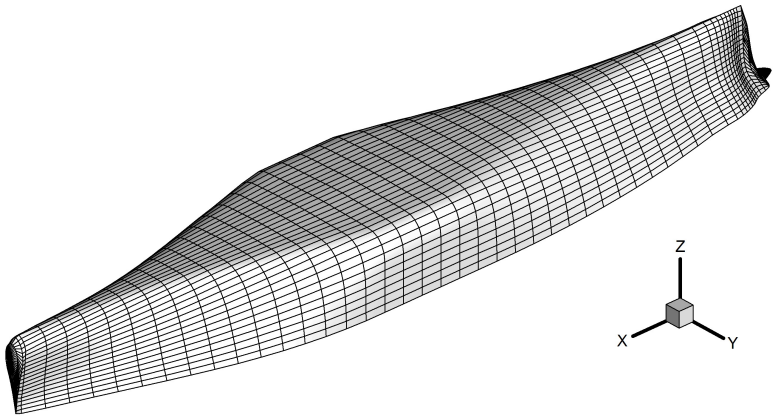

(b) Perspective view

FIGURE 6.11: Body plan and perspective view of four genes

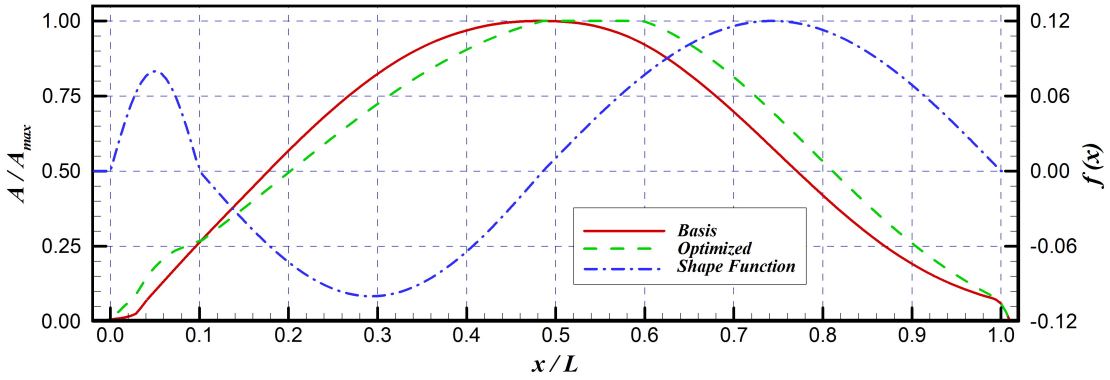

FIGURE 6.12: SAC and shape function of four genes

function, the resulting heave motion from this optimization also decreases as shown in Fig. 6.14. Nevertheless the amount of its reduction is smaller than that in the pitch motion. Due to large reduction of the amplitude of ship motions, it is appropriate to envisage that the corresponding result of the added resistance may also be reduced in large amount. This result can be seen in Fig. 6.16.

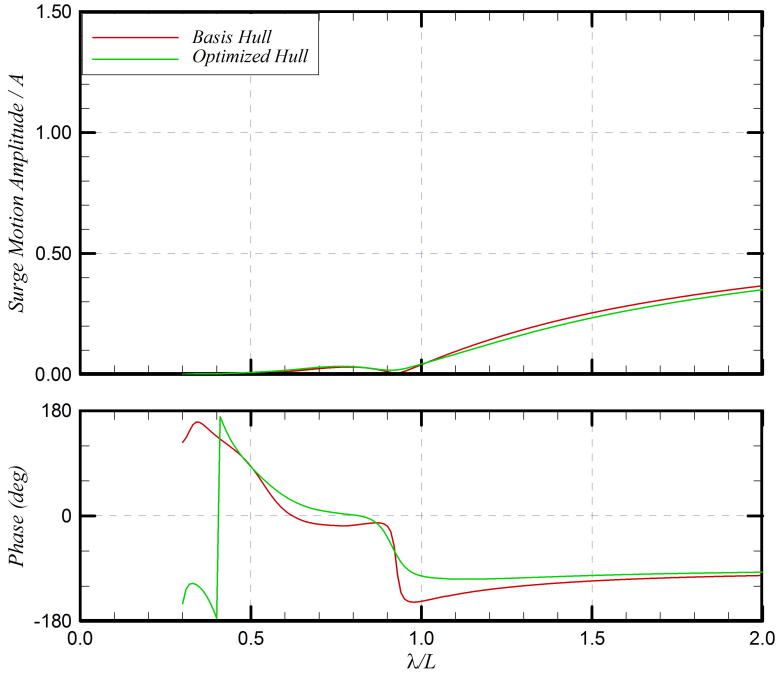

FIGURE 6.13: Surge motion of four genes

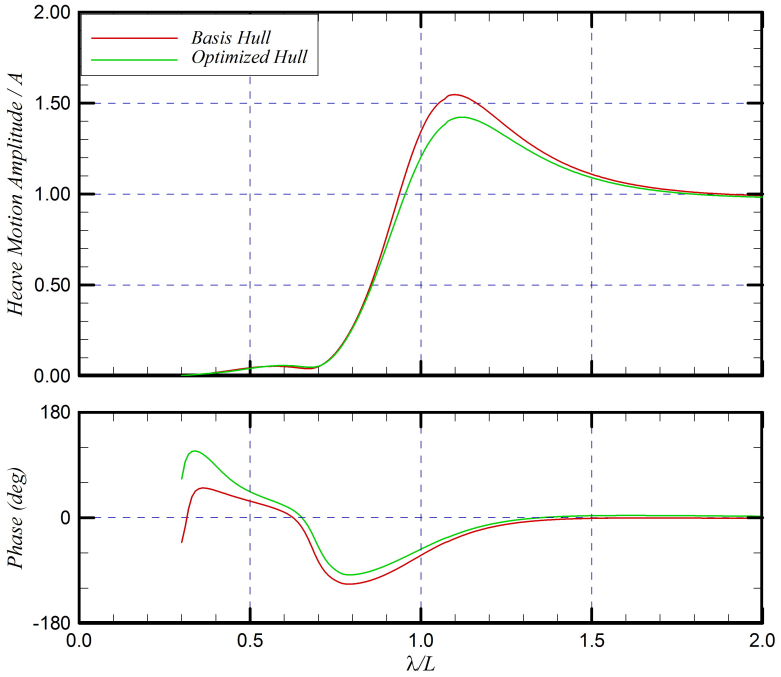

FIGURE 6.14: Heave motion of four genes

It should be noted again that this optimization is performed at $\lambda/L = 0.80 \sim 1.30$ and $Fn = 0.20$. From Fig. 6.16, it is clearly shown that the added resistance as the secondary fitness function remarkably decreases around its peak where the optimization is performed. However it slightly increases at short wavelength region. The added resistance of this optimized ship is also computed for several Froude numbers shown in

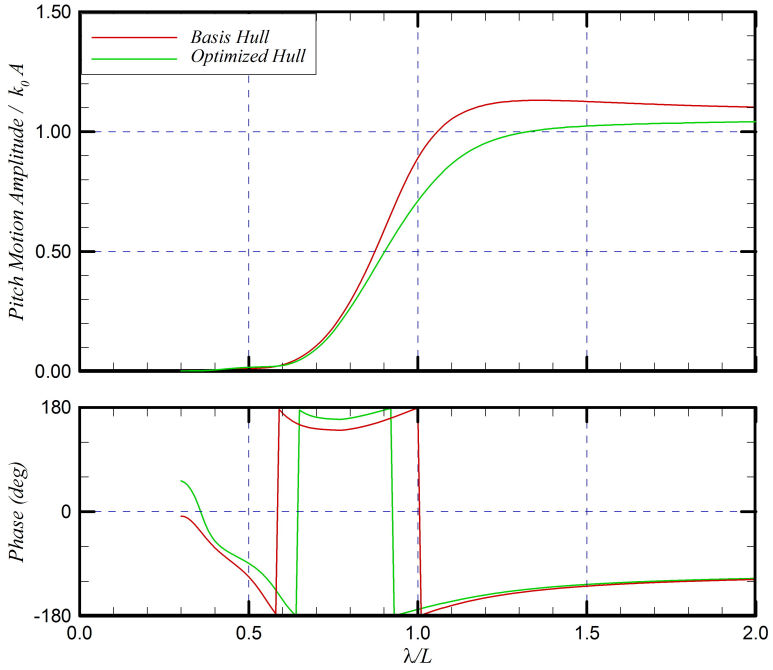

FIGURE 6.15: Pitch motion of four genes

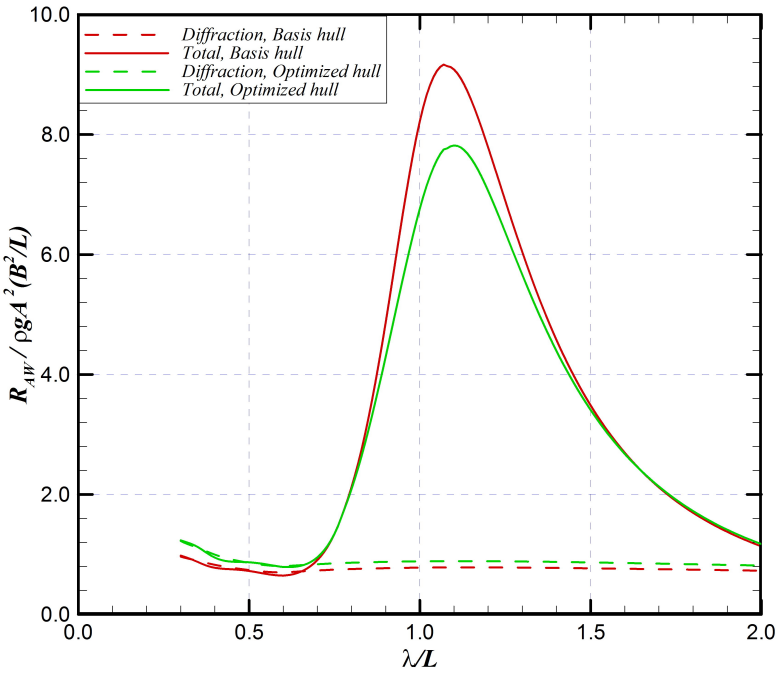

FIGURE 6.16: Added resistance of four genes

Fig. 6.17. It is noticeable that the discrepancy in the added resistance around its peak between the basis hull geometry and optimized ones increases as the Froude number increase. Besides that, in order to confirm reduction of the total wave resistance, the corresponding result of the steady wave resistance for several Froude numbers can be seen in Fig. 6.18. It is shown on this figure that the steady wave resistance is almost negligible at those Froude numbers, except that from around $Fn = 0.260$ to 0.335.

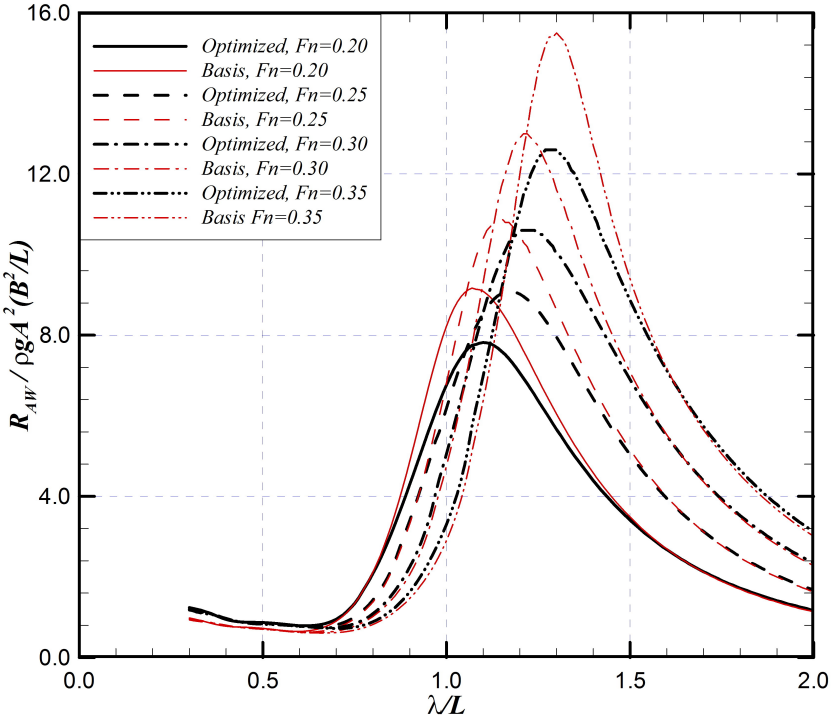

FIGURE 6.17: Added resistance of four genes for several F_n

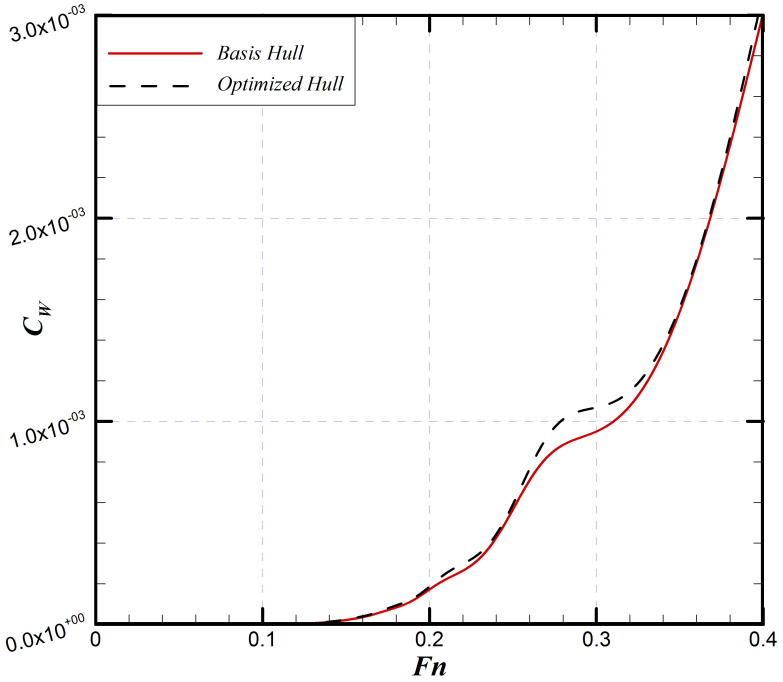

FIGURE 6.18: Wave resistance coefficient of four genes

Based on the results shown above, it might be concluded that this optimized hull can be operated at low and high speeds where the increase in the steady wave resistance becomes negligible at those Froude numbers.

Optimization with Six Genes

An optimization with six genes is also performed. In this case the range of genes for amplitude is set to be ±0.12 for both aft- and fore-bodies and for the fixed stations, it is exactly the same with the previous case including all parameters used in that optimization. Similar trend of the SAC and shape function with four genes is obtained in this optimization as shown in Fig. 6.19. The body plan and perspective view of the best optimized hull geometry obtained from this optimization can be seen in Fig. 6.20. The only difference is the shape around the parallel middle body of the fore body.

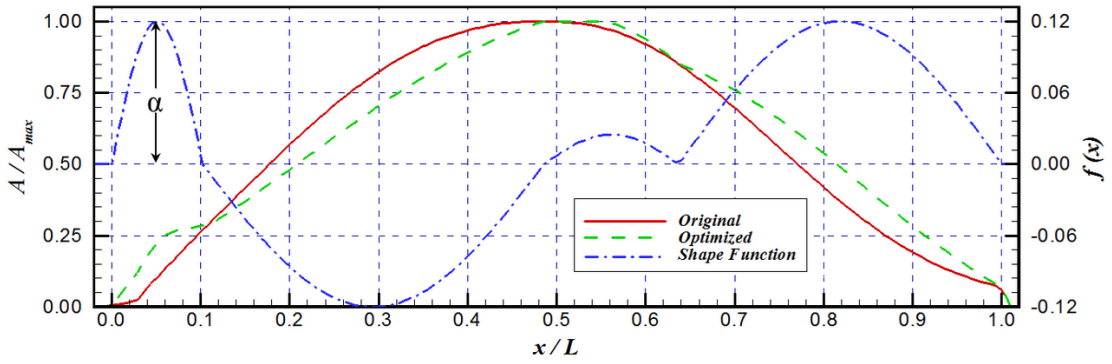

FIGURE 6.19: SAC and shape function of six genes

The results of this optimization can be seen in the following figures including its comparisons with the basis hull geometry and optimized ones with four genes. Fig. 6.21 through Fig. 6.25 show the results of the ship motions, the added resistance and the steady wave resistance of the best optimized ship, respectively. In Fig. 6.23 we could observe that the pitch motion of the optimized ship with six genes is lower than that of with four genes. Besides that, the heave motion also largely decreases around its peak as revealed in Fig. 6.22.

Consequently the corresponding result of the added resistance becomes the lowest among them which is shown in Fig. 6.24. The steady wave resistance shown in Fig. 6.25 looks negligible at $Fn = 0.20$ and becomes lower than that of the one optimized with four genes at $Fn = 0.260 \sim 0.335$. From these comparisons we could notice that the results of six genes are better than those of four genes for both the added resistance and steady wave making resistance.

Having a close look at the stern part of the perspective view shown in Fig. 6.20, an eccentric shape at stern part exists in this figure which is due to the amplitude of shape function denoted as α in Fig. 6.19. It also appears at the shape function of the best optimized ship with four genes shown in Fig. 6.12. To evade this, the amplitude of shape function (α) on that part is intentionally set to be zero. Thus the best optimized hull is intentionally modified and its new perspective view is given in Fig. 6.26.

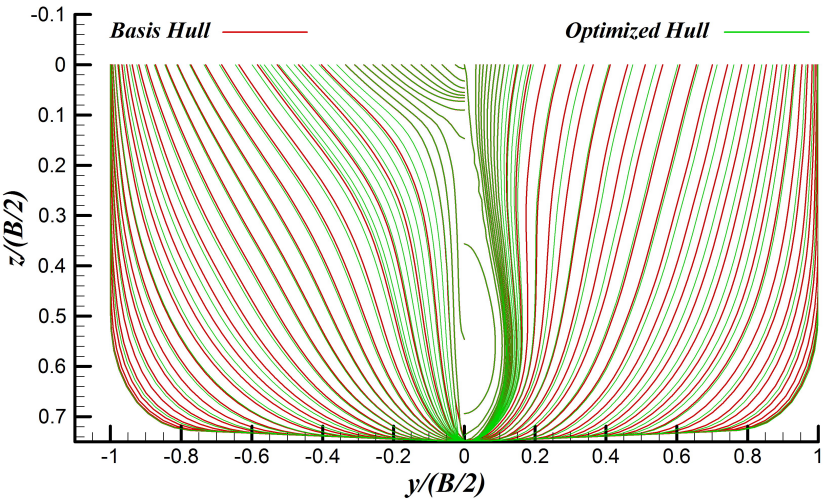

(a) Body plan

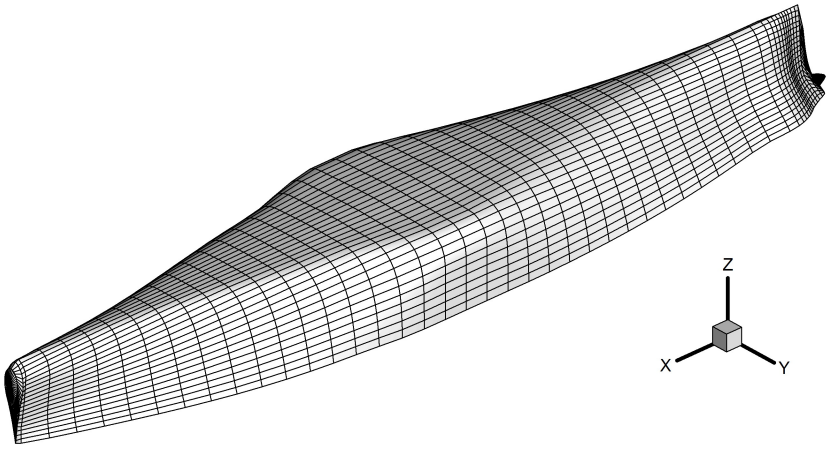

(b) Perspective view

FIGURE 6.20: Body plan and perspective view of six genes

The added resistance resulting from this intentional change for several Froude numbers can be seen in Fig. 6.27. From this result, we could understand that the added resistance still decreases in large amount from that of the basis hull, although its quantity is lower than that when the amplitude of the shape function is not equal to zero ($\alpha = 0.12$). Different with the added resistance, in Fig. 6.28 we could not observe the discrepancy of the steady wave resistance coefficient between the basis hull and the optimized ones with six genes and $\alpha = 0.00$ for all Froude numbers. Therefore it can be confirmed that the total wave resistance of the optimized ship is reduced from the decrease in the added resistance with the steady wave resistance being almost unchanged [20].

After obtaining the best optimized hull geometry from this optimization, let us now investigate the contribution from each term of the Kochin function in the resulting added resistance as shown in Fig. 6.27, especially at $Fn = 0.20$. In this case, the Kochin function is decomposed into diffraction and radiation terms as well as a cross

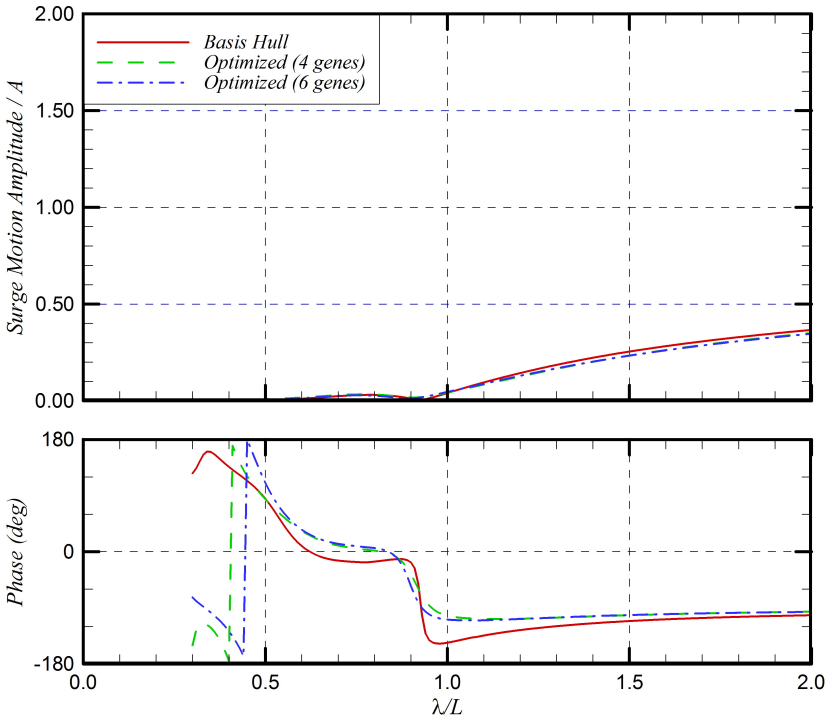

FIGURE 6.21: Surge motion of six genes

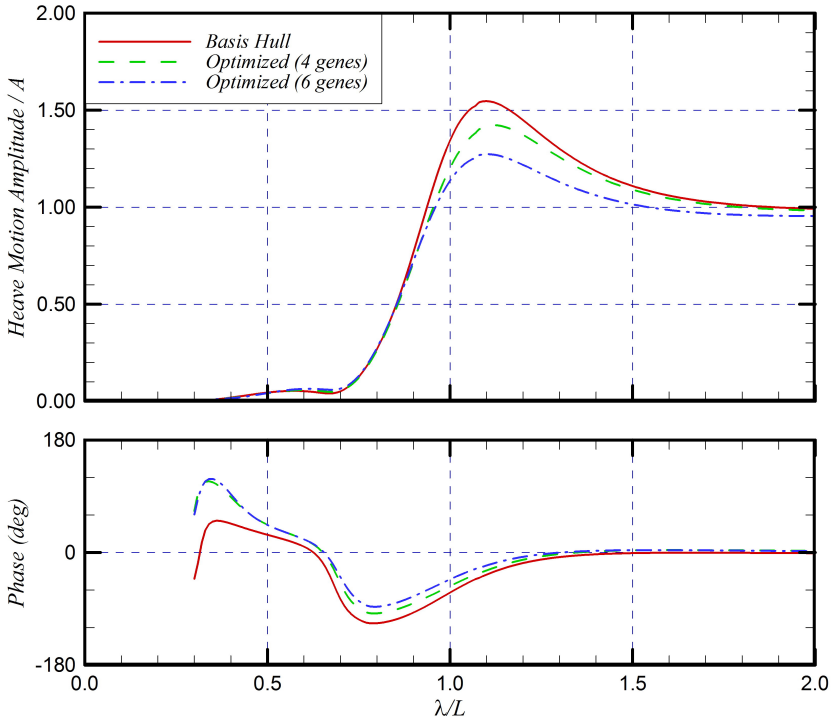

FIGURE 6.22: Heave motion of six genes

term between them as given in Eq.2.178 to Eq.2.180. The resulting added resistance due to these decompositions is shown in the following Fig. 6.29. The added resistance of the basis hull form is also given in the same figure for comparison.

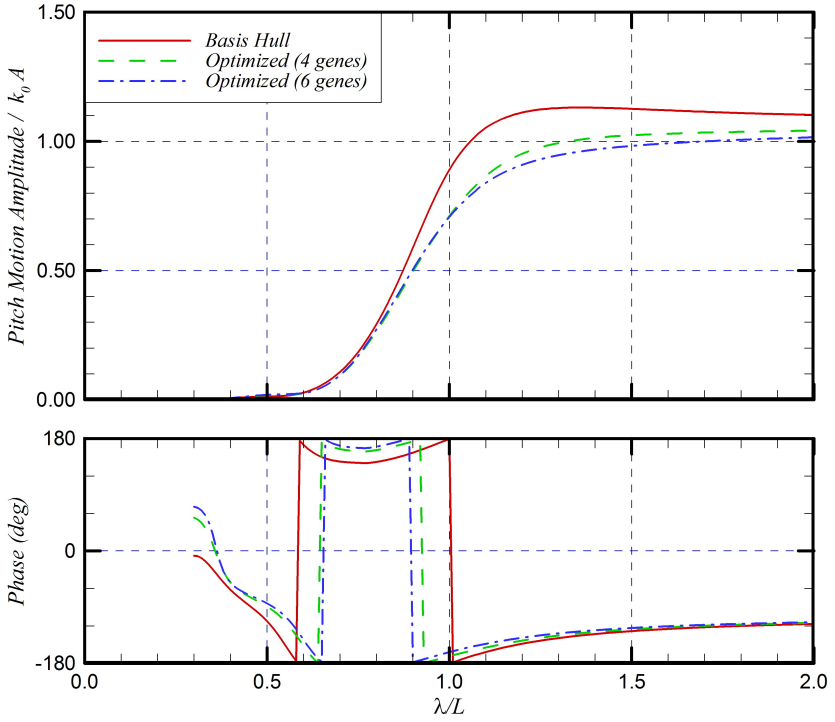

FIGURE 6.23: Pitch motion of six genes

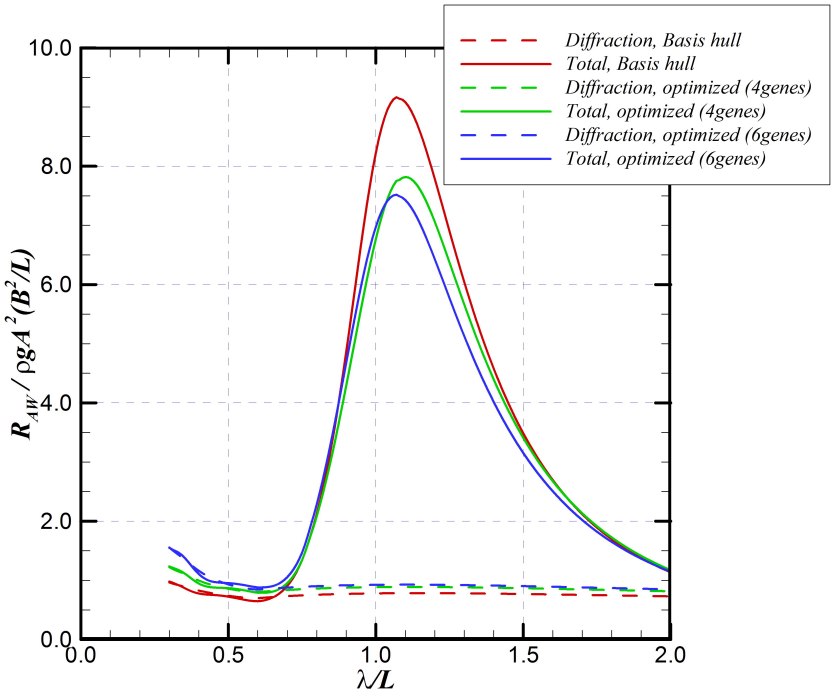

FIGURE 6.24: Added resistance of six genes

From Fig. 6.29, we could observe that the total added resistance resulting from this optimization is lower than that of the original ones, particularly around its peak to the longer wavelength region. However slightly increase of it is also observable in shorter wavelength region. If we look at each component of the added resistance, it is clearly

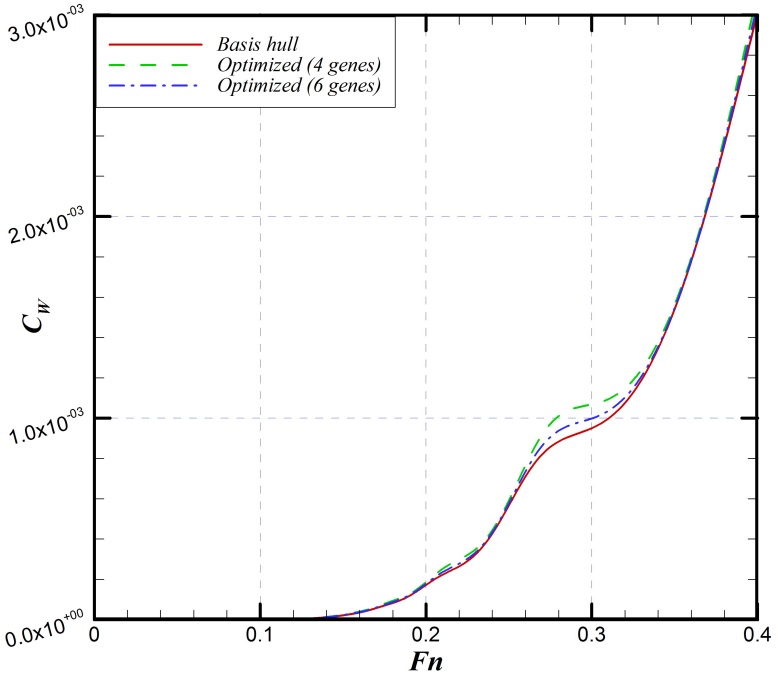

FIGURE 6.25: Wave resistance coefficient of six genes

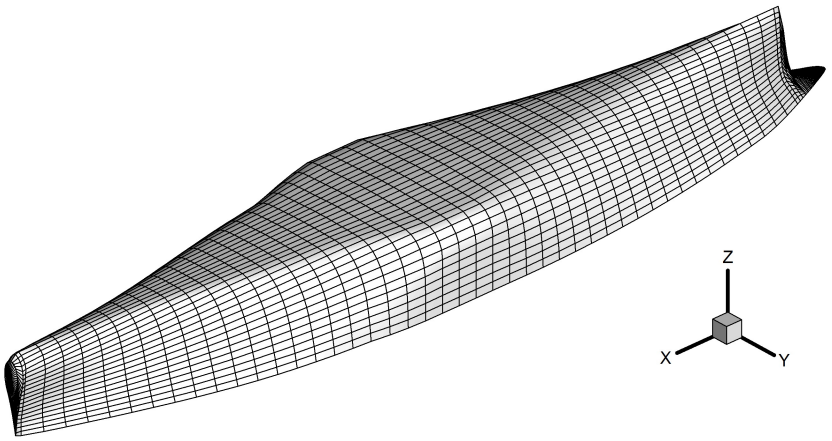

FIGURE 6.26: Perspective view of six genes with $\alpha = 0.00$

shown on Fig. 6.29 that the discrepancy of the added resistance in shorter waves is due to the diffraction component given as dotted line. However around its peak to the longer waves, it is atributed to the radiation components given as dashed-dotted line.

For more investigation, the Kochin function of radiation problem is further decomposed into surge, heave and pitch motions as we only consider the symmetric mode of motion. However, according to the sensitivity study described in Chapter 4, contribution of the surge motion is negligible in determining the peak value of the added resistance. The result of these decomposition can be seen in Fig. 6.30. From this figure we could observe that the prominent component of radiation problem in determining the peak value of the added resistance is due to the pitch motion given as dashed-double-dotted line on

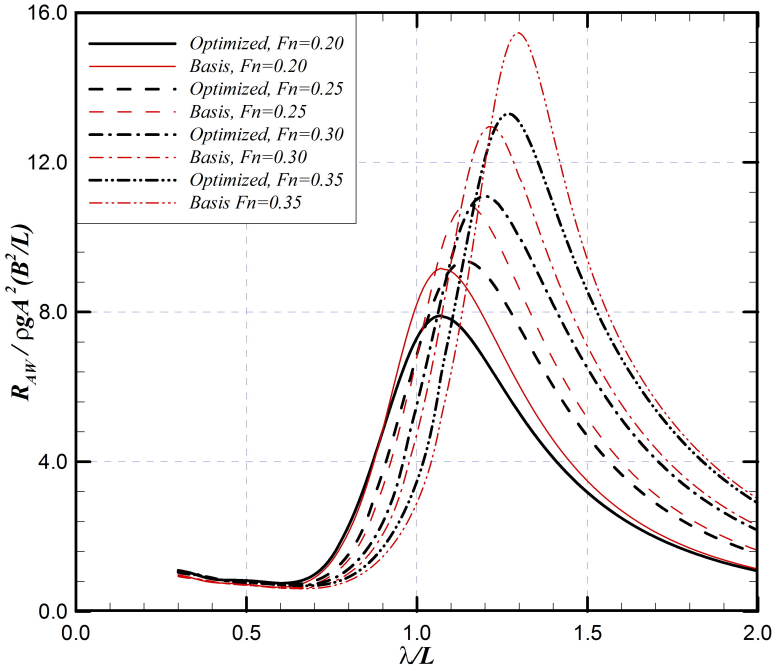

FIGURE 6.27: Added resistance of six genes with $\alpha = 0.00$ for several F_n

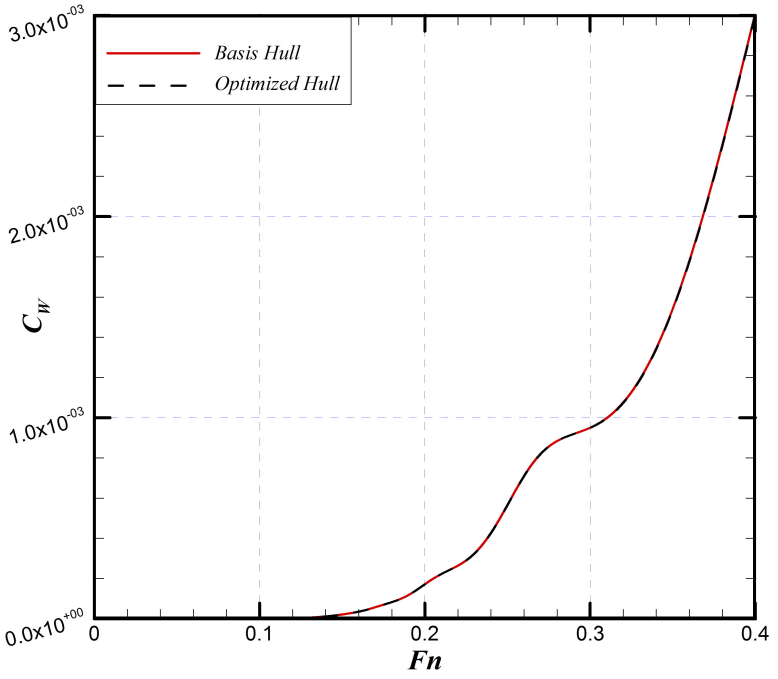

FIGURE 6.28: Wave resistance coefficient of six genes with $\alpha = 0.00$

that figure. It is almost the same with that due to the total component of radiation problem given as dashed line.

In Fig. 6.30, we could observe that the added resistance due to heave motion decreases in very large quantity due to the amplitude reduction of it shown in Fig. 6.22. However

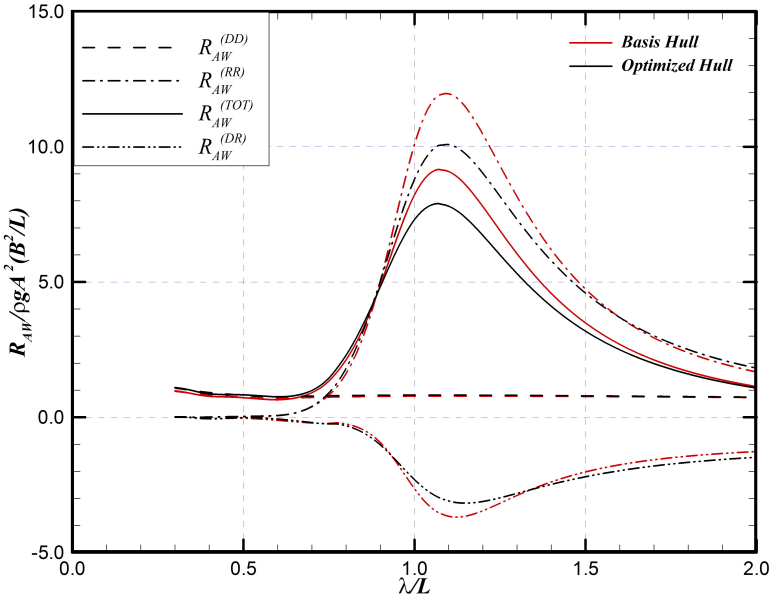

FIGURE 6.29: Main Component of R_{AW}

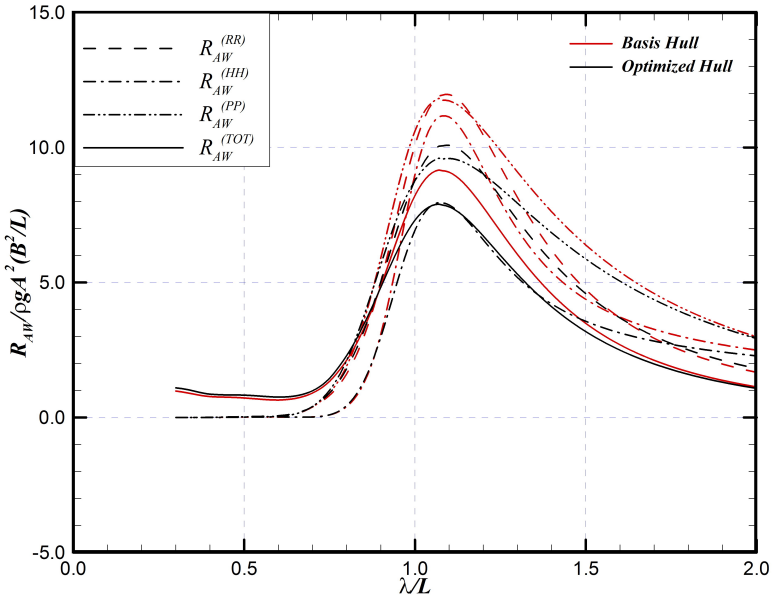

FIGURE 6.30: Radiation Component of R_{AW}

its effects are not significant to the total added resistance which only diminishes in relatively small amount as shown in Fig. 6.24.

Chapter 7

Conclusions

Performance of a ship has been improved by a practical integrated optimization method which was newly developed in this study. Namely, the Binary-Coded Genetic Algorithm (BCGA) and Enhanced Unified Theory (EUT) were integrated together to reduce the resistance of a ship in waves through the shape function and Lagrangian interpolation. A modified Wigley model was firstly employed as a basis hull, followed by an actual ship i.e. SR-108 for practical purposes. For modified Wigley model, the optimization was performed at short ($\lambda/L = 0.30 \sim 0.80$) and middle ($\lambda/L = 0.80 \sim 1.30$) wavelengths regions with the total added resistances being the objective function. For SR-108, it was optimized only at middle wavelength region based on sensitivity study to the peak value of the added resistance. The results obtained in this study may be summarized as follows:

a. For the modified Wigley model at short wavelength region, a finer shape of bow and stern with combination of inserting the parallel middle body (P_{MB}) to the aft- and fore-bodies of a ship would reduce the added resistance at concerned wavelengths but increase around its peak to longer wavelengths.

b. For middle wavelength region, a slightly blunter bow shape with inserting the P_{MB} only to the fore-body of a modified Wigley model would reduce the added resistance around its peak. It might be attributed to the pitch motion but slightly increases at short wavelengths as its bow shape becomes blunter.

c. By doing a sensitivity study to the added resistance, especially at its peak, it was found that the pitch motion is the most sensitive to the peak value of the added resistance. Hence it was used as the primary fitness function to be optimized for an actual container ship, SR-108.

d. The best optimized shape of SR-108 in which the P_{MB} was inserted and the blunter bow was acquired would reduce the added resistance in large amount around its peak at concerned wavelengths due to reduction of the pitch motion as well as reduction of the heave motion.

e. Removing an eccentric shape i.e. small bump near stern of the best optimized SR-108 did not increase the steady wave resistance but slightly increased the peak value of the added resistance. Nevertheless, compared to the basis hull, the amount of reduction of the resistance was remarkable.

f. The bow shape of a ship was the most important part in determining the added resistance followed by the stern part which was also influential in reducing the steady wave resistance.

Bibliographies

[1] M. Tasrief and M. Kashiwagi, "Relation between the added resistance and resonant frequency in ship motion," *Proc. of the Japan Society of Naval Architects and Ocean Engineers (JASNAOE)*, vol. 12, pp. 513–514, 2011.

[2] M. Tasrief and M. Kashiwagi, "Improvement of ship geometry by optimizing the sectional area curve with binary-coded genetic algorithms (bcgas)," *Proc. of the 23^{th} International Society of Offshore and Polar Engineers Conference (ISOPE)*, pp. 869–875, 2013.

[3] H. Lackenby, "On the systematic geometrical variation of ship forms," *Transaction, RINA*, vol. 92, pp. 289–316, 1950.

[4] D. Coley, *An Introduction to GA for Scientists and Engineers.* World Scientific Publishing, 1998.

[5] S. Sivandam and S. Deepa, *Introduction to Genetic Algorithms.* Springer, 2008.

[6] R. Chakraborty, "Fundamental of genetic algorithms," *Lecture Note*, 2010.

[7] H. Kim, C. Yang, and F. Noblesse, "Hull form optimization for reduced resistance and improved seakeeping via practical designed-oriented cfd tools," *Proceeding of the GCMS*, no. 89, 2010.

[8] J. Newman, *Marine Hydrodynamics.* MIT Press, 1977.

[9] M. Kashiwagi, "Theory of ship waves," *Study Handout*, pp. 1–47, 2010.

[10] M. Kashiwagi, "Calculation formulas for the wave-induced steady horizontal force and yaw moment on a ship with forward speed," *Reports of Research Institute for Applied Mechanics*, vol. XXXVII, no. 107, 1991.

[11] H. Maruo, "Wave resistance of a ship in regular head seas," *Bulletin of the Faculty of Eng. Yokohama National Univ.*, vol. IX, no. 107, pp. 73–91, 1960.

[12] J. Newman and P. Sclavounos, "The unified theory of ship motions," *Proc. of 13th Symp. on Naval Hydrodynamics*, pp. 373–394, 1980.

[13] M. Kashiwagi, "Numerical seakeeping calculation based on the slender ship theory," *Ship Technology Research*, vol. 44, pp. 167–188, 1997.

[14] M. Kashiwagi, "Prediction of surge and its effect on added resistance by means of the enhanced unified theory," *Trans West-Japan Society of Naval Architecture*, no. 89, pp. 77–89, 1995.

[15] T. Ogilvie and E. Tuck, "A rational strip theory of ship motions: Part i," *Tech. Rep. 013, University of Michigan, Dept. of Naval Architecture and Marine Engineering*, 1969.

[16] J. Holtrop and G. Mennen, "An approximate power prediction method," *International Shipbuilding Progress*, vol. 29, no. 335, 1982.

[17] M. Tasrief and M. Kashiwagi, "Improvement of ship geometry in light of ship performance in actual sea," *Proc. of the 6^{th} Asia Pacific Workshop on Marine Hydrodynamics*, pp. 83–88, 2012.

[18] M. Kashiwagi, T. Ikeda, and T. Sasakawa, "Effects of forward speed of a ship on added resistance in waves," *Int. Journal of Offshore and Polar Engineering*, vol. 20, pp. 196–203, 2010.

[19] M. Kashiwagi and K. Sumi, "Development of hull form of ship with high performance in waves," *International Conference on Fast Sea Tranportation, FAST*, June 2005.

[20] M. Tasrief and M. Kashiwagi, "Improvement of ship performance based on sensitivity study to the added resistance," *Proc. of the 24^{th} International Society of Offshore and Polar Engineers Conference (ISOPE)*, 2014.